CHALMERS

HAMIDREZA ABEDI

Aerodynamic Loads On Rotor Blades

Department of Applied Mechanics
Division of Fluid Dynamics
Chalmers University of Technology
Göteborg Sweden, 2011

Master's Thesis [2011 : 18]

Master's Thesis 2011:18

Aerodynamics Loads On Rotor Blades

Master's Thesis

Hamidreza Abedi

Department of Applied Mechanics
Division of Fluid Dynamics
Chalmers University of Technology
Göteborg, Sweden, 2011

AERODYNAMIC LOADS ON ROTOR BLADES
Master's Thesis
HAMIDREZA ABEDI

Master's Thesis 2011:18
ISSN: 1652-8557

Department of Applied Mechanics,
Division of Fluid Dynamics
Chalmers University of Technology
Se-412 96 Göteborg, Sweden
Phone +46-(0)31-7721400
Fax: +46-(0)31-180976

Printed at Chalmers Reproservice
Göteborg, Sweden 2011

Aerodynamics Loads On Rotor Blades

Master's Thesis

by

Hamidreza Abedi

abedih@student.chalmers.se

Department of Applied Mechanics

Division of Fluid Dynamics

Chalmers University of Technology

Abstract

In the last decade, we have heard more and more about the need of renewable clean energy, but not much has been done. Currently, the wind power energy is the most popular of all of these green technologies. Thousands of wind turbines are being invested and installed everywhere worldwide. Thus, many questions arise.

The aerodynamic loads on the rotor blades are the largest loads acting on a wind turbine. The horizontal wind turbine types of blades are usually made of two or three airfoils such as a propeller. In these types of blades, it is the lift force which makes the rotor turn. The drag force acts perpendicular to the lift force due to the resistance of the airfoil from the wind and counteracts the rotation to rotor. Therefore, predicting these loads accurately is one of the most important parts of the calculations in wind turbine aerodynamics. Another reason for computing the aerodynamic loads on rotor blades is to model the aeroelastic response of the entire wind turbine construction. There are different methods to calculate the aerodynamic loads on a wind turbine rotor with different level of complexity such as Blade Element Momentum Method (BEM), Vortex Method, Panel Method and Computational Fluid Dynamics (CFD). Most aerodynamic codes use BEM (together with many additions) which is very fast and gives fairly accurate results.

The main goal of this project is studying the Helical Vortex Method. In this text, helical vortex method has been developed and compared with Blade-Element Momentum (BEM) theory for the analysis of wind turbine aerodynamics.

Keywords: Incompressible Flow, Aerodynamics, Wind Turbine, Vortex Theory, BEM Method, Lifting Line Theory, Helical Vortex

Acknowledgment

The present work has been conducted at the Division of Fluid Dynamics, Applied Mechanics Department, Chalmers University of Technology.

I would like to express my sincere gratitude to my supervisor, Professor Lars Davidson for his support, guidance and encouragement. This thesis would never reach to this point without his enlightening discussions and brilliant advice. On my path, he has instructed me as a guide with his crystal spirit.

I would like to thank Ingemar Carlen at Teknikgruppen AB for his valuable advice and insights. I should thank Björn Montgomerie for the novel ideas that he has shared with me, and also my best friend, Alireza Majlesi for his excellent contribution.

My warmest and deepest sense of gratitude goes to my family; my father Abbas, the first teacher in my life, who taught me dignity and loyalty; my mother, Maryam, the teacher of love and selflessness and my sister Fatemeh, for her companionship and patience. Thanks for their interminable love and support.

Nomenclature

Upper-case Roman

A	Rotor area, Area, Arbitrary vector field
C	Constant
C_D	Drag coefficient
C_F	Axial force coefficient
C_L	Lift coefficient
C_n	Power coefficient in normal direction
C_P	Power coefficient
C_Q	Torque coefficient
C_t	Power coefficient in (parallel) tangential direction
C_T	Thrust coefficient
D_i	Induced drag
D'_i	Induced drag per unit length
$\mathbf{F}_{viscous}$	Viscous force
F	Prandtl tip loss factor
H	Hydraulic head
L	Lift
L'	Lift per unit length
NB	Number of blades
P	Shaft power, Arbitrary point
P_N	Force per unit length in normal direction
P_T	Force per unit length in (parallel) tangential direction
R	Rotor radius
S	Surface area, Curve defining the vortex line, Finite wing area
S'	Parametric variable along the curve
T	Thrust, Period
V	Velocity
V_a	Axial velocity
V_{ij}	Tangential normalized induced velocity
V_r	Radial velocity
V_{rel}	Local velocity, Relative velocity
V_{rot}	Rotational velocity
V_θ	Tangential velocity
V_0	Free stream velocity (wind velocity)
W	Resultant velocity, Downwash velocity
W_{ij}	Axial normalized induced velocity

W_n	Normal induced velocity, Induced velocity
W_t	Tangential induced velocity
W_y	Tangential induced velocity
W_z	Axial induced velocity
W'	Undisturbed resultant velocity vector

Lower-case Roman

a	Axial induction factor
a'	Tangential induction factor
b	Length of rotor blade
c	Chord length
$c(r)$	Local chord
$d\mathbf{A}$	Area of annual element of infinitesimal thickness dr
$d\mathbf{l}$	Segment of vortex filament
$d\mathbf{s}$	Distance element, Vector path of the helix
$d\boldsymbol{\eta}$	An Infinitesimal segment of the helix
ds	An infinitesimal portion of the vortex sheet
dM	Normal torque on the control volume, Angular momentum element
dT	Normal force on the control volume
dv	Vortex filament volume, Fluid element volume
$\mathbf{f}$	Body force
f	Glauert correction
h	Perpendicular distance
m	Number of blades
$\dot{m}$	Mass flow rate
$\mathbf{n}$	Normal vector to the rotor plane
n	Number of revolution
p	Pressure close upstream of the rotor blade
p_0	Atmospheric pressure
$\mathbf{r}$	Distance vector
r	Radius, Radial position (distance)
u	Wind speed at the rotor plane
v_i	Tangential induced velocity
w_i	Axial induced velocity
u_1	Wind speed in the wake
x	Arbitrary point where the potential is computed, Local rotational speed

Upper-case Greek

Γ	Circulation

Δp	Pressure loss
Ω	Angular velocity

Lower-case Greek

α_i	Induced velocity
α_{eff}	Effective angle of attack
$\alpha_{L=0}$	Zero-incident angle of attack
α	Angle of attack
β	Twist of the blade
γ	Strength of the vortex sheet per unit length
δ	Line Dirac delta function
θ	Airfoil or local blade pitch
θ_p	Blade pitch
λ	Tip speed ratio
ρ	Air density
σ	Solidity
ϕ	Flow angle, Scalar potential, Constant number
ψ	Vector potential
$\boldsymbol{\omega}$	Vorticity
ω	Angular velocity

Abbreviations

HAWT	Horizontal Axis Wind Turbine

subscripts

i	Direction, node number
ij	Tensor indices
j	Direction, node number
k	Direction
N	Normal
n	Normal
T	Tangential
t	Tangential

Contents

Chapter 1

Introduction

1.1 Aerodynamic Loads Philosophy

Studying the aerodynamics of a wind turbine is very crucial to predict accurately the blade loads and power output. The wind turbine performance is connected to different subjects such as creation of three-dimensional, atmospheric turbulence, the ground boundary layer, directional and spatial variations in wind shear, and the effects of an upstream support structure (tower shadow) [1]. Also, unsteady aerodynamics should be considered to look into the periodic loads by wind shear in the boundary layer of the earth and also the effect of the tower shadow [2].

For the last few decades, the aerodynamic performance methods for wind turbines were based on the blade element momentum (BEM) theory. This method is fast and simple but it is acceptable only for a limited range of flow conditions and break-down in the turbulent wake state and the vortex ring state. There are some modifications based on empirical corrections to modify the (BEM) method in order to defeat this restriction. But, they are not relevant for all operating conditions and often go wrong at higher tip speed ratios.

On the other side, the vortex theory can be a better choice for predicting aerodynamic performance of wind turbine. The major purpose of the vortex theory is to build up a solution which considers the effect of finite number of blades and secondary effects due to wake rotation. So, the complete vortex system of the rotor should be modeled [2].

There are two different approaches for vortex theory:

- Free Wake Modelling
- Prescribed Vortex Wake (Rigid Wake)

Free Wake Modelling has been used in rotorcraft applications, but it has not been used extensively for wind turbine research. In this model, all vortex elements affect all other vortex elements, so there will be a self-development in the vortex system translation. As can be seen in next chapters, the fundamental equation for vortex method analysis is Biot-Savart law, but in reality, the nature does not follow the Biot-Savart law for potential flows [3]. One reason for this deviation of the vortex system development is the viscous effects. One spectacular characteristic of reality is to concentrate the trailing vorticity from the blades into distinct tip vortices, one for each blade tip which occurs very rapidly. This fact also occurs for a fixed wing. The reason for using free wake modelling is the weakness of the rigid wake like the momentum theory in the turbulent wake/vortex ring condition [2]. On the other side, the computation cost (CPU time) of the free wake modelling is high.

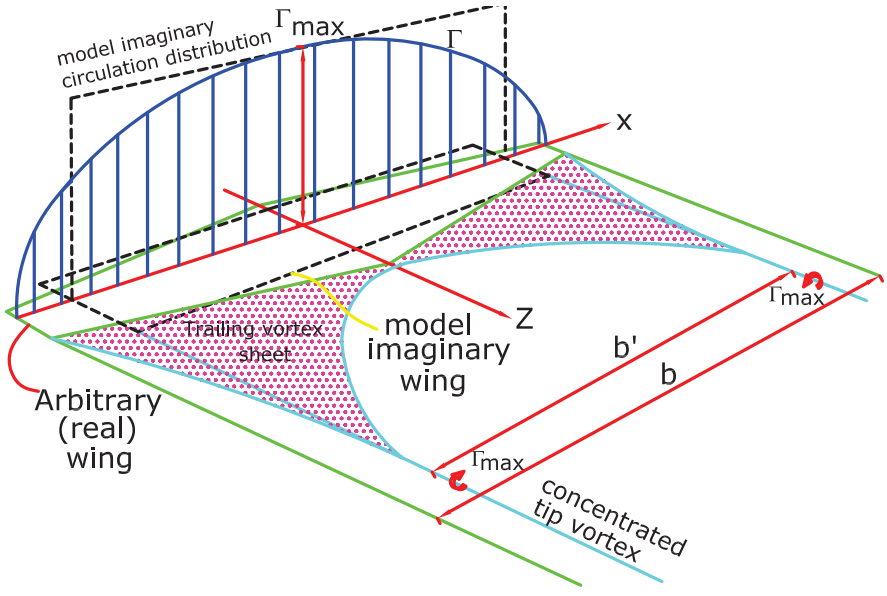

Figure 1.1: Schematic of the concentrated tip vortices for an fixed wing

Prescribed vortex wake models such as helical vortex theory have been used for analysis of wind turbine's aerodynamics. In the helical vortex

method, the rotor blades and trailing vorticity are modeled by lifting line and helical vortex sheet respectively. The bound circulation which originates from the lift force created sectionally by the flow passing over the blades, determines the vortex strength. By dividing the blade into a number of spanwise sections and knowing the strength and position of the vortices, the induced velocity around the blade can be found in each section using the Biot-Savart law and affect the flow as well as the forces acting on the blades. The relationship between the bound circulation and the lift is defined by the Kutta-Jukowski theorem and using this together with the definition of the lift, gives a simple relationship between the bound circulation and the lift coefficient. It is assumed that a helical filament of the trailing vortices traveling downstream with a constant velocity, extends sufficiently far downstream of the rotor and has a constant diameter. The interactions between the wake elements are ignored. This method requires an iterative procedure. Finally, when the iteration is completed and the effective angle of attack at each section is computed, then the performance parameters of a wind turbine like lift force, drag force, torque and shaft power can be calculated.

1.2 Basic Model for Vortex Method

In this section, the 3-D inviscid aerodynamic model is discussed [4]. The aim of this model is to find a more detailed description of the 3-D flow which develops around a wind turbine. The viscous effects are neglected. In vortex method, the rotor blades, trailing and shed vorticity in the wake are introduced by lifting line and surface. On the blade, the vortex strength is determined from the bound circulation stemming from the amount of lift which is created locally by the flow past the blades. The spanwise variation of bound circulation generates the trailing vortices while the shed wake is generated by a temporal variation and ensures that the total circulation over each section along the blade remains constant in time. It is recalled that knowing the strength and position of the vortices, makes it possible to calculate the induced velocity in any point using the Biot-Savart law (see Appendix A for its derivation). Also, the bound circulation is found from airfoil data like the BEM method. The inflow is determined as the vector sum of the induced velocity, the blade rotational velocity and the undisturbed wind velocity. The relationship between the bound circulation and the lift is denoted by the Kutta-Jukowski theorem and using this together with the definition of the lift coefficient, a simple relationship between the bound circulation and the lift coefficient can be derived as

$$L = \rho V_{rel}\Gamma = \frac{1}{2}\rho c V_{rel}^2 C_L \Rightarrow \Gamma = \frac{1}{2} c V_{rel} C_L \tag{1.1}$$

Moreover, according to vector analysis of fluid dynamics, any velocity field can be decomposed in a solenoidal part and a rotational part as [5]

$$\boldsymbol{V} = \nabla \times \boldsymbol{\Psi} + \nabla\phi \tag{1.2}$$

where $\boldsymbol{\Psi}$ is a vector potential and ϕ a scalar potential. Curl of the eq.(1.2) yields

$$\nabla \times \boldsymbol{V} = \nabla \times \nabla \times \boldsymbol{\Psi} + \nabla \times \nabla\phi \tag{1.3}$$

Vector identity gives

$$\nabla^{\mathbf{2}}\boldsymbol{\Psi} = \nabla\left(\nabla \cdot \boldsymbol{\Psi}\right) - \nabla \times \nabla \times \boldsymbol{\Psi} = -\nabla \times \nabla \times \boldsymbol{\Psi} \tag{1.4}$$

where $\nabla\left(\nabla \cdot \boldsymbol{\Psi}\right) = 0$ since $\boldsymbol{\Psi}$ is a solenoidal vector field (also known as an incompressible vector field) with divergence zero. From eqs.(1.3), (1.4) and the definition of vorticity, the Poisson equation for the vector potential is derived as

$$\nabla^{\mathbf{2}}\boldsymbol{\Psi} = -\boldsymbol{\Omega} \tag{1.5}$$

where $\boldsymbol{\Omega}$ denotes the rotational velocity ($\nabla \times \mathbf{V} = \boldsymbol{\Omega}$). The solution of the Poisson equation is

$$\boldsymbol{\Psi}\left(\mathbf{x}\right) = \frac{1}{4\pi}\int \frac{\boldsymbol{\Omega}\left(\mathbf{x}'\right)}{\mid \mathbf{x} - \mathbf{x}' \mid} dv \tag{1.6}$$

where $\mathbf{x}$ and v denote the point where the potential is computed and the vortex filament volume, respectively. A prime denotes evaluation at the point of integration $\mathbf{x}'$ which is taken over the region where the vorticity is non-zero, designated by v. So, the induced velocity field is obtained by taking the curl of eq.(1.6) as

$$\mathbf{W}\left(\mathbf{x}\right) = -\frac{1}{4\pi}\int \frac{\left(\mathbf{x} - \mathbf{x}'\right) \times \boldsymbol{\Omega}}{\mid \mathbf{x} - \mathbf{x}' \mid^3} dv \tag{1.7}$$

1.3 Vortex Wake's Regions

There is a loss momentum downstream of a wind turbine because of the wake. The wake shape is produced by interaction between free stream and vorticity sheets at the blades and trailed downstream of the rotor [6]. As

mentioned before, this trailing vorticity is similar to the horseshoe vortex system at finite wing because of the spanwise variation of the bound circulation. On a wind turbine rotor, since the circulation and lift force are forced to be zero at the tip and root. So, the gradient of circulation in the radial direction would be great at the blade tip, where a strong trailing vortex results. The trailing vorticity get the helix form downstream and spatial variation of the wake velocity change the diameter and pitch of the sheet. Then the induced velocity at any position in the wake can be determined by the vorticity at all other points by Biot-Savart law. Moreover, the vortex sheets tend to be rolled up concisely downstream of the rotor blade.

As a result, the vorticity is concentrated at the outer edge of the wake. The wake shape changes, so we deal with two different regions:

- Outer region with strong tip vortex spiral
- Inner region as a weak diffused vortex sheet

Chapter 2

Theory of 3-D Aerodynamics

In this chapter, we explain the aerodynamic theory and the fundamental definitions for Horizontal Axis Wind Turbine (HAWT). Since the rotor blade of an HAWT is very similar to the fixed wing, the aerodynamic concept of finite wing will be applicable.

2.1 Vortex Flow

In aerodynamics, we consider a series of non-lifting elementary incompressible flows to model complex incompressible flows, such as uniform flow, source flow, doublet flow and vortex flow [7]. In simple words, the vortex flow which includes vortices produces finite lift, and it is modelled as the flow where all the streamlines are concentric circles about a given point and a velocity along any circular streamline is constant (but vary from one streamline to another inversely with distance from the common center). Generally, the vortex flow properties are

- It is an incompressible flow ($\nabla.\mathbf{V} = 0$) at every point.
- The vortex flow is irrotational ($\nabla \times \mathbf{V} = 0$) at every point except at the origin where the velocity is infinite.

By introducing V_θ as tangential velocity (see fig.(2.1)), the flow for an ideal vortex line is given by

$$V_\theta = \frac{C}{r} \tag{2.1}$$

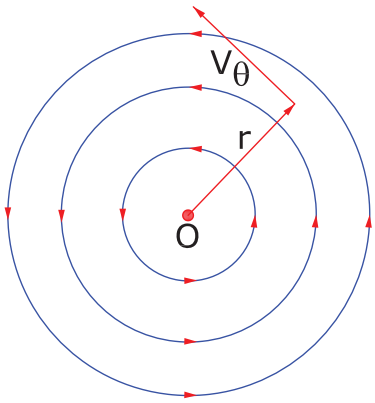

Figure 2.1: Vortex flow

where C is obtained by taking the circulation around a given circular streamline of radius r as

$$\Gamma = \oint_c \mathbf{V}.d\mathbf{s} = V_\theta(2\pi r)$$
$$V_\theta = \frac{\Gamma}{2\pi r} \tag{2.2}$$

So, by comparing eqs.(2.1) and (2.2), we get

$$C = \frac{\Gamma}{2\pi} \tag{2.3}$$

where Γ is called the strength of the vortex flow. Equation (2.3) shows that the circulation taken about all streamlines is the same value as $\Gamma = 2\pi C$. Also, eq.(2.2) gives the velocity field for a vortex flow of strength Γ.

2.2 Vortex Sheet

To define a vortex sheet [7], we basically consider a straight line perpendicular to the page, going through point O and extending to infinity from both sides. This line is a straight vortex filament of strength Γ. The induced flow by straight vortex filament in any plane normal to itself (see fig.(2.2)), is similar to a point vortex of strength Γ. So, it can be concluded that the point vortex is a section of a straight vortex filament. We can define vortex sheet as an infinite number of adjacent straight vortex filaments with infinitesimally small strength. By introducing $\gamma = \gamma(s)$ as the strength of the vortex sheet per unit length along s, the strength of an infinitesimal portion ds of the sheet is γds. As can be seen in fig.(2.3), the small section of the vortex sheet

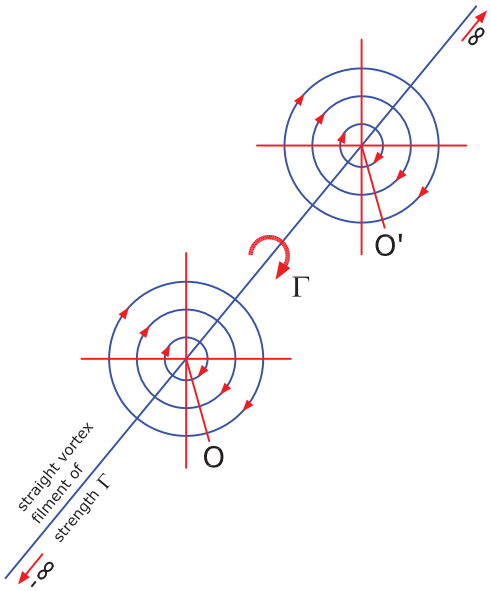

Figure 2.2: Vortex filament

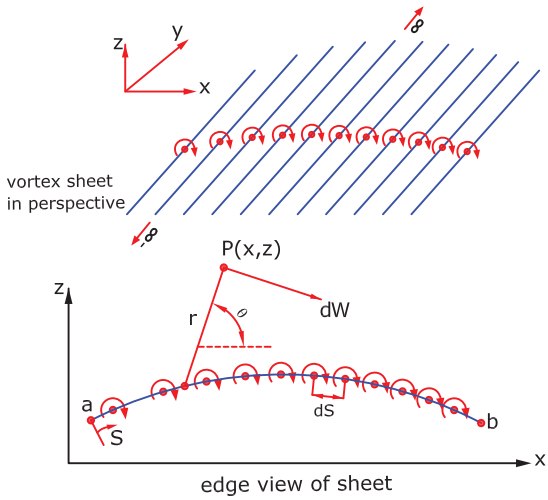

Figure 2.3: Vortex sheet

of strength γds induces an infinitesimally small velocity dW at point $P(x, z)$ located at the distance of r from ds, so we get

$$dW = \frac{\gamma ds}{2\pi r} \tag{2.4}$$

which is perpendicular to r. The induced velocity at point P by the entire vortex sheet is the vector summation of eq.(2.4) from point a to point b. Therefore we get

$$dW = \int_a^b \frac{\gamma ds}{2\pi r\,(s)}$$

The circulation around the airfoil is given by $\Gamma = \int \gamma ds$ where the integral is taken around the total surface of the airfoil. So, we can calculate the lift force by the Kutta-Jukowski theorem as

$$L = \rho V_0 \Gamma$$

where ρ is the density of the fluid and V_0 is the uniform velocity far from the airfoil.

2.3 Finite Wing and Downwash

In this section, we describe flow over the finite wing (3-D wing) and evaluate how the spanwise lift distribution affects the upstream flow and modifies the angle of attack [7].

To find the above, we must study the vortex theory, since a real wind turbine has blades (wings of finite span) and the aerodynamic characteristics of a finite wing is different from the properties of its airfoil section because usual airfoil data is related to flow over 2-D airfoil.

A wing is similar to a beam of finite length whose cross section has the form of airfoil and therefore the presence of a high pressure region on the bottom surface and low pressure region on the top surface produces the lift force. Also, there is a component of flow in the spanwise direction for the finite wing as a 3-D body.

Due to pressure imbalance, there is air leakage at the wing tip where air flows from the bottom surface to the top surface and curl around the tip. As a result, the spanwise component of flow makes the top surface flow to be deflected from the tip toward the wing root and bottom surface to be deflected from the root toward the wing tip (see fig.(2.4). Furthermore, at the trailing edge, there is a jump in the tangential velocity. The air leakage around the wing tip also creates a circulatory motion as a continuous sheet of

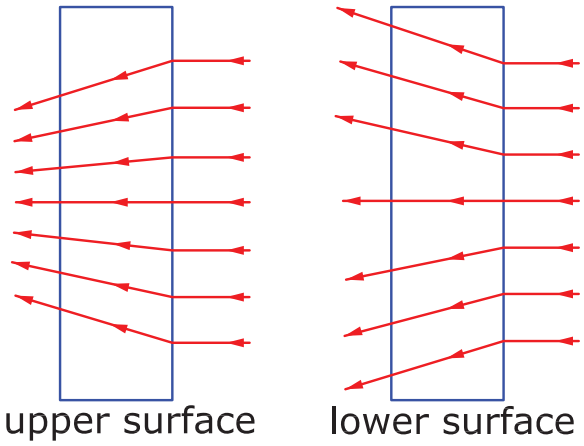

Figure 2.4: Streamlines flowing upper and lower surface of a wing

streamwise vorticity in the wake behind the wing. Since the trailing vortices curl up around the strong tip vortices in a real flow, the vortex system looks like fig.(2.6). These wing-tip vortices downstream of the wing, induce a small

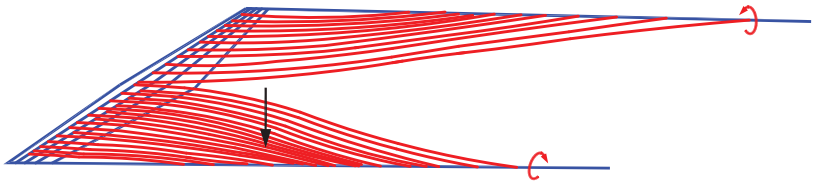

Figure 2.5: Vortex system on a wing

downward component of air velocity in the neighborhood of the wing itself. These wing-tip vortices contain a large amount of translational and rotational kinetic energy. In fig.(2.7), the two vortices tend to entrain the surrounding air and this secondary movement induces a small velocity component in the downward direction at the wing. This downward component from all vortices at a section of the wing is called *downwash*, denoted by W. In turn, the vector combination of the downwash with the free stream velocity V_0 produces

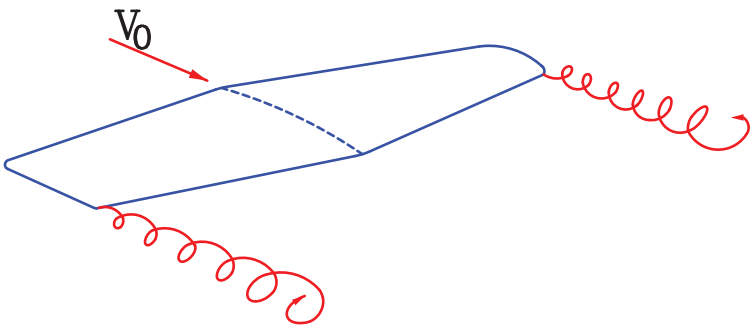

Figure 2.6: Schematic of wing-tip vortices

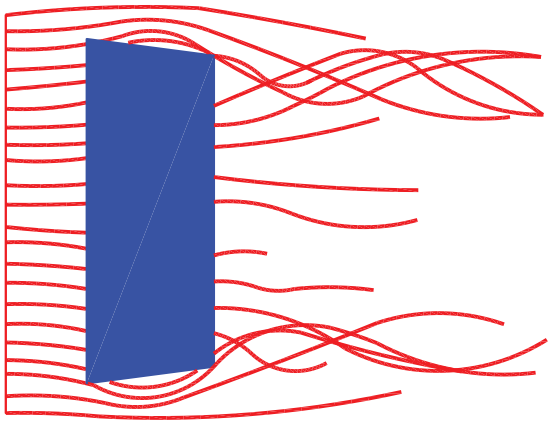

Figure 2.7: Wing-tip vortices from a rectangular wing

a local relative wind tilted downward in the vicinity of each section of the wing, so the local angle of attack at each section is reduced by α_i . The local

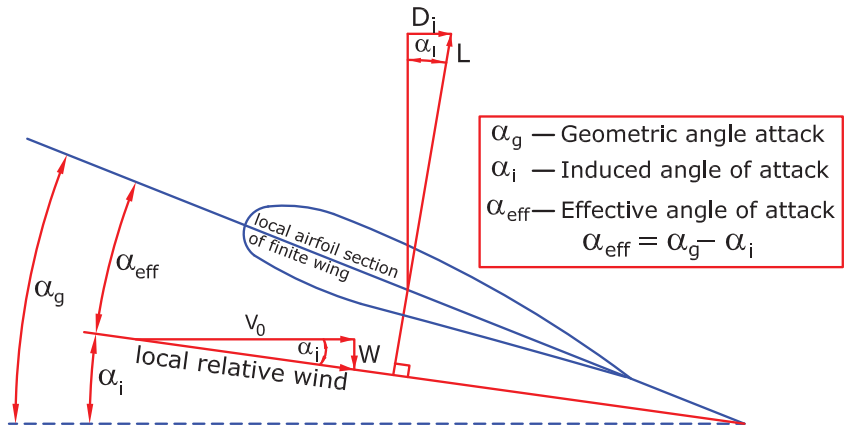

Figure 2.8: Effect on downwash on the local flow over a local airfoil section of a finite wing.

lift force by definition is perpendicular to the local relative wind. So, there is a component of the local lift force in the direction of V_0 which means that there is a drag force created by the downwash. This drag force is defined as induced drag which is a type of pressure drag denoted by D_i.[1]Also, at the tip of the wing, the induced velocity obtains a value which exactly ensures zero lift force. According to fig.(2.8), we can categorize the downwash effects as

- Reducing the angle of attack for each section.
- Creating a component of drag force (induced drag D_i).

2.4 The Biot-Savart Law and Helmholtz's Theorems

As mentioned before, the vortex filament of strength Γ induces a flow field in the surrounding space and it can be used as a model for the flow over an airfoil for small angles of attack [7].

[1]The local lift force is different from the global lift force which is perpendicular to the free stream V_0.

According to Biot-Savart law, the velocity induced by the segment of a vortex filament which is created by trailing vortices (free vortices) at any arbitrary point P in space is equal to (see eq.(A.37))

$$d\mathbf{W} = \frac{\Gamma}{4\pi} \frac{d\mathbf{s} \times \mathbf{r}}{|\ \mathbf{r}\ |^3} \tag{2.5}$$

In the analysis of inviscid incompressible flow, the Helmholtz's theorem

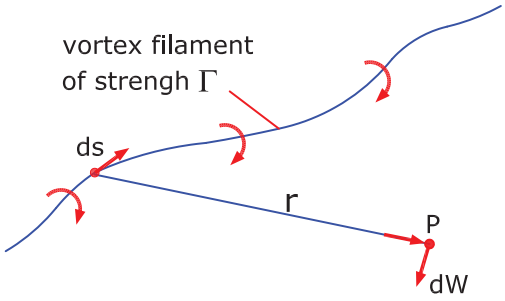

Figure 2.9: Vortex filament and Biot-Savart law concept

describes the behaviour of the vortex filament as

- The strength of a vortex filament is constant along its length.
- A vortex filament cannot end in a fluid; It must extend to the boundaries of the fluid (which can be $\pm\infty$) or form a closed path.

These theorems are inevitable to explain the following sections. Finally, the concept of lift distribution along the span of a finite wing is presented. In general, most finite wings have variable chords and they are also twisted so that the angle of attack α is not the same at different spanwise locations. Likewise, most wings are constructed by different airfoil sections along the span. Accordingly, the lift force per unit span at different locations is not the same. Hence, there will be a lift distribution per unit length along the wing (blade), i.e. $L' = L'(y)$ where L' denotes the lift per unit length. Therefore, according to the Kutta-Jukowski theorem, the circulation is also a function of y, i.e.

$$\Gamma(y) = \frac{L'(y)}{\rho V_0}$$

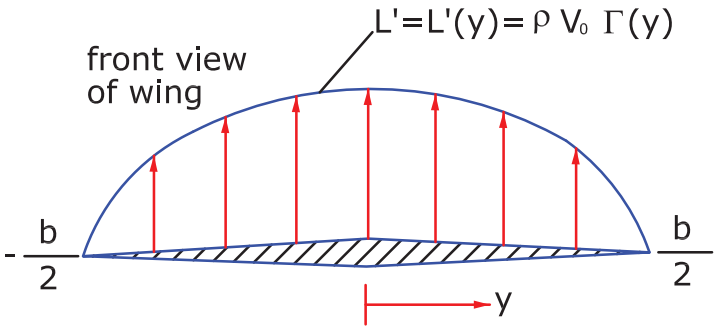

Figure 2.10: Lift distribution along a wing

Because of the pressure balancing from the bottom to the top of the wing exactly at $y = -b/2$, $y = b/2$, there is no lift at the tips, see fig.(2.10). Now, we need to calculate the lift distribution $L(y)$ (or the circulation distribution $\Gamma(y)$) for a finite-wing.

2.5 Prandtl's Classical Lifting-Line Theory

This theory is used to calculate the characteristics of a finite-wing (or blade) [7]. According to this theory, a vortex filament of strength Γ bounded to a fixed location in a flow (a so-called bound vortex) will sense a force $L = \rho V_0 \Gamma$ according to the Kutta-Jukowski theorem. This bound vortex is in contrast to a free vortex moving with the same fluid elements throughout a flow. So, a finite wing of span b can be modeled as a bound vortex from $y = -b/2$ to $y = b/2$. Since a vortex filament cannot end in the fluid (according to the Helmholtz's theorem and also because $\nabla \cdot \boldsymbol{\omega} = 0$), so it is concluded that that the vortex filament continues as two free vortices trailing downstream of the wing tips to infinity as in fig.(2.11). This vortex including the bound and the two free vortices is like a horseshoe, a so-called horseshoe vortex. According to fig.(2.12), it is obvious that the bound vortex induces no velocity along its axis whereas the two trailing vortices both contribute to the downward induced velocity along the bound vortex. By taking the origin at the center of the bound vortex (see eq.(2.5)), the contributions from the left trailing vortex (trailing from $-b/2$) and form the right trailing vortex (trailing from $+b/2$), respectively are as belows. Recall that Biot-Savart law reads as

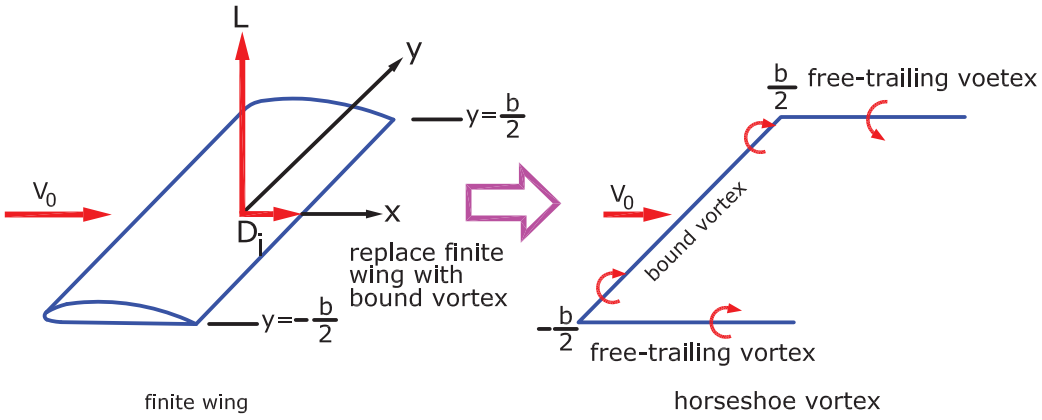

Figure 2.11: Modelling of the finite wing with a bound vortex

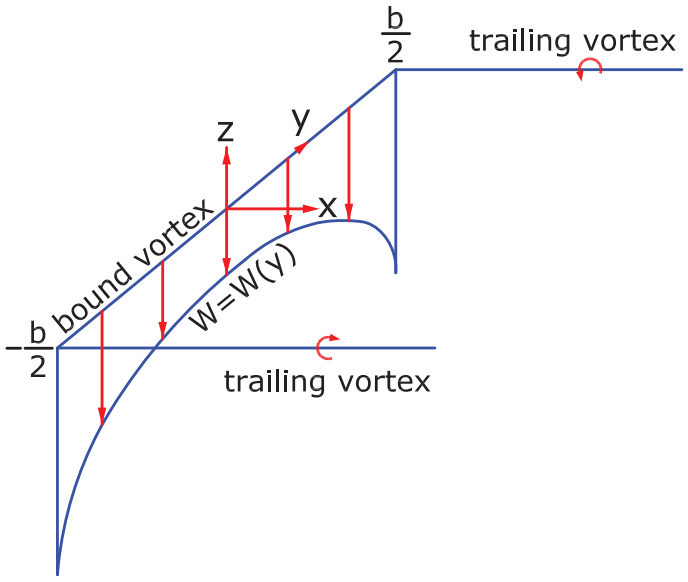

Figure 2.12: Downwash distribution for a single horseshoe vortex along the y axis.

$$\mathbf{W} = \frac{1}{4\pi}\int \frac{\mathbf{\Gamma}\times \mathbf{r}ds}{|\mathbf{r}|^3}$$

For the left trailing vortex, $\mathbf{r} = (x, -(b/2-y), 0)$ and $\mathbf{\Gamma} = (\Gamma, 0, 0)$ which gives

$$\begin{aligned} W_L(y) &= \frac{\Gamma}{4\pi}\int_0^\infty \frac{(b/2-y)\,dx}{\left(x^2+(b/2-y)^2\right)^{3/2}} = \frac{\Gamma}{4\pi(b/2-y)}\left[\frac{x}{\left(x^2+(b/2-y)^2\right)^{1/2}}\right]_0^\infty \\ &= -\frac{\Gamma}{4\pi}\frac{1}{(b/2-y)} \end{aligned}$$

For the right trailing vortex, $\mathbf{r} = (x, b/2+y, 0)$ and $\mathbf{\Gamma} = (-\Gamma, 0, 0)$ which yields

$$\begin{aligned} W_R(y) &= \frac{\Gamma}{4\pi}\int_0^\infty \frac{(b/2+y)\,dx}{\left(x^2+(b/2+y)^2\right)^{3/2}} = \frac{\Gamma}{4\pi(b/2+y)}\left[\frac{x}{\left(x^2+(b/2+y)^2\right)^{1/2}}\right]_0^\infty \\ &= -\frac{\Gamma}{4\pi}\frac{1}{(b/2+y)} \end{aligned}$$

Since both contributions are in the downward directions, then we get

$$\begin{aligned} W(y) &= -\frac{\Gamma}{4\pi(b/2+y)} - \frac{\Gamma}{4\pi(b/2-y)} \\ W(y) &= -\frac{\Gamma}{4\pi}\frac{b}{(b/2)^2-y^2} \end{aligned} \tag{2.6}$$

Simulation of a finite wing with downwash distribution due to the single horseshoe cannot be realistic, so instead of modeling the wing by a single horseshoe vortex, we can superimpose a large number of horseshoe vortices while each of them has a different length of the bound vortex but with all the bound vortices coincident along a single line, called the lifting line. By considering an infinite number of horseshoe vortices of small strength $d\Gamma$ which are superimposed along the lifting line (see fig.(2.14)), we can get the related equation as

$$W(y_0) = -\frac{1}{4\pi}\int_{-b/2}^{+b/2}\frac{(\frac{d\Gamma}{dy})dy}{y_0-y} \tag{2.7}$$

Equation (2.7) gives the value of the induced velocity W at y_0 due to all trailing vortices. In practice, the singularity in eq.(2.7) (where $y_0 = y$) is avoided because the point y is located at a distance x_0 downstream of y_0.

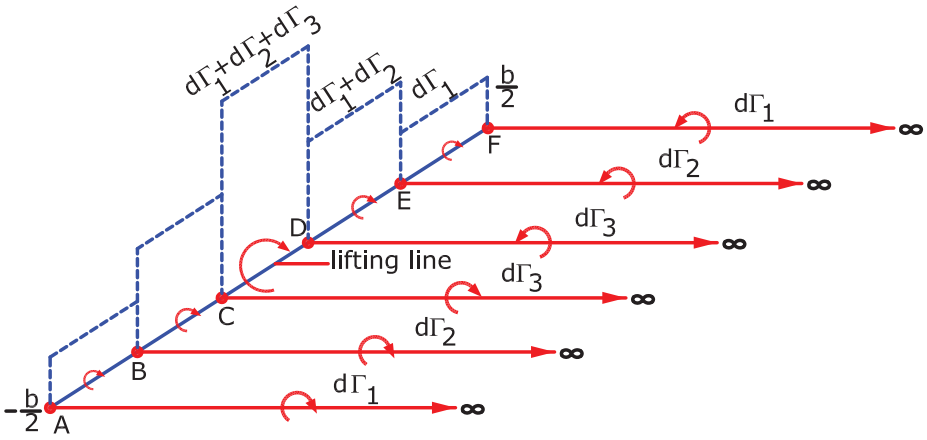

Figure 2.13: Superposition of a finite number of horseshoe vortices along the lifting line

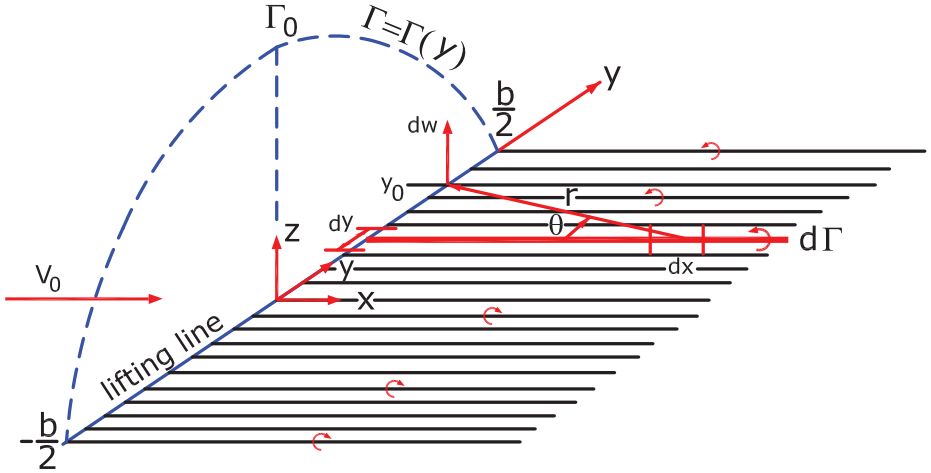

Figure 2.14: Superposition of an infinite number of horseshoe vortices along the lifting line

The integral limits will change from (0 to ∞) to (x_0 to ∞). Now, we are interested to find out $\Gamma(y)$ for a given finite wing, along with its corresponding total lift and induced drag. From fig.(2.8), we get

$$\alpha_i(y_0) = \tan^{-1}\left(-\frac{W(y_0)}{V_0}\right)$$

If α_i is small, it can be approximated as

$$\alpha_i(y_0) = -\frac{W\left(y_0\right)}{V_0} \tag{2.8}$$

By substituting eq.(2.7) into eq.(2.8), we get

$$\alpha_i(y_0) = \frac{1}{4\pi V_0}\int_{-b/2}^{+b/2}\frac{\left(\frac{d\Gamma}{dy}\right)dy}{y_0 - y} \tag{2.9}$$

From eq.(2.7), it is obvious that the downwash varies across the span. According to the relation of $\alpha_{eff} = \alpha_g - \alpha_i$ and eq.(2.8), we find that α_{eff} also varies along the span, i.e. $\alpha_{eff} = \alpha_{eff}\left(y_0\right)$. By combination of the lift coefficient definition and the Kutta-Jukowski theorem for the local airfoil section located at y_0 we get

$$\begin{aligned} L' &= \frac{1}{2}\rho V_0^2 c\left(y_0\right) C_L = \rho V_0 \Gamma\left(y_0\right) \\ C_L &= \frac{2\Gamma\left(y_0\right)}{V_0 c\left(y_0\right)} \end{aligned} \tag{2.10}$$

where $c\left(y_0\right)$ is the local chord length. Also, from the thin airfoil theory, we know that

$$C_L = 2\pi[\alpha_{eff}(y_0) - \alpha_{L=0}] \tag{2.11}$$

Substituting eq.(2.10) into eq.(2.11) gives

$$\alpha_{eff} = \frac{\Gamma(y_0)}{\pi V_0 c(y_0)} + \alpha_{L=0} \tag{2.12}$$

As we know, $\alpha_{eff} = \alpha_g - \alpha_i$, so we obtain

$$\alpha_g\left(y_0\right) = \frac{\Gamma\left(y_0\right)}{\pi V_0 c\left(y_0\right)} + \alpha_{L=0}\left(y_0\right) + \frac{1}{4\pi V_0}\int_{-b/2}^{+b/2}\frac{\left(\frac{d\Gamma}{dy}\right)dy}{y_0 - y} \tag{2.13}$$

The above equation is the fundamental equation of Prandtl's lifting line theory. The solution of eq.(2.13) gives $\Gamma = \Gamma(y_0)$ where y_0 changes along the span from $-b/2$ to $b/2$. Then we can calculate the parameters of a finite wing as below

- The lift distribution (from Kutta-Jukowski theorem) by

$$L'(y_0) = \rho V_0 \Gamma(y_0) \tag{2.14}$$

- The total lift by

$$L = \int_{-b/2}^{+b/2} L'(y)\, dy \Rightarrow L = \rho V_0 \int_{-b/2}^{+b/2} \Gamma(y)\, dy \tag{2.15}$$

  and the lift coefficient as

$$C_L = \frac{L}{\frac{1}{2}\rho V_0^2 S} = \frac{2}{V_0 S} \int_{-b/2}^{+b/2} \Gamma(y)\, dy \tag{2.16}$$

  where S is area of a finite wing.

- The induced drag by

$$D_i' = L_i' \sin\alpha_i \Rightarrow D_i' = L_i' \alpha_i \tag{2.17}$$

$$D_i = \int_{-b/2}^{+b/2} L'(y)\alpha_i(y) dy \Rightarrow D_i = \rho V_0 \int_{-b/2}^{+b/2} \Gamma(y)\alpha_i(y) dy \tag{2.18}$$

  and the induced drag coefficient as

$$C_D = \frac{D_i}{\frac{1}{2}\rho V_0^2 S} = \frac{2}{V_0 S} \int_{-b/2}^{+b/2} \Gamma(y)\, \alpha_i(y)\, dy \tag{2.19}$$

2.6 Vortex Wake System of a Wind Turbine

The rotor of Horizontal-Axis Wind Turbine (HAWT) consists of a number of blades [5]. These blades are in the form of a finite wing. By cutting the rotor blades at radial distance r parallel to the rotational axis as in fig.(2.15), we find a cascade of airfoils. The relation between the local velocity V_{rel}, axial

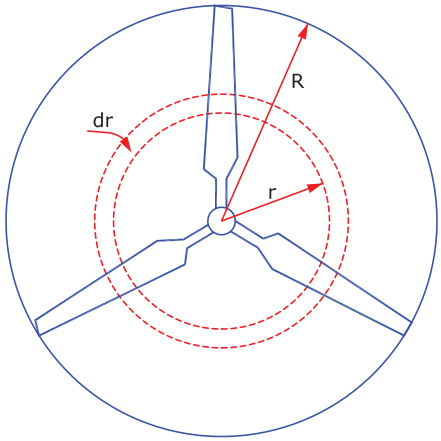

Figure 2.15: Rotor of a three-bladed wind turbine with rotor radius R

velocity V_a, rotational velocity V_{rot}, the local angle of attack α and the local pitch of airfoil θ are shown in fig.(2.16). It is obvious that

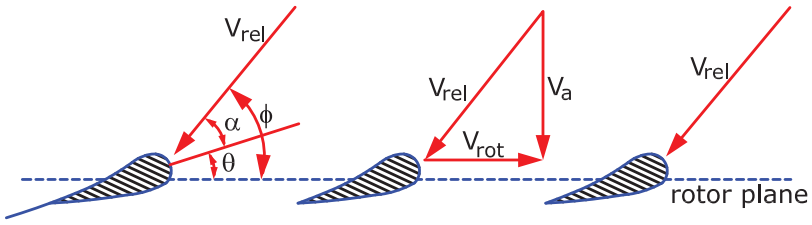

Figure 2.16: Rotor radial cut in a wind turbine showing airfoils at r/R

$$\tan\phi = \frac{V_a}{V_{rot}} \tag{2.20}$$

so, the local angle of attack at each section of blade is determined by

$$\alpha = \phi - \theta \tag{2.21}$$

since θ is constant at each section of the blade. On a horizontal axis wind turbine, the free vortices due to the rotating blades create a vortex sheet aligned in a helical path behind the rotor. The strong tip vortices are located at the edge of the rotor wake and the root vortices are located along the axis of the rotor as fig.(2.17). The vortex system induces an axial velocity

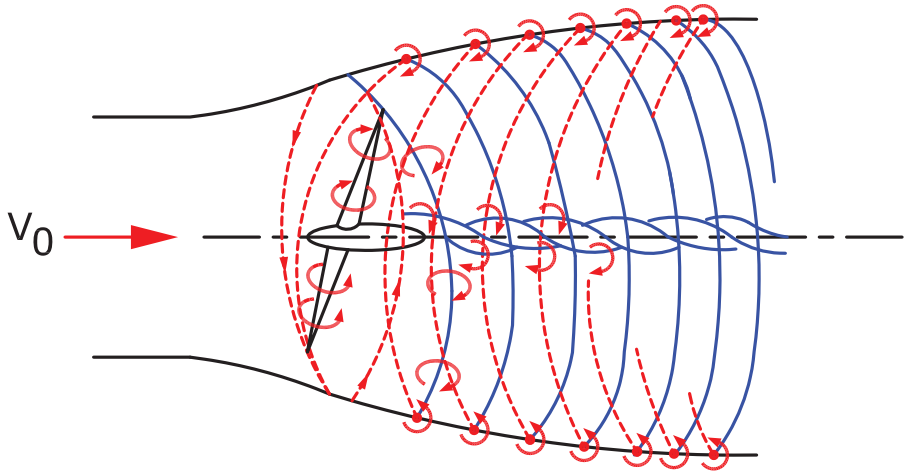

Figure 2.17: Schematic of the vortex system behind the rotor of a wind turbine

component opposite to the direction of the wind and a tangential velocity component opposite to the rotation of the wind turbine's rotor blades. The induced velocity in the axial direction is estimated by the axial induction factor a as aV_0, where V_0 is the free stream. The induced tangential velocity due to the rotor wake is estimated by the tangential induction factor a' as $2a'\Omega r$. Note that the induced tangential velocity is opposite to the tangential velocity of the rotor blade. Since the upstream flow of the rotor does not rotate, the tangential induced velocity in the rotor plane is approximately $a'\Omega r$ (an average of upstream and downstream value), where Ω denotes the angular velocity of the rotor and r is the radial distance from the rotational axis.

If a and a' are known, a 2-D equivalent angle of attack could be found from eqs.(2.20) and (2.21), where

$$V_a = (1 - a)V_0 \tag{2.22}$$

$$V_{rot} = (1 + a')\Omega r \tag{2.23}$$

Moreover, if the lift $C_L(\alpha)$ and drag $C_D(\alpha)$ coefficients are known for the airfoils used along the blades, it is easy to compute the force distribution. By integrating this distribution along the span, the global loads such as the shaft power output and the root bending moments of the blades are found. It is the purpose of the Blade Element Momentum (BEM) method to compute the induction factors a and a' as well as the loads on a wind turbine.

2.6.1 Axial Momentum Theory

The application of a wind turbine is to extract mechanical energy from the kinetic energy of the wind. In this section, we try to find a simple 1-D model for an ideal rotor [5]. In this model, the rotor is simulated as an ideal actuator disk so that it is frictionless and without any rotational velocity component in the wake. In our assumption, the rotor disc acts as a drag device (sudden pressure reduction in the rotor plane) which reduces the wind speed from V_0 far upstream of the rotor to u at the rotor plane and u_1 in the wake. Thus, we see the divergence streamlines as fig.(2.18).

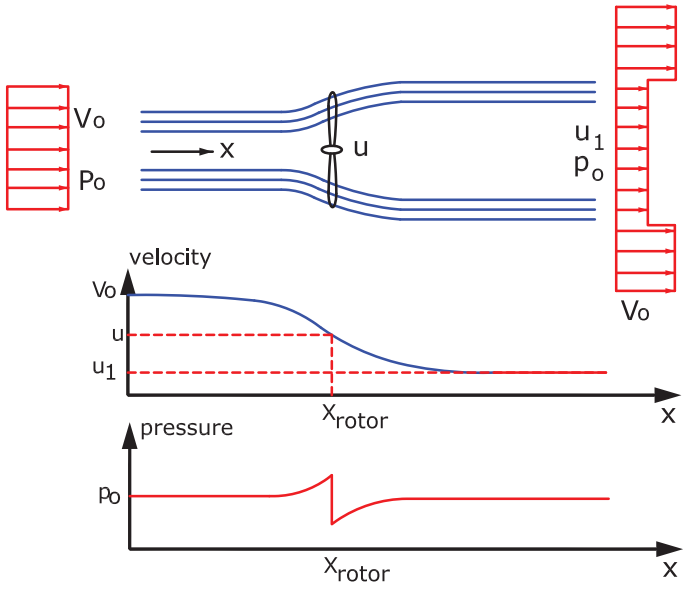

Figure 2.18: Streamline around the rotor blade and the axial velocity and pressure upstream and downstream of the rotor

The drag force can be calculated by the pressure drop over the rotor. As can be seen, there is a small pressure rise from the atmospheric level p_0 to p close upstream of the rotor blade before a discontinuous pressure drop Δp over the rotor. Downstream of the rotor, the pressure has continuously regained its original value p_0. The Mach number is small and since the flow is incompressible, so the density is constant and as a result, the axial velocity must decrease continuously from V_0 to u as fig.(2.18). By using the ideal rotor assumption, it is convenient to derive some relationship between the velocities V_0, u, u_1, thrust T and the shaft power P. By definition, the thrust is the force in the streamwise direction obtained from the pressure drop over the rotor and it is the reason for the wind speed reduction from V_0 to u_1. So, we can write

$$T = \Delta p A \tag{2.24}$$

where $A = \pi R^2$ is the rotor area. Since our flow is stationary, incompressible and frictionless and there is no external force on the fluid (both upstream and downstream), we can use the Bernoulli equation from far upstream to just in front of the rotor and from just behind the rotor to far downstream in the wake as

$$p_0 + \frac{1}{2}\rho V_0^2 = p + \frac{1}{2}\rho u^2 \tag{2.25}$$

$$p - \Delta p + \frac{1}{2}\rho u^2 = p_0 + \frac{1}{2}\rho u_1^2 \tag{2.26}$$

by combination of the eqs.(2.25) and (2.26)

$$\Delta p = \frac{1}{2}\rho(V_0^2 - u_1^2) \tag{2.27}$$

Now, we can apply the axial momentum equation integral form on the circular control volume as shown in fig.(2.19). The general form of the momentum equation is

$$\frac{\partial}{\partial t}\iiint_{cv} \rho \mathbf{V} dv + \iint_{cs} (\rho \mathbf{V}.d\mathbf{A})\mathbf{V} = -\iint_{cs} p d\mathbf{A} + \iiint_{cv} \rho \mathbf{f} dv + \mathbf{F}_{viscous} \tag{2.28}$$

for our case, we get

$$\frac{\partial}{\partial t}\iiint_{cv} \rho u(x,y,z) dv + \iint_{cs} (\rho \mathbf{V}.d\mathbf{A}) u(x,y,z) = -T \tag{2.29}$$

by applying the assumptions of an ideal rotor, eq.(2.29) gives

$$\rho u_1^2 A_1 + \rho V_0^2 (A_{cv} - A_1) + \dot{m}_{side} V_0 - \rho V_0^2 A_{cv} = -T \tag{2.30}$$

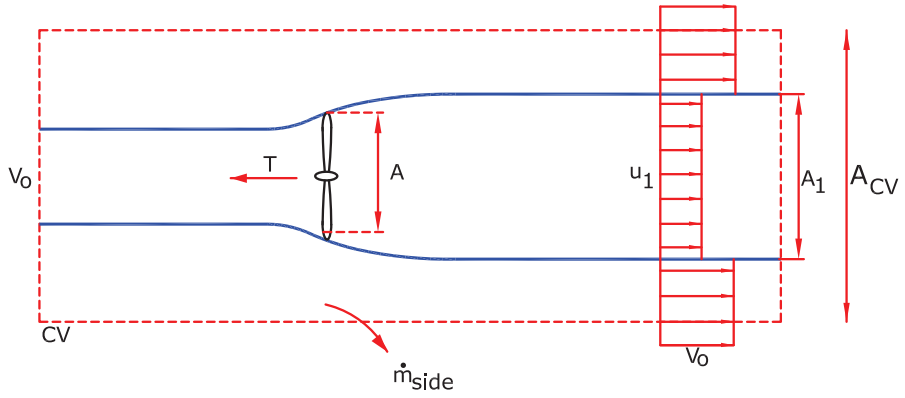

Figure 2.19: Circular control volume around the wind turbine

from the mass conservation we have

$$\dot{m}_{side} = \rho A_1 (V_0 - u_1) \tag{2.31}$$

and by applying mass conservation between A and A_1, we get

$$\dot{m} = \rho u A = \rho u_1 A_1 \tag{2.32}$$

Combining eqs.(2.30), (2.31) and (2.32) gives

$$T = \rho u A (V_0 - u_1) = \dot{m}(V_0 - u_1) \tag{2.33}$$

Replacing the thrust by the pressure drop over the rotor as eq.(2.24) and using the pressure drop from eq.(2.27) yields

$$u = \frac{1}{2}(V_0 + u_1) \tag{2.34}$$

It is seen that the velocity in the rotor plane is the arithmetic mean of the wind speed V_0 and the velocity in the wake u_1.[2] We assumed that the flow is frictionless. So, by applying the integral energy equation on the previous circular control volume, we can get the shaft power P.

$$P = \dot{m}(\frac{1}{2}V_0^2 + \frac{p_0}{\rho} - \frac{1}{2}u_1^2 - \frac{p_0}{\rho}) \tag{2.35}$$

[2]In general, this is not true when rotation occurs in the slipstream.

since $\dot{m} = \rho u A$, then we get

$$P = \frac{1}{2}\rho u A \left(V_0^2 - u_1^2\right) \tag{2.36}$$

As we discuss later, the axial induction factor a is defined as

$$a = \frac{V_0 - u}{V_o} \tag{2.37}$$

so, we get

$$u = (1 - a)V_0 \tag{2.38}$$

Combining eq.(2.34) with eq.(2.38) yields

$$u_1 = (1 - 2a)V_0 \tag{2.39}$$

and by substituting eq.(2.39) into eqs.(2.36) and (2.33), we get

$$P = 2\rho V_0^3 a(1 - a)^2 A \tag{2.40}$$

$$T = 2\rho V_0^2 a(1 - a)A \tag{2.41}$$

The available power by the rotor is

$$P_{available} = \frac{1}{2}\dot{m}V_0^2 = \frac{1}{2}\rho A V_0^3 \tag{2.42}$$

The power coefficient C_P and the thrust coefficient C_T are defined as

$$C_P = \frac{P}{\frac{1}{2}\rho A V_0^3} \tag{2.43}$$

$$C_T = \frac{P}{\frac{1}{2}\rho A V_0^2} \tag{2.44}$$

Applying the eqs.(2.40) and (2.41) for the power and thrust equations give

$$C_P = 4a(1 - a)^2 \tag{2.45}$$

$$C_T = 4a(1 - a) \tag{2.46}$$

To obtain the maximum value of C_P, differentiating gives

$$\frac{dC_P}{da} = 4(1 - a)(1 - 3a) \tag{2.47}$$

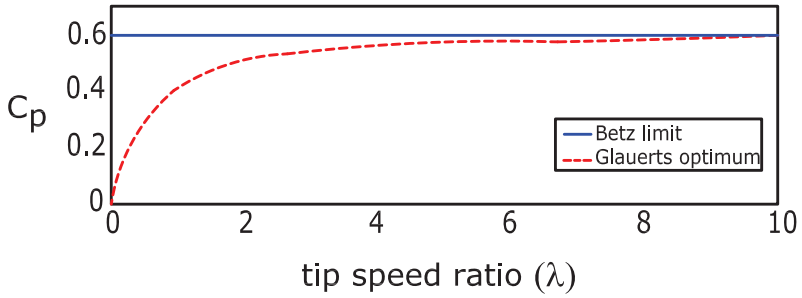

Figure 2.20: Power coefficient vs. Tip speed ratio (Betz limit vs. Glauert optimum)

We can see that for $a = 1/3$ the theoretical power coefficient for ideal wind turbine has its maximum value as $C_{P,max} = 16/27$ which is known as Betz limit.

When the rotation of the wake is not included, C_P is constant for all tip speed ratios due to the Betz limit ($C_{P,max} = 16/27$). By considering the wake rotation, the value of the power decreases as the tip speed ratio decreases due to the Glauert optimum. The thrust coefficient C_T has a maximum value of 1 at $a = 0.5$. There is a problem for values of $a \geq 0.5$ because of the wake velocity where it becomes zero or even negative (see eq. 2.39). So, the momentum theory is not applicable in this condition and an empirical correction has to be made. The eqs.(2.45) and (2.46) are shown in fig.(2.21). We must also note that experiments prove that the assumption of an ideal wind turbine resulting in eq.(2.44) are applicable for an axial induction factor a of less than approximately 0.4 [5]. If the momentum theory was valid for higher values of a, the velocity in the wake become negative (see eq.(2.39)). In a wind turbine, at low wind speeds, we have a high thrust coefficient C_T and thus a high axial induction factor a. The reason that the simple momentum theory is not valid for values of a greater than approximately 0.4, is that the free shear layer at the edge of the wake becomes unstable when the velocity jump $(V_0 - u_1)$ becomes too large and eddies transporting momentum from the outer flow into the wake are created. This phenomena is called turbulent wake state. Also, the higher values of axial induction factor give a negative wake velocity according to eq.(2.38).

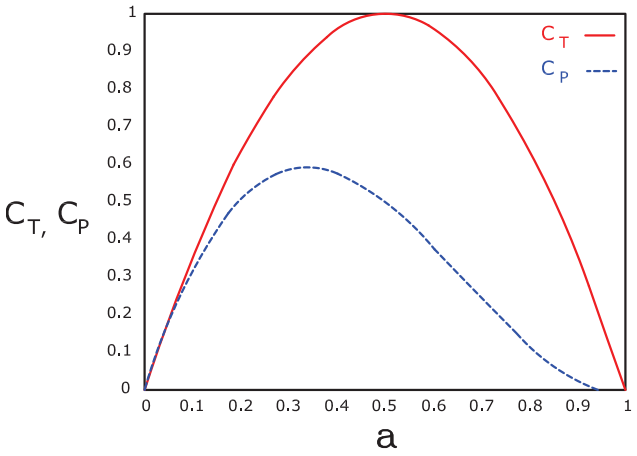

Figure 2.21: Variation of C_P and C_T with axial induction factor for an ideal HAWT.

2.6.2 General Momentum Theory

The blade element theory assumes that each blade element operates independently of all the other elements [8]. It is obvious that this theory cannot give more than a rough approximation. The dominant part of the energy loss occurs in the operation of a rotor blade even if it operates in a perfect fluid. The momentum theory assumes that the air to be a perfect fluid. On the other hand, the momentum theory does not try to solve the complete rotor blade problem and must be modified for practical issues. The general momentum theory replaces rotor blade by an ideal mechanism, the so-called actuator disk. The action that this disk is supposed to exert on the fluid represents the main features of the action exerted by the rotor blade. Since the axial velocity of the air is decreased by the rotor blade, this body of revolution must have a larger diameter downstream compared to upstream. In the case of an actual rotor blade rotating with the angular velocity, the flow is not strictly steady but it is quasi-steady, even periodic with mn periods per second where m is the number of blades and n is the number of revolution as $\Omega = 2\pi n$. But, the idealized flow pattern in the momentum theory is supposed to be strictly steady, at least outside an infinitesimal region surrounding the actuator disk. In a strictly steady continuous flow no exchange of power between the perfect fluid and a rigid body immersed in it is possible. To account for the energy exchange occurring in the case of a rotor blade, the momentum theory needs another assumption. The regions upstream and downstream of the rotor blade are supposed to be separated

by an infinitesimal region in which sudden changes of pressure and velocity occur. That is, the flow between the boundaries is assumed to be continuous except in the immediate neighborhood of the actuator disk where the following discontinuities are accepted:

- The pressure has different values on the two sides of this disk (p on the upstream side and $p - \Delta p$ downstream). The integral extended over the disk area represents the rotor blade thrust T.
- The fluid particles passing through the disk region can here suddenly change their tangential velocity component to the circular paths due to the rotating rotor blade.

The assumption of a steady (not periodic) motion outside the disk region will be justified the larger the number of blades, since the number of periods per second increases with m. This is why the theory of the actuator disk is often referred to as the theory of a rotor blade with an infinite number of blades.

In the previous section, the axial momentum theory was based on the assumption of the no rotational motion in the slipstream and therefore, the rotor blade was replaced by an actuator disc. In general, the slipstream will have a rotational motion given to it by the reaction of the torque of the rotor blade and its rotational motion denotes a more energy loss. So, we must extend the previous theory to involve the effects of the rotational motion. To do this, another assumption must be made so that the actuator disc can also give a rotational component to the fluid velocity while the axial and radial components remain unaltered.

Let r be the radial distance of any annular element of the rotor blade and let u and v be the axial and radial components of the fluid velocity respectively. Let p be the pressure immediately in front of the rotor blade and Δp be the decrease of the pressure behind the rotor blade, associated with an angular velocity ω. In the final wake, let p_1 be the pressure, u_1 the axial velocity and ω_1 the angular velocity at a radial distance r_1 from the axis of the slipstream. The continuity equation for the annular element of flow gives

$$u_1 r_1 dr_1 = u r dr \tag{2.48}$$

since the angular momentum of the fluid moving down the slipstream is constant, we get

$$\omega_1 r_1^2 = \omega r^2 \tag{2.49}$$

Furthermore, the element of torque of the rotor blade is equal to the angular momentum given in unit time to the corresponding annular element of the

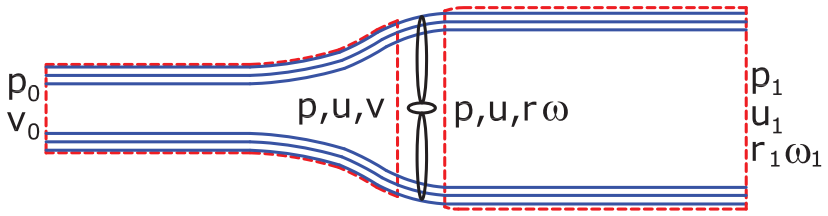

Figure 2.22: control volume around the wind turbine

slipstream. So, it gives

$$dM = \rho u \omega r^2 dA \tag{2.50}$$

Using the Bernoulli equation to the flow upstream and downstream the rotor blade yields

$$H_0 = p_0 + \frac{1}{2}\rho V_0^2 = p + \frac{1}{2}\rho(u^2 + v^2) \tag{2.51}$$

$$H_1 = p - \Delta p + \frac{1}{2}\rho(u^2 + v^2 + \omega^2 r^2) = p_1 + \frac{1}{2}\rho(u_1^2 + \omega_1^2 r^2) \tag{2.52}$$

so,

$$\Delta H = H_1 - H_0 = -\Delta p + \frac{1}{2}\rho\omega^2 r^2 \tag{2.53}$$

Also, the total pressure head can be stated as

$$p_0 - p_1 = \frac{1}{2}\rho(u_1^2 - V_0^2) + \frac{1}{2}\rho\omega_1^2 r_1^2 - (H_1 - H_0) \tag{2.54}$$

or

$$p_0 - p_1 = \frac{1}{2}\rho(u_1^2 - V_0^2) + \frac{1}{2}\rho(\omega_1^2 r_1^2 - \omega^2 r^2) + \Delta p \tag{2.55}$$

In general, the pressure p_1 in the slipstream is more than the external pressure p_0 owing to the rotation of the slipstream about its axis. Applying the Bernoulli equation to the flow relative to the rotor blades rotating with the angular velocity Ω, the relative angular velocity increases from Ω to $\Omega + \omega$ and hence the decrease of pressure is

$$\Delta p = \frac{1}{2}\rho[(\Omega + \omega)^2 - \Omega^2]r^2 = \rho(\Omega + \frac{1}{2}\omega)\omega r^2 \tag{2.56}$$

Finally, by combination of the eq.(2.49), (2.54) and (2.56), we get the pressure drop in the wake.

$$p_0 - p_1 = \frac{1}{2}\rho(u_1^2 - V_0^2) + \frac{1}{2}\rho(r_1^2\omega_1^2 - r^2\omega^2) + \Delta p \tag{2.57}$$

$$p_0 - p_1 = \frac{1}{2}\rho(u_1^2 - V_0^2) + \rho\omega_1^2 r_1^2(\Omega + \frac{1}{2}\omega) \tag{2.58}$$

To solve the above equations, we need some assumptions. In general, the angular velocity ω given to the slipstream is very small compared with the angular velocity Ω of the rotor blade, so the terms including ω^2 are negligible. Another assumption is that the pressure in the wake p_1 is equal to the far upstream pressure p_0 of the fluid and the pressure drop Δp across the rotor blade is equal to the total pressure head reduction $(H_1 - H_0)$. The equations related to the thrust and axial velocity are then similar to the axial momentum theory. Again, the axial velocity at the rotor plane is considered as the arithmetic mean of the axial velocity V_0 and slipstream velocity u_1. Thus, by applying the equations of axial momentum in the differential form at an arbitrary cut of the rotor plane, we get

$$dT = 2\rho u(u - V_0)dA = 4\pi\rho V^2(1 - a)ardr \tag{2.59}$$

alternatively,

$$dT = \Delta p dA = 2\pi\rho(\Omega + \frac{1}{2}\omega)\omega r^3 dr \tag{2.60}$$

By introducing $\omega = 2a'\Omega$, then we get

$$dT = 4\pi\rho\Omega^2(1 + a')a'r^3dr \tag{2.61}$$

The relation between axial and rotational induced factors a and a' is obtained by comparing the eq.(2.59), (2.60), so,

$$V_0^2(1 - a) = \Omega^2 r^2(1 + a')a' \tag{2.62}$$

At the end, the torque element regarding the eq.(2.50) is

$$dM = \rho u\omega r^2 dA = 4\pi\rho V_0\Omega(1 - a)a'r^3dr \tag{2.63}$$

As we know, $dP = \omega dM$, so the total power is obtained by integrating dP from 0 to R as

$$P = 4\pi\rho\Omega^2 V_0 \int_0^R a'(1 - a)r^3 dr \tag{2.64}$$

By introducing $\lambda = \dfrac{\Omega R}{V_0}$ as the tip speed ratio [3] and $x = \dfrac{\Omega r}{V_0}$ as the local rotational speed at radius r, we get from eq.(2.62) that

$$x^2(1 + a')a' = (1 - a)a \tag{2.65}$$

If the local angles of attack are below stall, then a and a' are not independent because the reacting force according to potential flow theory is perpendicular to the local velocity seen by the blade according to the Kutta-Jukowski theorem. The total induced velocity W must be in the direction of the force and thus perpendicular to the local velocity.

2.6.3 The Vortex System of a Rotor Blade

According to the airfoil theory, the lift force L per unit length of an airfoil section in 2-D motion is related to the circulation Γ around its contour by the Kutta-Jukowski theorem as $L = \rho V_0 \Gamma$. By defining the chord length of the airfoil section as c , the lift force can be stated as below related to the lift coefficient C_L,

$$L = \frac{1}{2}\rho C_L V_0^2 c \tag{2.66}$$

so, we get from the Kutta-Jukowski theorem

$$\Gamma = \frac{1}{2} C_L V_0 c \tag{2.67}$$

It is obvious that there must be a circulation of the flow around the rotor blade to produce the aerodynamic force experienced by the blades. In general, the circulation Γ around the blade element will vary along the blade, but for simplification, we assume that the circulation is constant along the blade although it is not possible physically. Also, we can describe the existence of this circulation in different way, so that there is a vortex line of strength Γ bound to the blade and running along it from root to the tip. According to the Helmholtz's theorem, a vortex line cannot begin or end suddenly; unless it develops closed curve around the body and to be continued as a free vortex line in the fluid. Thus, it follows that the general motion of the fluid is a trailing vortex behind the body.[4] The free vortex springing from the root of the rotor blade will be a straight line along the axis of the rotor and its strength will be $B\Gamma$ for a rotor with B blades. The tip vortices, each

[3] The tip speed ratio imposes the operating condition of a wind turbine and has a direct effect on the induction factors a and a'.

[4] In reality, the trailing vortices are dissipated by viscosity far behind the rotor.

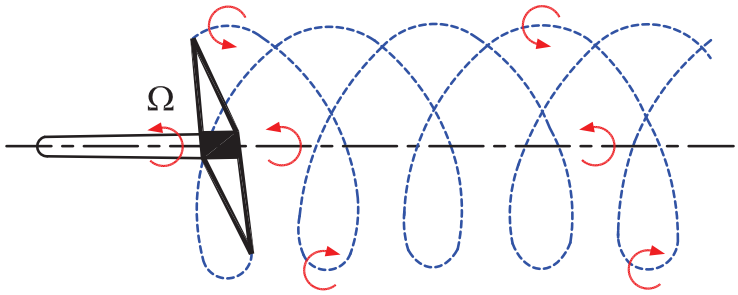

Figure 2.23: The schematic of the system of trailing vortices of a rotor blade

of strength Γ, will be of helical shape and will trace out roughly the paths described by the tips of the rotor blades. The rotation of the axial vortex is the same as that of the rotor whereas the rotation of the tip vortices is of the opposite direction. These vortex lines constitute the slipstream of the rotor and the motion of the fluid in the slipstream can be calculated as the induced velocity of this vortex system. Due to the variation of circulation along the blade, trailing vortices will arise not only at the root and tip of the blade, but also from each point of its trailing edge. So, the increase of circulation between the two points of the blade is equal to the strength of the helical vortex springing from this element but with opposite sign. The disturbance of the flow by a rotor can be considered as the induced velocity of the complete vortex system, including the bound vortices of the rotor blades and the free vortex sheets of the slipstream. Finally, by considering the induced velocity of the system of free vortices springing from the airfoil, the behaviour of an element of an airfoil is the same as in 2-D motion based on the theory of airfoils of finite span developed by Prandtl.

2.6.4 The Induced Angular Velocity

The force on the blades not only has a component in the flow direction, but also it must have a tangential component due to the shaft torque [8]. The reaction of the shaft torque must be transmitted with opposite sign to the wind as a change of angular velocity. As a result, the streamlines in the wake follow a helical path from the superposition of the streamwise and rotational velocities (see fig.(2.24)).

The transfer of rotational motion takes place entirely across the thickness

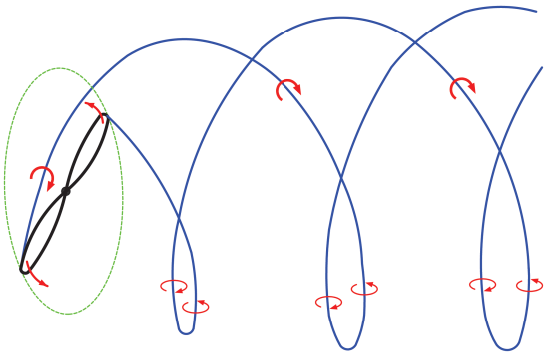

Figure 2.24: Helical wake of a HAWT

of the disk. The change in angular velocity is expressed in terms of a angular flow induction factor a'. Upstream the disk, the angular velocity is zero and the induced angular velocity at the rotor plane is equal to the $a'\Omega r$ (an average of upstream and downstream value) where r is a radial distance from the axis of rotation. Downstream of the disk, the tangential velocity is $2a'\Omega r$. Since the induced tangential velocity is produced in reaction to the torque, it is in opposite direction of the blade motion. Now, we can complete the velocity triangle as fig.(2.25).

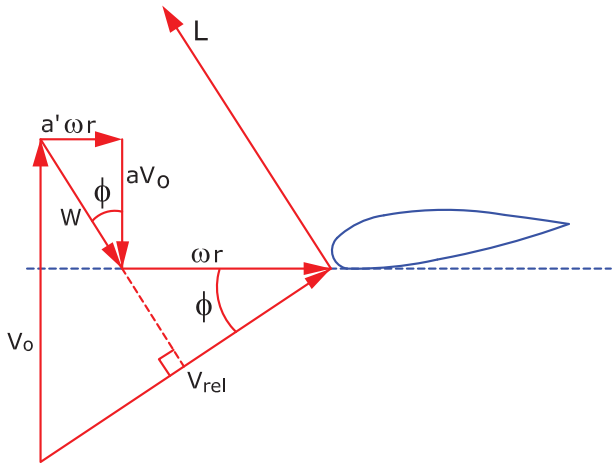

Figure 2.25: Velocity triangle for a section of the blade

Chapter 3

The Blade Element Momentum (BEM) Method

The Blade Element Momentum method combines the Blade Element Theory and the Momentum Theory[1]. In this method, we assume that aerodynamic forces acting on a blade element can be estimated as the force on a airfoil of the same cross-section, advancing through the air with the uniform velocity V_{rel} at the angle of attack α and that the force on the whole blade can be derived by adding the contributions of all the elements along the blade. Also, there is no induction between consecutive blade elements except in so far as such induction modifies the characteristics of the same airfoil section. In the Blade Element Theory, we also consider some assumptions related to the blade behaviour. These are:

1. The operation of an element is not affected by the adjacent elements of the same blade.

2. The effective velocity of the element through the air is the vector resultant of the axial velocity V_0 and the rotational velocity Ωr.

3. The airfoil characteristics is used for the blade elements.

4. The force from the blades acting on the flow is constant at each annular element. This stands for the rotor with an infinite number of blades.[2]

According to the Blade Element Momentum (BEM) method, the steady loads, thrust and power can be calculated for different operation conditions

[1]Most part of this chapter has been extracted from [5].

[2]The Prandtl's tip loss factor is applied to modify this assumption for a rotor with a finite number of blades.

of wind speed, rotational speed and pitch angle. For unsteady purposes to calculate time series of the loads, some engineering models must be implemented. As mentioned above, the BEM method joins the momentum theory with the local conditions at the actual blades and dividing the stream tube into N annular elements of height dr as shown in fig.(3.1). Therefore, the lateral boundary of these elements consists of streamlines and thus there is no flow across the elements.[3] From the ideal rotor, we obtained the required

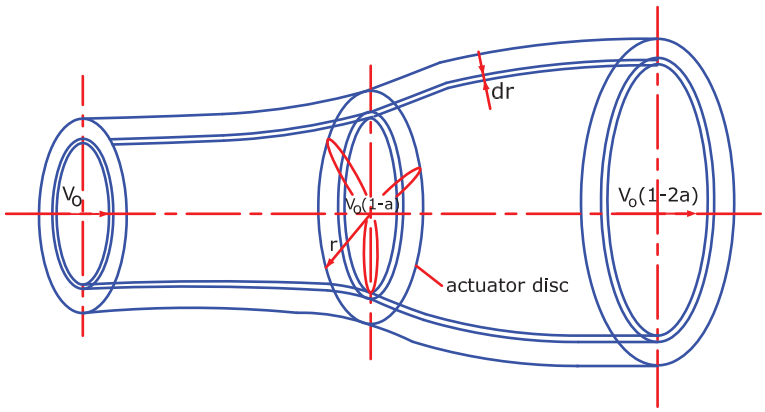

Figure 3.1: Annular control volume

equations (eq.2.59 and 2.63) for the thrust and torque in previous sections.

$$dT = 4\pi\rho V_0^2 a\,(1-a)\,r dr \tag{3.1}$$

$$dM = 4\pi\rho V_0 \Omega\,(1-a)\,a' r^3 dr \tag{3.2}$$

It is obvious that the relative velocity V_{rel} seen by a section of the blade is a combination of the axial velocity $V_0\,(1-a)$ and the angular velocity $(1+a')\,\Omega r$ at the rotor plane as fig.(3.2). By definition, θ is the local pitch of the blade (the angle between the chord line and the plane of rotation). It consists of the pitch angle[4] θ_p (the angle between the tip chord and the rotor plane) and the twist of the blade β which is measured relative to the tip chord. Hence, $\theta = \theta_p + \beta$. Also, ϕ is the angle between the plane of

[3]The only difference between the actuator annulus and the actuator disk is that the pressure on the surfaces of a thin-walled tube is not uniform. This may give rise to an axial force on the tube since it is not cylindrical.

[4]The pitch angle is the angle at which the blade surface contacts the wind. It is often variable to ensure optimum operation of the turbine in varying wind conditions and to prevent electrical overload and over speed in high winds. Gears in the hub of the rotor allow the pitch to be varied.

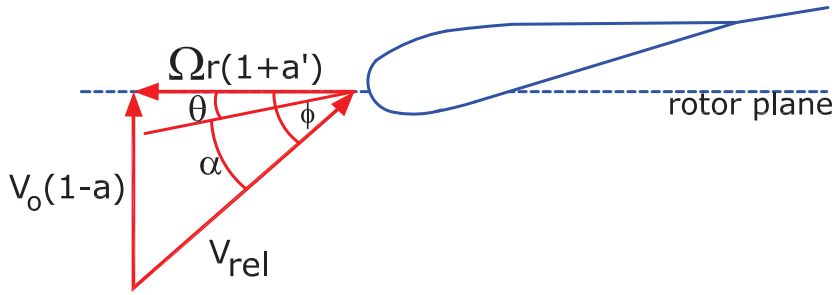

Figure 3.2: Velocities at the rotor plane

rotation and the relative velocity V_{rel}. According to fig.(3.2), the local angle of attack α is defined as

$$\alpha = \phi - \theta \tag{3.3}$$

Moreover, it is found that

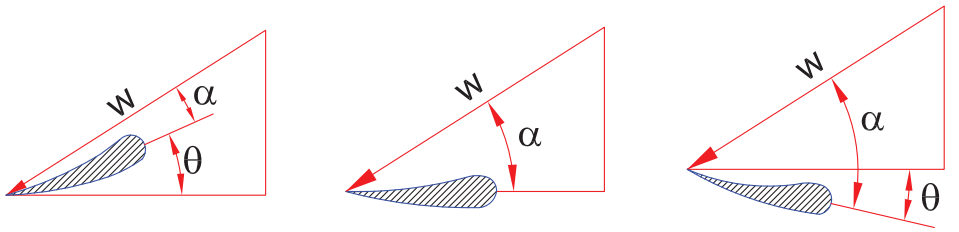

(a) positive pitch angle (b) zero pitch angle (c) negative pitch angle

Figure 3.3: Flow and blade angles of a blade element

$$\tan\phi = \frac{(1-a)\,V_0}{(1+a')\,\Omega r} \tag{3.4}$$

In addition, by knowing the lift coefficient C_L , drag coefficient C_D and the chord length c of each airfoil, the lift L and drag D forces per length can be computed as

$$L = \frac{1}{2}\rho C_L V_{rel}^2 c \tag{3.5}$$

$$D = \frac{1}{2}\rho C_D V_{rel}^2 c \tag{3.6}$$

By definition, the lift and drag forces are perpendicular and parallel to the velocity seen by the rotor respectively. In order to calculate the forces which are normal and tangential to the rotor plane, we must decompose the above lift and drag forces into these directions as fig.(3.4). Therefore, we get

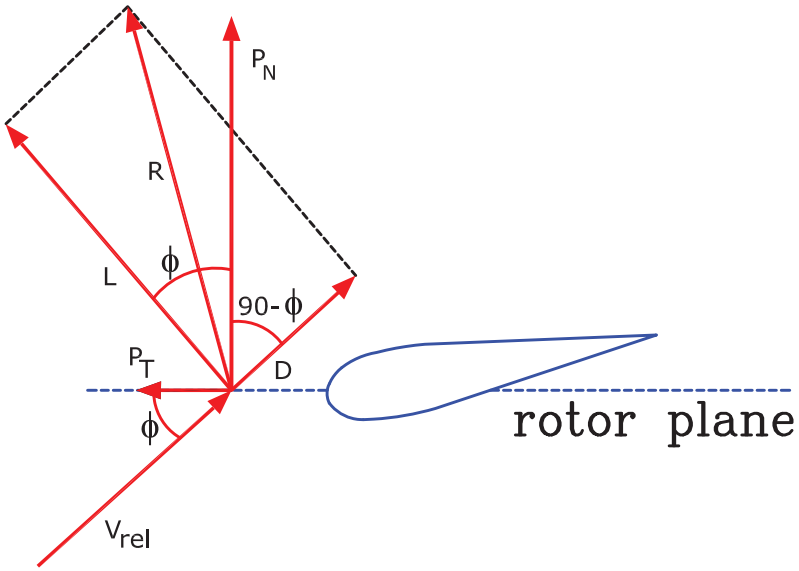

Figure 3.4: Decomposition of the lift L and drag D forces into the rotor plane

$$P_N = L\cos\phi + D\sin\phi \tag{3.7}$$

$$P_T = L\sin\phi - D\cos\phi \tag{3.8}$$

By normalizing the eqs.(3.7) and (3.8) with $\frac{1}{2}\rho V_{rel}^2 c$, we get

$$C_n = C_L\cos\phi + C_D\sin\phi \tag{3.9}$$

$$C_t = C_L\sin\phi - C_D\cos\phi \tag{3.10}$$

where

$$C_n = \frac{P_N}{\frac{1}{2}\rho V_{rel}^2 c} \tag{3.11}$$

$$C_t = \frac{P_T}{\frac{1}{2}\rho V_{rel}^2 c} \tag{3.12}$$

From fig.(3.2), it can be seen that

$$V_{rel} \sin\phi = V_0 (1 - a) \tag{3.13}$$

$$V_{rel} \cos\phi = \Omega r (1 + a') \tag{3.14}$$

Now, we define the solidity as the portion of the annular area in the control volume covered by the blades as

$$\sigma(r) = \frac{c(r) NB}{2\pi r} \tag{3.15}$$

where NB, $c(r)$ and r denote the number of blades, the local chord and the radial position of the control volume, respectively. Since P_N and P_T are forces per unit length, the normal force and the torque on the control volume of thickness dr are

$$dT = NBP_N dr \tag{3.16}$$

$$dM = rNBP_T dr \tag{3.17}$$

Combination of eqs.(3.11), (3.13) and (3.16) gives

$$dT = \frac{1}{2}\rho c NB \frac{V_0^2 (1 - a)^2}{\sin^2\phi} C_n dr \tag{3.18}$$

Similarly, combination of eqs.(3.12), (3.13), (3.14) and (3.17) yields

$$dM = \frac{1}{2}\rho c NB \frac{V_0 (1 - a) \Omega r (1 + a')}{\sin\phi \cos\phi} C_t r dr \tag{3.19}$$

Finally, if eqs.(3.18) and (3.1) for dT are equalized and eq.(3.15) is applied, then the axial induction factor is obtained as

$$a = \frac{1}{\frac{4\sin^2\phi}{\sigma C_n} + 1} \tag{3.20}$$

If eqs.(3.19) and (3.2) for dM are equalized, the angular induction factor is obtained as

$$a' = \frac{1}{\frac{4\sin\phi\cos\phi}{\sigma C_t} - 1} \tag{3.21}$$

Now, we have all required equations in BEM model. As we assumed that there is no radial dependency for different control volumes in BEM method, so each section can be evaluated separately. The BEM model algorithm includes the following steps:

1. Initialize a and a'; generally $a = a' = 0$.
2. Calculate the flow angle ϕ using eq.(3.4)
3. Calculate the local angle of attack using eq.(3.3)
4. Read $C_L(\alpha)$ and $C_D(\alpha)$ from the table.
5. Calculate C_n and C_t from eqs.(3.9) and (3.10)
6. Calculate a and a' from eqs.(3.20) and (3.21)
7. If a and a' has changed more than a certain tolerance, go to step (2) otherwise finish.
8. Calculate the local loads on the portion of the blades.

The above steps are shown in fig.(3.5). Because of the assumption which was made at the BEM model, here we need two corrections to the above algorithm. The first one corrects the assumption of the infinite number of blades and the second one is an empirical relation between the thrust coefficient C_T and an axial induction factor a when it becomes greater than approximately 0.4. The corrections are:

1. Prandtl's Tip Loss Factor

   Prandtl's tip loss factor adjusts the assumption of an infinite number of blades. So, instead of using eqs.(3.20) and (3.21), the following relations are used for a and a'

$$a = \frac{1}{\frac{4F\sin^2\phi}{\sigma C_n} + 1} \tag{3.22}$$

$$a' = \frac{1}{\frac{4F\sin\phi\cos\phi}{\sigma C_n} - 1} \tag{3.23}$$

   where F and f (Glauert Correction) are defined as

$$F = \frac{2}{\pi}\cos^{-1}\left(\exp\left(-f\right)\right) \tag{3.24}$$

$$f = \frac{NB}{2}\frac{R-r}{r\sin\phi} \tag{3.25}$$

   Recall that NB, R, r and ϕ are defined as the number of blades, rotor radius, local radial position and flow angle, respectively.

2. Glauert Correction

The simple momentum theory is valid only for small values of axial induction factor and it is not valid for values larger than approximately 0.4. In this condition, empirical relations between the thrust coefficient C_T and a would be performed to meet the experiments. The relation is given by [5]

$$C_T = \begin{cases} 4a\left(1-a\right)F & \text{if } a < a_c \\ 4\left(a_c^2 + \left(1-2a_c\right)a\right)F & \text{if } a > a_c \end{cases} \tag{3.26}$$

where $a_c = 0.2$ and F is Prandtl's tip loss factor. So instead of eqs.(3.22) and (3.23), for $a < a_c$

$$a = \frac{1}{\dfrac{4F\sin^2\phi}{\sigma C_n} + 1} \tag{3.27}$$

otherwise

$$a = \frac{1}{2}[2 + K\left(1-2a_c\right) - \sqrt{\left(K\left(1-2a_c\right)+2\right)^2 + 4\left(Ka_c^2 - 1\right)}] \tag{3.28}$$

where

$$K = \frac{4F\sin^2\phi}{\sigma C_n} \tag{3.29}$$

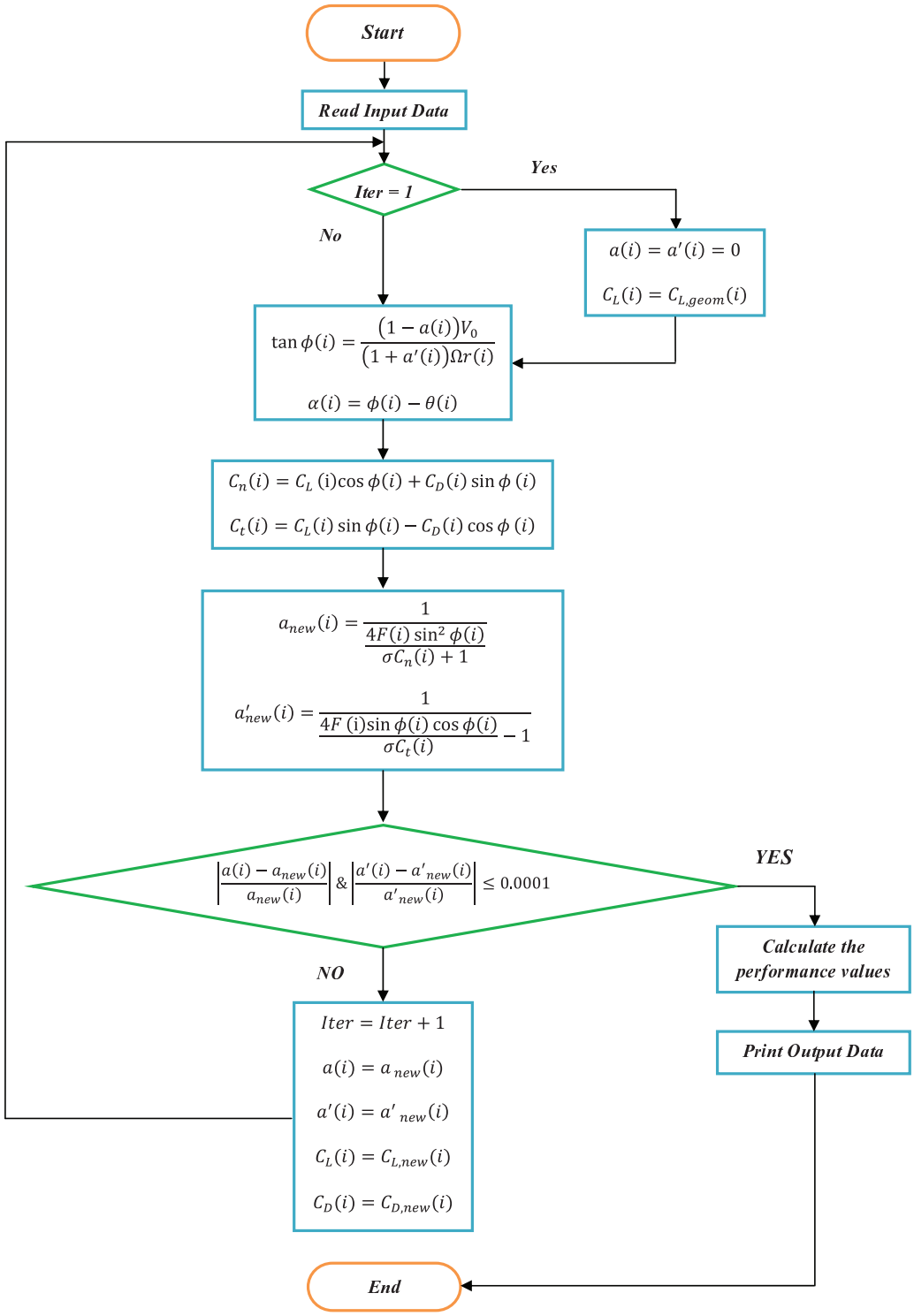

Figure 3.5: Flow chart for the numerical procedure

Chapter 4

Helical Vortex Method (Influence Coefficient Method)

4.1 Introduction

In this chapter, the Helical Vortex Method (Influence Coefficient Method) is introduced for analysis of wind turbine aerodynamic performance [9]. In this method, the turbine blade is modeled as a lifting line where the trailing vortices are shed along the blade span. It should be noted that this model is based on the prescribed wake model which means that the geometry of the wake is known as a helix. For evaluation of aerodynamic performance, the Biot-Savart law and Kutta-Jukowski theorem have been used. Therefore, the induced velocity and circulation can be calculated at the blade section.

The rotor blade is replaced by a lifting line with the bound circulation varying along its span. Then, the blade is divided into a number of segments. Each segment is presented by a helical horseshoe vortex. The induced velocities produced by all trailing vortices at the control point of each segment are calculated by the Biot-Savart law. Then, by using the Kutta-Jukowski theorem and 2-D sectional airfoils data (lift and drag coefficients vs. angle of attack), the aerodynamic forces acting on the blade are calculated. Recall that the air flow is modeled as inviscid-incompressible flow.

Also, in this model the local pitch of each trailing vortex leaving the blade has been taken into account. This means that the rotor blade does not create a uniform helical vortex surface with constant pitch in the radial, axial and tangential directions. It is assumed that for helical motion of the trailing vortices, the helix pitch angle is calculated by induced velocity at the point where this helical vortex is emanated. Finally, the dependency of the wake model to the induced velocity at each radial position causes a non-linearity

in the equation system, so an iterative method must be used.

4.2 Assumptions

Like every model, there are some assumptions to be made:

1. The flow streamline is steady and parallel to the rotating axis of wind turbine.
2. The blade is presented by a lifting line located at a quarter chord behind the leading edge with a varying circulation distribution along its span.
3. The 2-D flow conditions is considered for each blade segment while the influence of induced rotational and axial velocities is taken into account. The induced radial velocity is not taken into account since it does not influence lift or drag.
4. The elastic effects of the blades are disregarded, so it is assumed that the blades remain straight and stand in the rotational plane.
5. Each component of the trailing vortices springing from the blade has a helical shape with constant pitch angle along the axial direction. This pitch angle is equal to the pitch angle at the point where the trailing vortices shed from. So, there is no expansion of the wake.

4.3 Rotor Geometry

The rotor of radius R has been equally divided into N segments. The aerodynamic characteristics along the blade such as chord C and local pitch angle θ are known. Similarly, the rotational speed Ω and free stream velocity V_0 are known.

According to fig.(4.1), the (x, y, z) Cartesian coordinate system builds up from the hub center. The axis system is defined as x axis through the quarter chord line of the blade and z axis indicating to the positive down-wind direction. As mentioned before, the blade is divided into N segments and the points of each segment are referred by $x_j\,(j = 1, 2, .., N + 1)$. This segmentation may be either uniform or non-uniform. As shown in fig.(4.2), each segment consists of a bound vortex of constant strength Γ_i and a control point $C_i = (x_i, 0, 0)$. From the ends of the bound vortex segment, two free vortices shed at j, $j+1$ and develop as helical vortices to infinity. As a result, the bound vortex segment and the two trailing helical vortices build a helical horseshoe vortex.

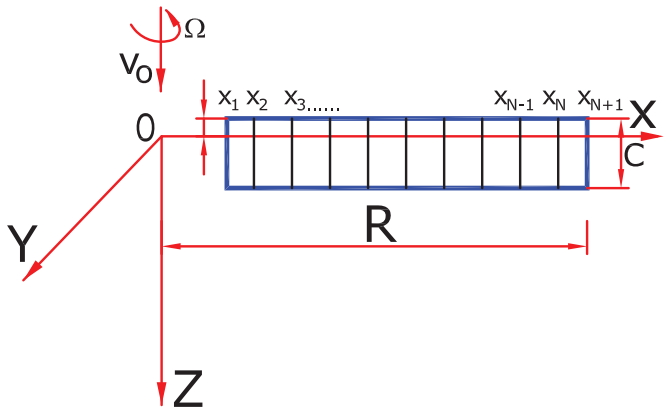

Figure 4.1: Coordinate axes and blade division

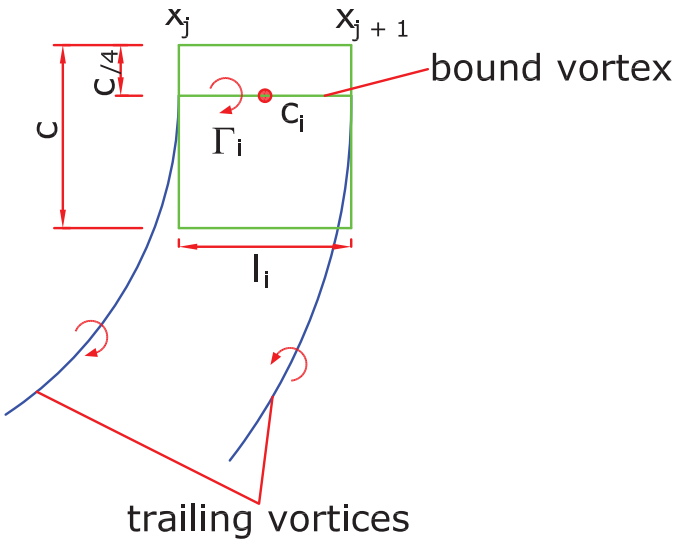

Figure 4.2: Helical horseshoe vortex for a segment of a blade

4.4 Induced Velocities

The components of induced velocity in the y and z directions are defined as v_{ij} and w_{ij} respectively at the blade, at the control point $(x_i, 0, 0)$. This induced velocity originates as a small helical vortex segment at point (x_j, y_j, z_j) on the helical trailing vortex line jumping from the point $(x_j, 0, 0)$ with circulation equal to one. Then the total normalized induced velocities induced by helical vortex lines V_{ij} and W_{ij} can be determined by applying the Biot-Savart law as

$$V_{ij} = \frac{1}{4\pi R} \int_0^\infty v_{ij} d\theta \tag{4.1}$$

$$W_{ij} = \frac{1}{4\pi R} \int_0^\infty w_{ij} d\theta \tag{4.2}$$

$$v_{ij} = \sum_{n=1}^{NB} \frac{h\left[-\eta\left(\cos\theta' + \theta\sin\theta'\right) + r\right]}{\left[h^2\theta^2 + \eta^2 + r^2 - 2r\eta\cos\theta'\right]^{\frac{3}{2}}} \tag{4.3}$$

$$w_{ij} = \sum_{n=1}^{NB} \frac{\eta^2 - r\eta\cos\theta'}{\left[h^2\theta^2 + \eta^2 + r^2 - 2r\eta\cos\theta'\right]^{\frac{3}{2}}} \tag{4.4}$$

where

$$\eta = \frac{x_j}{R}$$

$$r = \frac{x_i}{R}$$

$$\theta' = \theta + \frac{2\pi\left(n-1\right)}{NB}$$

where θ is azimuthal angle of the blade and $n = 1, ..., NB$. Also, h is defined as

$$h = \frac{V_0 - w_j}{R\left(\Omega - \left(\frac{v_j}{x_j}\right)\right)} \tag{4.5}$$

It should be noted that v_j and w_j are circumferential and axial induced velocities at the radial location of point of emanating of this vortex element. By introducing the following terms as non-dimensional parameters $\overline{\Gamma}_i = \frac{\Gamma_i}{R^2\Omega}$, $\overline{v}_i = \frac{v_i}{R\Omega}$ and $\overline{w}_i = \frac{w_i}{R\Omega}$, we find that all NB horseshoe vortices j of the

NB blades induce the non-dimensional velocities $\overline{V}_{ij}\overline{\Gamma}_{ij}$ and $\overline{W}_{ij}\overline{\Gamma}_{ij}$ at the control point x_i. The influence coefficients $\overline{V}_{ij}$ and $\overline{W}_{ij}$ are defined as

$$\overline{V}_{ij} = \frac{1}{4\pi}\int_0^\infty (v_{i,j+1} - v_{i,j})\, d\theta \tag{4.6}$$

$$\overline{W}_{ij} = \frac{1}{4\pi}\int_0^\infty (w_{i,j+1} - w_{i,j})\, d\theta \tag{4.7}$$

Then, the total induced velocities at the control point x_i will be the sum of the portions of all the horseshoe vortices.

$$\overline{v}_i = \sum_{j=1}^{NB} \overline{V}_{ij}\overline{\Gamma}_{ij} \tag{4.8}$$

$$\overline{w}_i = \sum_{j=1}^{NB} W_{ij}\overline{\Gamma}_{ij} \tag{4.9}$$

Since it has been assumed that we are dealing with the incompressible flow, so the numerical integration is done only to a limited azimuthal angle. Also, because of the symmetry, there is no any additional induction velocity along the blades by the bound vortices of the lifting lines.

4.5 Distribution of Circulation

By using the Kutta-Jukowski theorem, we can calculate the forces acting on the blade. The related equation can be written as

$$L_i = \rho W_i \Gamma_i \tag{4.10}$$

where ρ is density of air and W_i is the resultant velocity at x_i. According to fig.(4.3), it can be written that

$$\alpha_{eff} = \alpha_g - \alpha_i \tag{4.11}$$

where α_{eff}, α_g and α_i are effective, geometric and induced angles of attack respectively. The geometric and induced angle of attack are given by

$$\alpha_g\,(i) = \tan^{-1}\left(\frac{V_0}{x_i\Omega}\right) - \theta_i \tag{4.12}$$

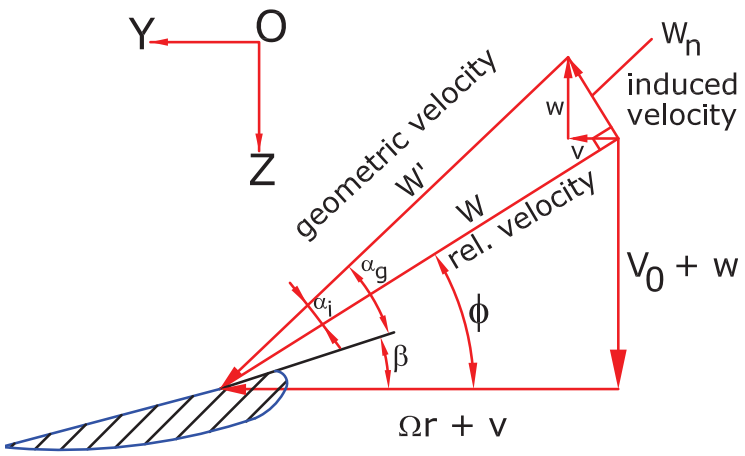

Figure 4.3: velocity component at the blade cross section

$$\alpha_i(i) = \frac{W_n(i)}{W_i} \tag{4.13}$$

where $W_n(i) = (v_i^2 + w_i^2)^{1/2}$. By using an iterative method, the circulation distribution along the blade can be computed. The above steps is shown in fig.(4.4). Then, the axial force, torque and power for each blade can be calculated by summing the axial force, torque and power elements over all of the segments. Finally, the total axial force, torque and power of the wind turbine rotor blades can be written as

$$F = \int_{x_{hub}}^{x_{tip}=R} \frac{1}{2}\rho N B c W^2 \left(C_L \cos\phi + C_D \sin\phi\right) dx \tag{4.14}$$

$$Q = \int_{x_{hub}}^{x_{tip}=R} \frac{1}{2}\rho N B c W^2 \left(C_L \sin\phi - C_D \cos\phi\right) x dx \tag{4.15}$$

$$P = \int_{x_{hub}}^{x_{tip}=R} \frac{1}{2}\rho N B c W^2 \left(C_L \sin\phi - C_D \cos\phi\right) x\Omega dx \tag{4.16}$$

where ϕ is the relative flow angle. The axial force, torque and power coefficients are defined as non-dimensional parameters as

$$C_F = \frac{F}{\frac{1}{2}\rho\pi R^2 V_0^2} \tag{4.17}$$

$$C_Q = \frac{Q}{\frac{1}{2}\rho\pi R^3 V_0^2} \tag{4.18}$$

$$C_P = \frac{P}{\frac{1}{2}\rho\pi R^2 V_0^3} \tag{4.19}$$

It should be noted that the analytical form of airfoil data have been used in the calculation of C_L and C_D as

If $\alpha < \alpha_s = 0.2rad\,(11.45^\circ)$

$$\begin{aligned} C_L &= 2\pi\alpha \\ C_D &= 0.01 + 0.5\alpha^2 \end{aligned} \tag{4.20}$$

If $\alpha \geq \alpha_s = 0.2rad\,(11.45^\circ)$

$$\begin{aligned} C_L &= 2\pi\alpha_{stall} \\ C_D &= 0.01 + 0.5\alpha^2 \end{aligned} \tag{4.21}$$

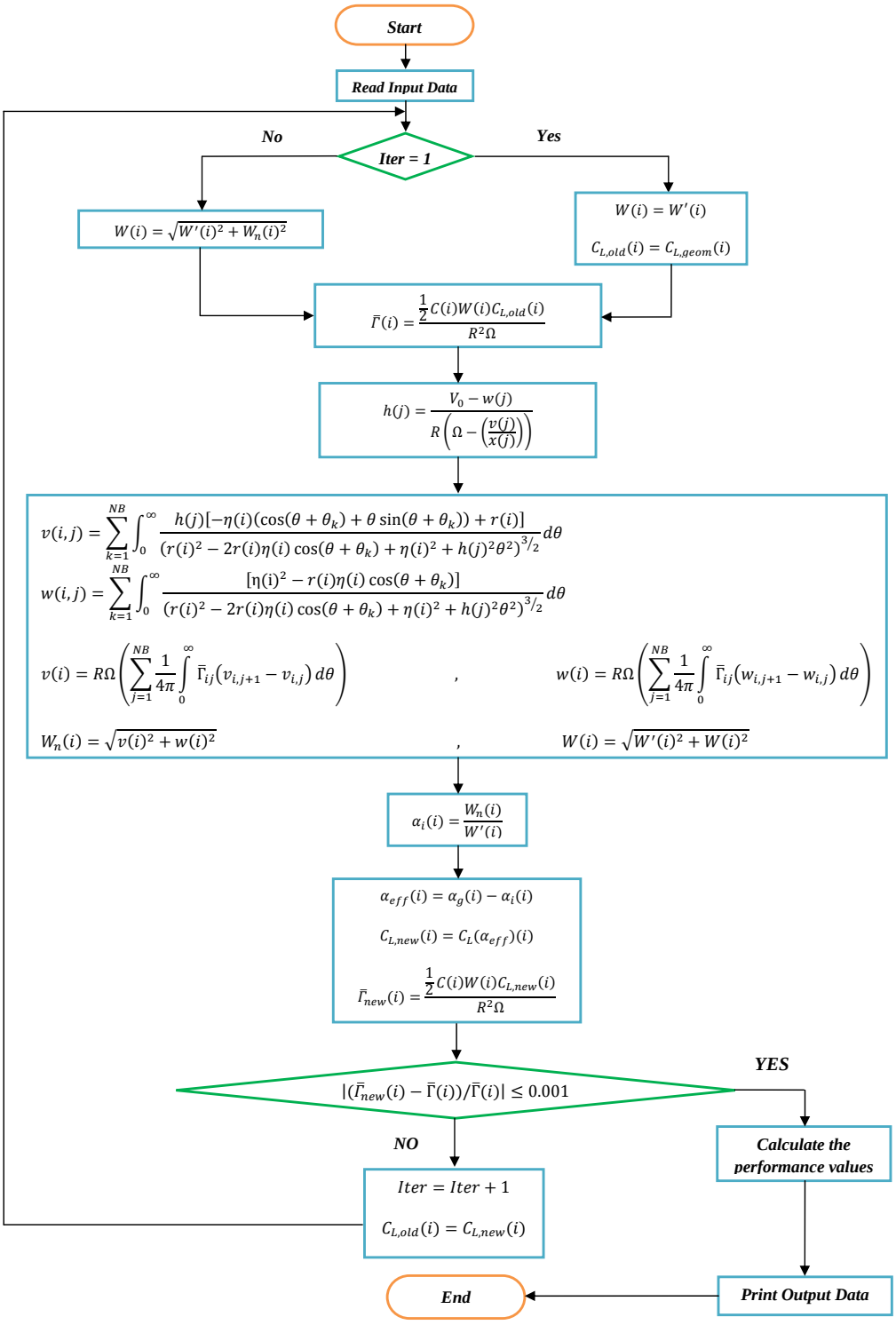

Figure 4.4: Flow chart for the numerical procedure

Chapter 5

Helical Vortex Sheet Method

In this chapter, the theoretical development of the helical vortex sheet method for prediction of the aerodynamics loads on wind turbine blades is introduced [10]. In this method, it is assumed that the collection of the trailing vortices which originate from each blade element construct a helical vortex sheet (due to blade rotation) behind of each rotor blade which continues to infinity far downstream of the blades. This vortex sheet creates induced velocities on each blade element. Therefore, the Biot-Savart law is applied to compute these induced velocities. Contrary to the BEM method, we avoid the axial induction factor a and tangential induction factor a'.

5.1 Introduction

In this analysis, the induced velocity is calculated by the Biot-Savart law. It is assumed that a filament of the trailing vortices has a helical shape and it extends to infinity down stream of the rotor blades with a constant diameter. Also, it is assumed that these helical vortices are moving downstream with a constant velocity which is equal to the inflow velocity through the rotor's plane of rotation. This means that the interactions between the wake elements are ignored. To model the blade, the lifting line theory is used. In addition, we consider a continuous variation of circulation in the radial direction, and the integration is performed for the whole helical vortex sheet in the trailing wake to compute the induced velocities.

5.2 Vortex Theory for HAWT

Generally, each element of the blade can be handled as a 2-D airfoil section subject to a local resultant velocity W. The local lift of the blade element, dL,

is related to the circulation Γ around the airfoil. The local resultant velocity is the vector sum of the free stream velocity V_0, the circumferential velocity of the section Ωr and the induced velocity W_n. For each blade element, the Kutta-Jukowski theorem can be written as

$$dL = \rho W \Gamma dr \tag{5.1}$$

where ρ is the local density of the air, dr is the length of the blade element and W is the relative velocity.

Generally, the circulation Γ around the blade changes along the blade length as $\frac{d\Gamma}{dr}dr$ between the points r and $r + dr$. From the vortex continuity, it can be concluded that a trailing vortex filament originates from the blade element and continues to infinity far downstream of the blade. Since trailing vortices emanate from all points along the blade, a helical vortex sheet is constituted. The number of vortex sheets are equal to the number of blades. The trailing vortex sheets induce velocity distribution in the rotor plane. The local resultant velocity W for each blade element is obtained by vector sum of this induced velocity along with the wind velocity and rotational velocity. This local resultant velocity is used to compute the lift on the blade element by using the Kutta-Jukowski theorem.

5.3 General Assumptions

There are some assumptions for analyzing the aerodynamic performance of HAWT which can be stated as follow:

1. The air stream is considered as inviscid-incompressible flow.

2. The wind velocity is always parallel to the rotor shaft axis and constant along the blade.

3. The relative velocity of a blade element to the air stream is equal to the velocity when the blade element is located in a 2-D stream with the same relative velocity.

4. The trailing vortex system is helical with constant pitch and diameter, continuing infinitely far down stream of the blade and traveling with a constant velocity determined at the rotor. In reality, the wake is not rigid and expands radially in the downstream direction.

5. The effect of hub on the rotor flow is neglected.

6. The slipstream expansion, related to the gradual decrease of axial velocity behind the rotor by reduction in pressure behind the rotor, is neglected.

5.4 Coordinate System

The physical model and coordinate systems for the analysis are shown in figs.(5.1) and (5.2). The Cartesian coordinates X, Y, Z are fixed in a space. The Z axis is the rotation axis and the XY plane is considered as the rotation plane. In addition, the Z coordinate is defined as the distance measured from the rotor to a segment of trailing vortex parallel to the axis of rotor rotation. The second coordinate system is a cylindrical coordinate system (r, θ, z) which is fixed to the rotating blade. The r axis is made along the blade, the θ axis measures the azimuthal angle measured from the kth blade and the z axis is the axis of rotation. It is assumed that the blade whose induced velocity is to be calculated, to be coincident with the X axis as in fig.(5.2).

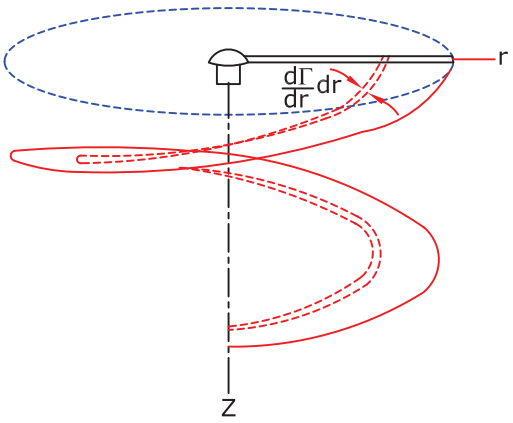

Figure 5.1: Physical model of helical vortex sheet

5.5 Calculation of Induced Velocity

As mentioned before, it is assumed that the trailing vortex filament from a blade element extends infinitely far downstream of the rotor. Moreover,

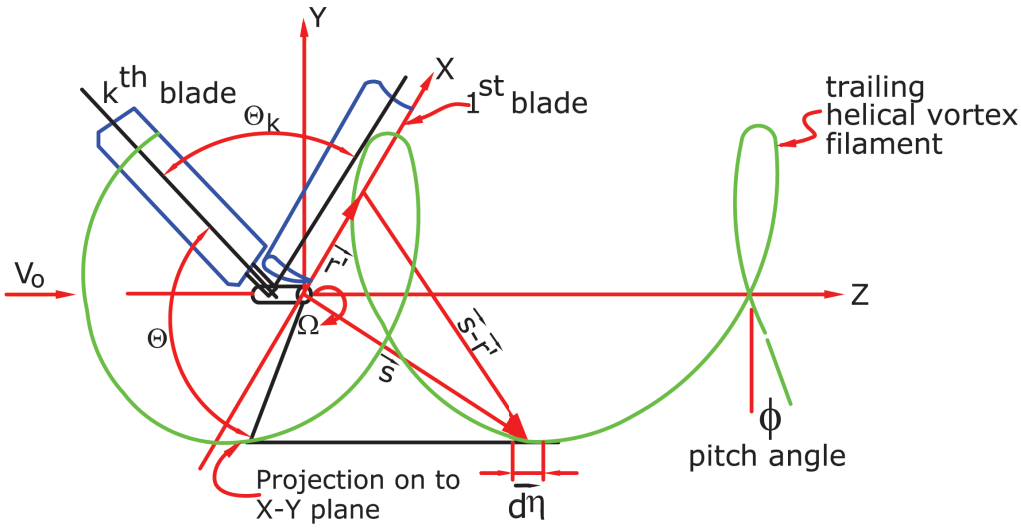

Figure 5.2: Geometry of helical vortex and the coordinate systems

this vortex induces a velocity field which can be calculated by Biot-Savart law. This law is expressed in vector differential form as

$$d\mathbf{W}_{\mathbf{induced}}\left(r'\right) = \frac{d\Gamma}{4\pi}\frac{\left(\mathbf{s}-\mathbf{r}'\right)\times d\boldsymbol{\eta}}{\left|\mathbf{s}-\mathbf{r}'\right|^3} \tag{5.2}$$

In this equation, $d\mathbf{W}_{\mathbf{induced}}$ is the differential velocity induced at a point r' on the blade due to a segment $d\eta$ of the trailing vortex filament emanated at point r on the kth blade. Also, $\dfrac{d\Gamma}{dr}dr$ is the circulation change between the points r and $r+dr$ along the blade which is equal to the circulation of the trailing vortex from the blade element dr. Vectors $\mathbf{s}$, $\mathbf{r}'$ and $d\boldsymbol{\eta}$ are defined as (see Appendix B)

$$\mathbf{r}' = r'\mathbf{i} \tag{5.3}$$

$$\mathbf{s} = r\cos\left(\theta+\theta_k\right)\mathbf{i} + r\sin\left(\theta+\theta_k\right)\mathbf{j} + r\theta\tan\phi\mathbf{k} \tag{5.4}$$

$$d\boldsymbol{\eta} = rd\theta\left\{-\sin\left(\theta+\theta_k\right)\mathbf{i} + \cos\left(\theta+\theta_k\right)\mathbf{j} + \tan\phi\mathbf{k}\right\} \tag{5.5}$$

In the above equations, θ is the azimuthal angular variable of the helix measured from the kth blade and ϕ is the helix pitch. For simplicity, $h = r\tan\phi$ and also it is considered that ϕ is related to the inflow velocity U and the

rotational velocity of rotor Ωr by

$$\tan\phi = \frac{U}{r\Omega + W_y} \tag{5.6}$$

then

$$h = r\tan\phi = \frac{U}{\Omega + \dfrac{W_y}{r}} \tag{5.7}$$

Now, eqs.(5.4) and (5.5) may be expressed as

$$\mathbf{s} = r\cos(\theta+\theta_k)\,\mathbf{i} + r\sin(\theta+\theta_k)\,\mathbf{j} + h\theta\mathbf{k} \tag{5.8}$$

$$d\boldsymbol{\eta} = d\theta\left\{-r\sin(\theta+\theta_k)\,\mathbf{i} + r\cos(\theta+\theta_k)\,\mathbf{j} + h\mathbf{k}\right\} \tag{5.9}$$

So, the cross product in the eq.(5.2) can be written as

$$\begin{aligned}(\mathbf{s}-\mathbf{r}')\times d\boldsymbol{\eta} = d\theta\,\{&hr\left[\sin(\theta+\theta_k) - \theta\cos(\theta+\theta_k)\right]\mathbf{i}\\ &+ h\left[r' - r\cos(\theta+\theta_k) - r\theta\sin(\theta+\theta_k)\right]\mathbf{j}\\ &+ \left[r^2 - rr'\cos(\theta+\theta_k)\right]\mathbf{k}\}\end{aligned} \tag{5.10}$$

$$|\,\mathbf{s}-\mathbf{r}'\,| = \left(r^2 - 2rr'\cos(\theta+\theta_k) + r'^2 + h^2\theta^2\right)^{1/2} \tag{5.11}$$

For simplicity, $A = |\,\mathbf{s}-\mathbf{r}'\,|$ and $d\mathbf{W}_{\mathbf{induced}}$ is decomposed into its components as

$$d\mathbf{W}_{\mathbf{induced}} = dW_x\mathbf{i} + dW_y\mathbf{j} + dW_z\mathbf{k} \tag{5.12}$$

Therefore, by combining eqs.(5.2), (5.10), (5.11) and (5.12) and considering the number of helical vortices NB originating from each blade element located at distance r from the rotation axis, the induced velocity components can be written

$$dW_x = \frac{\dfrac{d\Gamma}{dr}dr}{4\pi}\sum_1^{NB}\int_0^{\infty}\frac{hr\left[\sin(\theta+\theta_k) - \theta\cos(\theta+\theta_k)\right]}{A^3}d\theta \tag{5.13}$$

$$dW_y = \frac{\dfrac{d\Gamma}{dr}dr}{4\pi}\sum_1^{NB}\int_0^{\infty}\frac{h\left[r' - r\cos(\theta+\theta_k) - r\theta\sin(\theta+\theta_k)\right]}{A^3}d\theta \tag{5.14}$$

$$dW_z = \frac{\dfrac{d\Gamma}{dr}dr}{4\pi}\sum_1^{NB}\int_0^{\infty}\frac{\left[r^2 - rr'\cos(\theta+\theta_k)\right]}{A^3}d\theta \tag{5.15}$$

where NB is number of blades, k denotes the corresponding blade and

$$\theta_k = \frac{2\pi(NB - k)}{NB} \tag{5.16}$$

The induced velocity components at r' due to a single helical vortex filament originating from the kth blade section located at r along the blade can be calculated by integrating eqs.(5.13), (5.14) and (5.15) with respect to θ from zero to infinity. For simplicity and since we are dealing with inviscid-incompressible flow, the integrating can be computed from zero to $6D$ with respect to θ. Here, $6D$ is considered as a distance where the effect of the induced velocity on the blade by the helical vortex sheet is significant. Also, it is assumed that blade with $k = NB$ always coincide with the X axis.

If the diameter of the vortex helix is constant, then $dW_x = 0$. Also, if the induced velocity at radius r' is decomposed into the normal and parallel directions with respect to the undisturbed velocity W' of the blade element (see fig.(5.3.)), it can be written as

$$dW_n = dW_z \cos\phi' - dW_y \sin\phi' \tag{5.17}$$

$$dW_t = dW_z \sin\phi' + dW_y \cos\phi' \tag{5.18}$$

where

$$\phi' = \tan^{-1}\left(\frac{V_0}{r\Omega}\right) \tag{5.19}$$

By integrating eqs.(5.17) and (5.18) along the blade from the hub radius r_{hub} to the tip radius $r_{tip} = R$, the total components of induced velocity are calculated.

W_t is always zero everywhere on the blade. Therefore, the total induced velocity at point r' of the blade by all trailing vortices emanating from the blade is equal to the dW_n. In eq.(5.17) at point $r = r'$ when $\theta = \theta_k = 0$, a singularity occurs (a denominator goes to zero). In practice, it can never occur since r' is located at a quarter of the chord of the blade and r is always located downstream of the trailing edge. The parameter h is re-written as

$$h = \frac{V_0 - W_n \cos\phi'}{\Omega + \dfrac{W_n \sin\phi'}{r}}$$

5.6 Governing Equations

In order to formulate the governing equation, it should be noted that the blade section is placed at a geometric angle of attack α_g with respect to

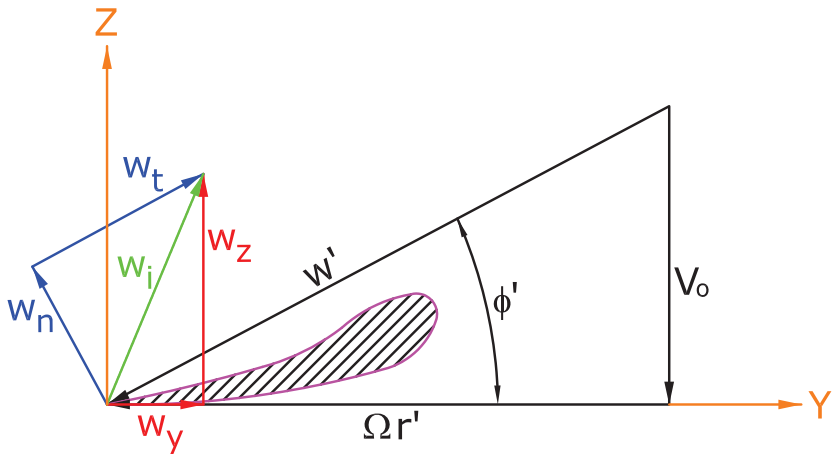

Figure 5.3: Velocity diagram and induced velocity components

the undisturbed incoming fluid velocity W', and the induced angle of attack α_i, which is created by induced velocity, makes each blade element to see a smaller angle of attack, the so-called effective angle of attack α_{eff}

$$\alpha_{eff} = \alpha_g - \alpha_i \tag{5.20}$$

The induced angle of attack may be expressed from fig.(5.4) as

$$\alpha_i = \tan^{-1} \frac{W_n}{W'} \tag{5.21}$$

The geometric angle of attack can be computed from fig.(5.4) as

$$\alpha_g = \tan^{-1} \left(\frac{V_0}{r\Omega} \right) - \theta \tag{5.22}$$

where θ is defined as the local pitch angle of the blade element. The Kutta-Jukowski theorem defines the relation between circulation and lift coefficient at each section as

$$L = \rho W \Gamma \tag{5.23}$$

Also, lift coefficient is defined as

$$C_L = \frac{L}{\frac{1}{2}\rho W^2 c} \tag{5.24}$$

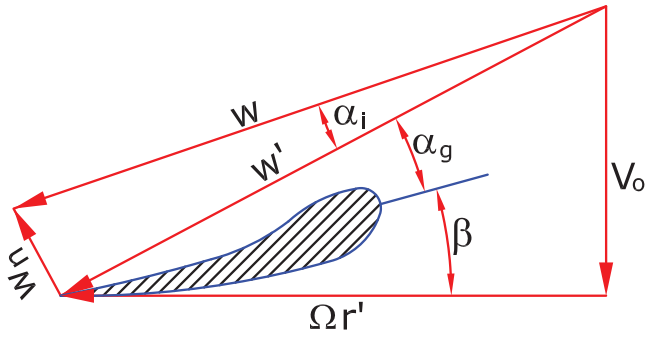

Figure 5.4: Velocity diagram and the induced velocity components

Combination of eqs.(5.23) and (5.24) yields

$$\Gamma = \frac{1}{2} c W C_L \tag{5.25}$$

where c is the chord of the blade section.

5.7 Numerical Procedure

To start the calculation, each blade of the wind turbine is divided into M sections with M nodes along the blade for computing the required variables. These partitions may be either uniform or non-uniform. For simplicity, each rotor blade of the wind turbine is divided into number of sections similarly. The induced velocity as mentioned before, is computed by direct integration of the Biot-Savart law. This induced velocity is used to calculate the induced angle of attack distribution which in turn may be used to evaluate different performance variables, e.g., rotor power, rotor thrust, etc. To accomplish all of these, the circulation distribution along the blade $\Gamma(r)$, must be known. This distribution is constructed so that the circulation at both the blade tip $r_{tip} = R$ and the blade hub $r = r_{hub}$ is zero. Now, all the required equations have been introduced. A numerical iterative method can be obtained as fig.(5.5).

5.8 Power, Torque and Drag On a HAWT

After finishing the iterative process and calculating the effective angle of attack, the rotor power P, torque Q and axial force F can be computed as follow

$$F = \int_{r_{hub}}^{r_{tip}} \left(\frac{1}{2}\rho N B c W^2\right) (C_L \cos\phi + C_D \sin\phi)\, dr \tag{5.26}$$

$$Q = \int_{r_{hub}}^{r_{tip}} \left(\frac{1}{2}\rho N B c W^2\right) (C_L \sin\phi - C_D \cos\phi)\, r dr \tag{5.27}$$

$$P = \int_{r_{hub}}^{r_{tip}} \left(\frac{1}{2}\rho N B c W^2\right) (C_L \sin\phi - C_D \cos\phi)\, \Omega r dr \tag{5.28}$$

where C_L and C_D are the sectional lift and drag coefficients respectively defined as

$$C_L = \frac{dL}{\frac{1}{2}\rho W^2 c dr} \tag{5.29}$$

$$C_D = \frac{dD}{\frac{1}{2}\rho W^2 c dr} \tag{5.30}$$

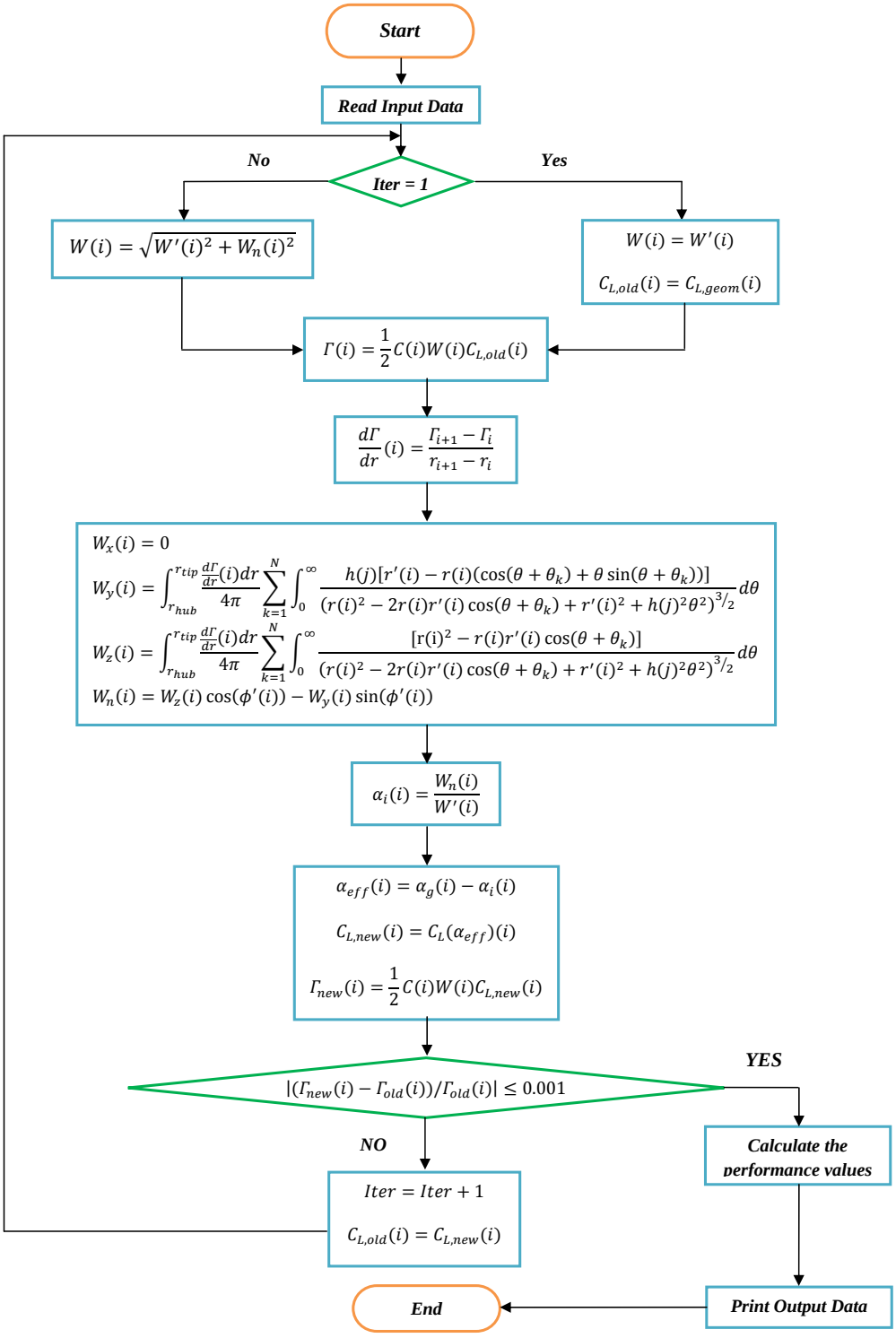

Figure 5.5: Flow chart for the numerical procedure

Chapter 6

Results

In this chapter, the aerodynamics performance of HAWT for four different cases have been evaluated by the three mentioned methods; BEM, Vortex Method 1 (Helical Vortex Method by Influence Coefficient Method) and Vortex Method 2 (Helical Vortex Sheet). The results are compared to each other. In each case, the Blade Aerodynamics Properties and Basic Machine Parameters have been introduced by related tables.

In the tables of the Distributed Blade Aerodynamic Properties, the blade nodes radial position, twist angle, pitch angle, element length, chord length and the airfoil type of each blade segment have been determined. Each node is located at the middle of the segment as control point and the calculated parameters such as circulation Γ, induced α_i and effective α_{eff} angles of attack are stored there.

In the tables of Basic Machine Parameters, the gross properties of each machine have been presented.

It may happen that the wind turbine blades operate in the stalled region occurring at large angles of attack. In this situation, airfoil data have to be modified. Since the existed tables are based on the 2-D measurements, so it is necessary to consider 3-D effects on the aerodynamics coefficient tables (C_L and C_D) such as rotational stall delay, dynamic-stall, etc. For each case, please see the related reference.

In all cases, the variation of Reynolds number along the blade has been neglected.

In order to calculate the wind turbine performance, first we must compute the circulation distribution along the blade. It should be noted that the calculated output power is not the rotor power because of the losses in the power transmission.

Node	Radial Position (m)	Twist (deg)	Pitch (deg)	Element Length (m)	Chord (m)	Airfoil Type
1	11.75	13.31	0	4.10	4.56	$DU40$
2	15.85	11.48	0	4.10	4.65	$DU35$
3	19.95	10.16	0	4.10	4.46	$DU35$
4	24.05	9.01	0	4.10	4.25	$DU30$
5	28.15	7.79	0	4.10	4.01	$DU25$
6	32.25	6.54	0	4.10	3.75	$DU25$
7	36.35	5.36	0	4.10	3.50	$DU21$
8	40.45	4.18	0	4.10	3.26	$DU21$
9	44.55	3.12	0	4.10	3.01	$NACA64$
10	48.65	2.32	0	4.10	2.76	$NACA64$
11	52.75	1.52	0	4.10	2.52	$NACA64$
12	56.16	0.86	0	2.73	2.31	$NACA64$
13	58.90	0.37	0	2.73	2.09	$NACA64$
14	61.63	0.11	0	2.73	1.42	$NACA64$

Table 6.1: Blade aerodynamics properties of "NREL Offshore $5-MW$ Baseline" HAWT

Item	Description
Rating Power $[MW]$	5
No. of Blades	3
Rotor Radius $[m]$	63.0
Hub Radius $[m]$	1.5
Rated Wind Speed $[m/s]$	11.4
Rated Rotor Speed $[rpm]$	12.1
Tip Speed Ratio $(R\Omega/V_0)$	7

Table 6.2: Basic machine parameters of "NREL Offshore $5-MW$ Baseline" HAWT

6.1 Case 1

- NREL Offshore $5-MW$ Baseline

The blade aerodynamics properties and basic machine parameters of the "NREL Offshore $5-MW$ Baseline" [11] are given in tables (6.1) and (6.2). According to fig.(6.1), it can be seen that the effective circulation (Γ) values

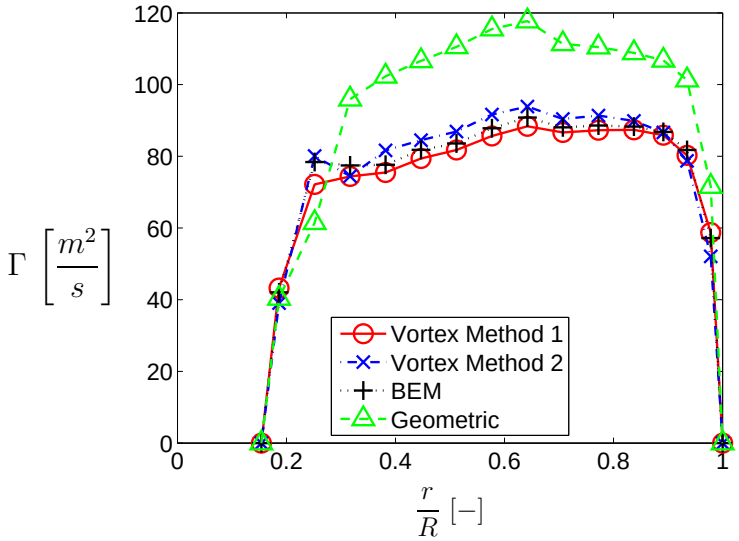

Figure 6.1: Distribution of circulation (Γ) along the blade

have been decreased compared with the geometric circulation. The reason for this reduction is the effect of the induced velocity. In nodes where the effective circulation value is larger than the geometric ones it is due to stall condition. In this condition, instead of circulation reduction, there will be an increasing value for the circulation. The results show good agreement between the different methods. As we discussed before, fig.(6.2) verifies the theory of rotating blades and downwash effect (induced velocity) where it decreases the angle of attack seen by the blade airfoil sections. Figure (6.3) shows the values of axial induction velocity along the blade.The negative values of the axial induction velocity approves the wake theory behind the rotor blade. The positive effect of the tangential induced velocity can be seen in fig.(6.4). Near the hub, the BEM method shows a larger values for tangential induced velocities compared with the vortex methods.

Figure (6.5) shows the total induced velocity along the blade. It shows that the induced tangential velocity is dominant component compared with the induced axial velocity.

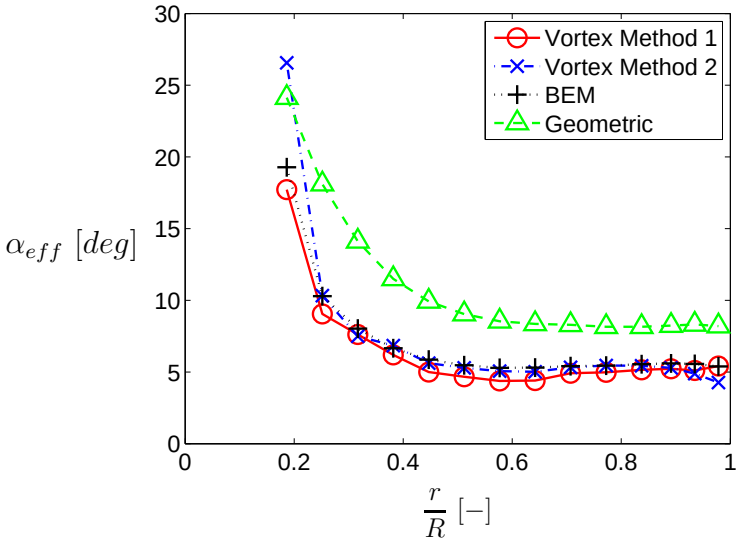

Figure 6.2: Distribution of angle of attack (α_{eff}) along the blade

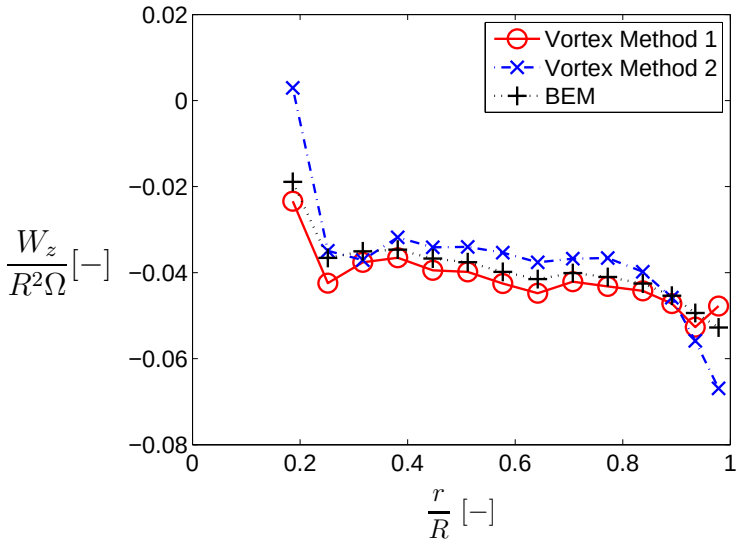

Figure 6.3: Distribution of axial induction velocity (W_z) along the blade normalized by $R^2\Omega$

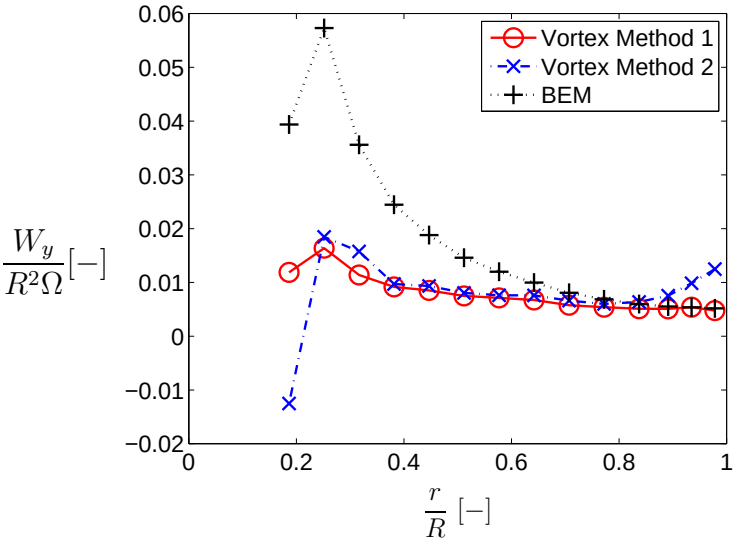

Figure 6.4: Distribution of tangential induction velocity (W_y) along the blade normalized by $R^2\Omega$

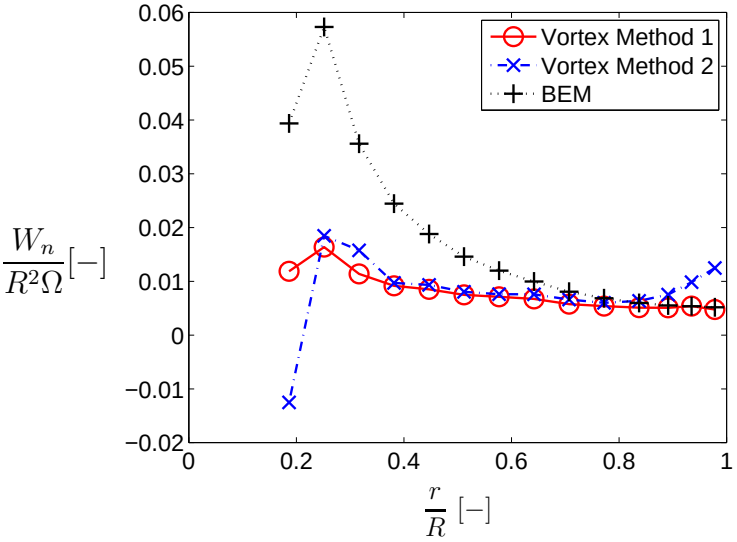

Figure 6.5: Distribution of total induction velocity (W_n) along the blade normalized by $R^2\Omega$

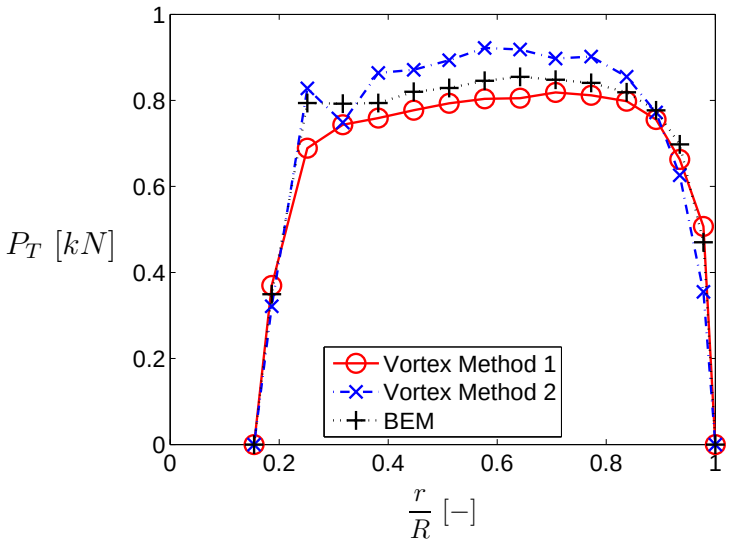

Figure 6.6: Distribution of tangential force (P_T) with respect to the rotor plane

The tangential and normal force at the rotor plane are shown in figs.(6.6) and (6.7). There is a uniform tangential force, except at the tip and root, along the blade. The normal force increases linearly and reaches its maximum value at the tip. Also, the magnitude of the normal force compared with tangential force is significant. Figures (6.8) and (6.9) show the distribution

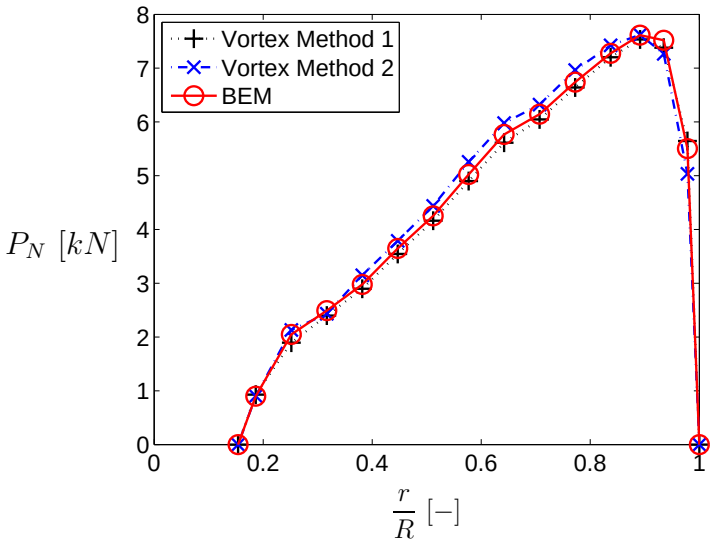

Figure 6.7: Distribution of normal force (P_N) with respect to the rotor plane

of geometric properties (twist angle and chord length) for the blade.

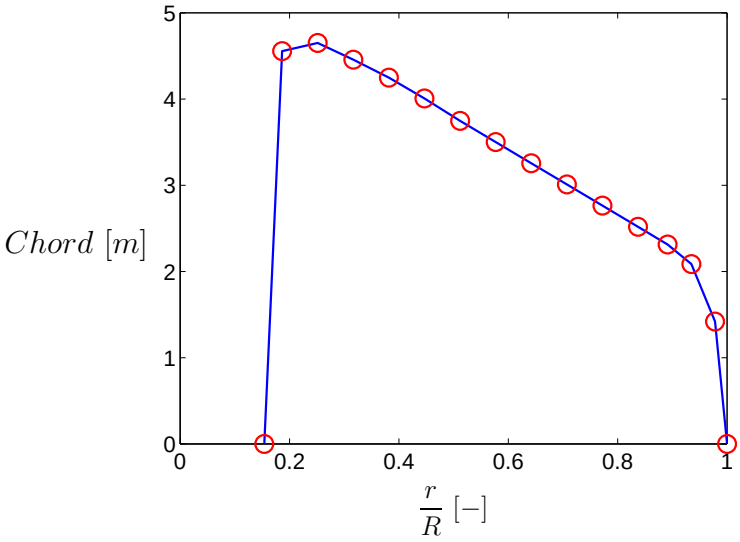

Figure 6.8: Distribution of chord length along the blade

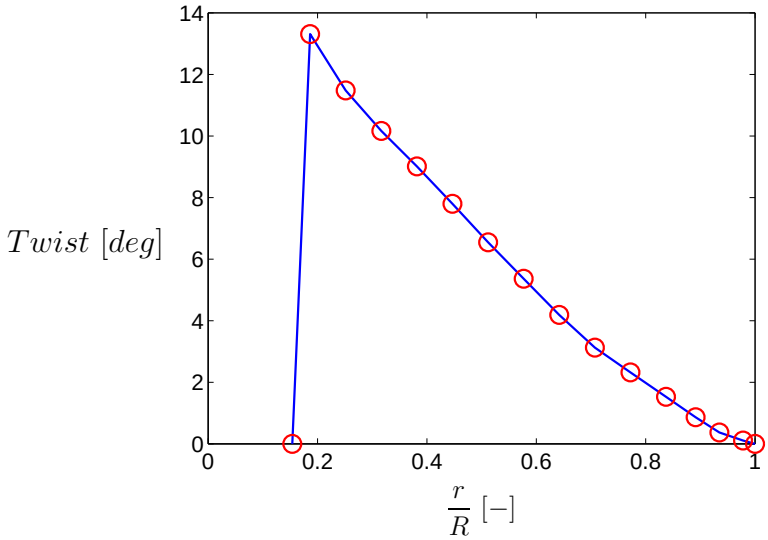

Figure 6.9: Distribution of twist angle along the blade

Node	Radial Position (m)	Twist (deg)	Pitch (deg)	Element Length (m)	Chord (m)	Airfoil Type
1	1.50	0	4.00	0.60	1.00	Thin Airfoil
2	2.10	0	4.00	0.60	1.00	Thin Airfoil
3	2.70	0	4.00	0.60	1.00	Thin Airfoil
4	3.30	0	4.00	0.60	1.00	Thin Airfoil
5	3.90	0	4.00	0.60	1.00	Thin Airfoil
6	4.35	0	4.00	0.30	1.00	Thin Airfoil
7	4.80	0	4.00	0.60	1.00	Thin Airfoil
8	5.25	0	4.00	0.30	1.00	Thin Airfoil
9	5.55	0	4.00	0.30	1.00	Thin Airfoil
10	5.85	0	4.00	0.60	1.00	Thin Airfoil

Table 6.3: Blade aerodynamics properties of "AA" HAWT

Item	Description
Rating Power $[kW]$	41.0
No. of Blades	2
Rotor Radius $[m]$	6.0
Hub Radius $[m]$	1.2
Rated Wind Speed $[m/s]$	11.4
Rated Rotor Speed $[rpm]$	117.8
Tip Speed Ratio ($R\Omega/V_0$)	6.5

Table 6.4: Basic machine parameters of "AA" HAWT

6.2 Case 2

- Analytical Airfoil (AA)

The blade aerodynamics properties and basic machine parameters of the "AA" [9] are given in tables (6.3) and (6.4). Figure (6.10) shows the difference between the effective circulation (Γ) values and the geometric circulation. The rotor blade experiences smaller circulation values compared to the geometric ones. There is a good agreement between different methods, however vortex method 2 predicts smaller values for the region near the tip. According to fig.(6.11), we can see that the reduction of effective angle of attack is larger near the hub compared with the tip region. It means that the induced velocity magnitude near the root is larger than near the tip.

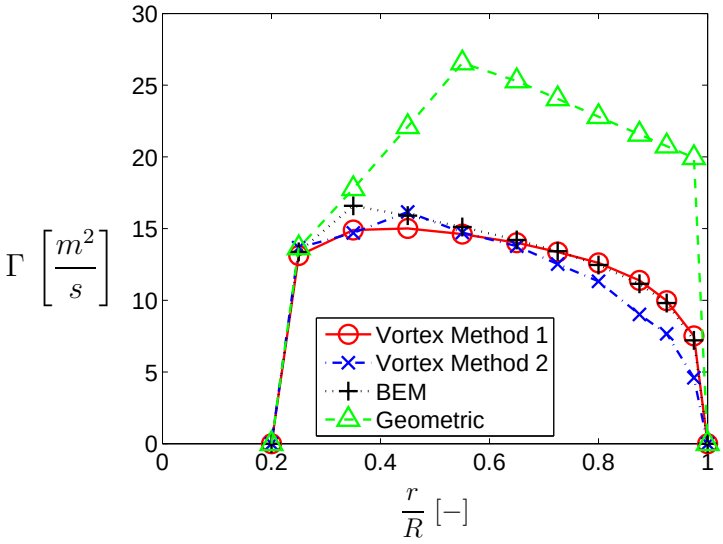

Figure 6.10: Distribution of circulation (Γ) along the blade

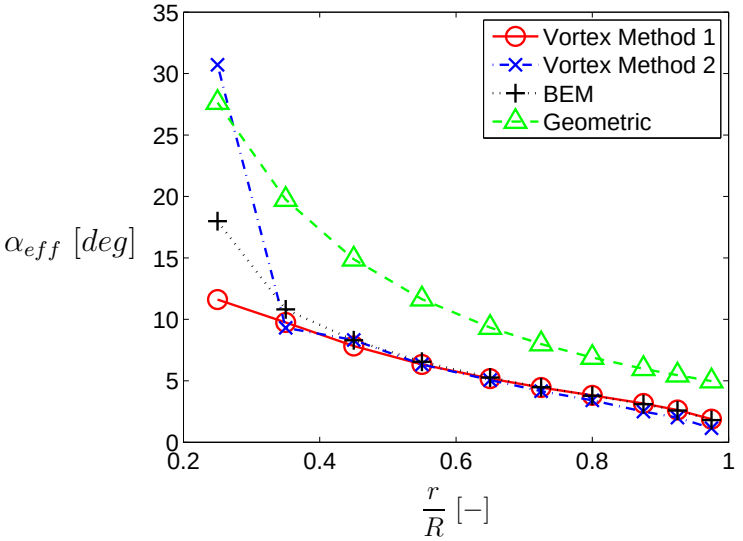

Figure 6.11: Distribution of angle of attack (α_{eff}) along the blade

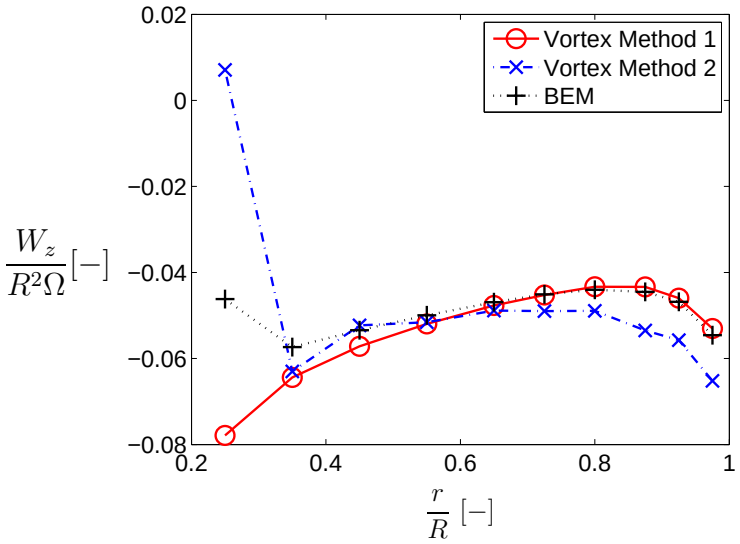

Figure 6.12: Distribution of axial induction velocity (W_z) along the blade normalized by $R^2\Omega$

The values of axial induction velocity along the blade can be seen in fig.(6.12). The larger values of the axial induced velocity for the vortex method 2 (near the tip) is connected to the smaller value of the circulation predicted by this method.Figure (6.13) shows larger values for the BEM method near the hub compared with the vortex methods.

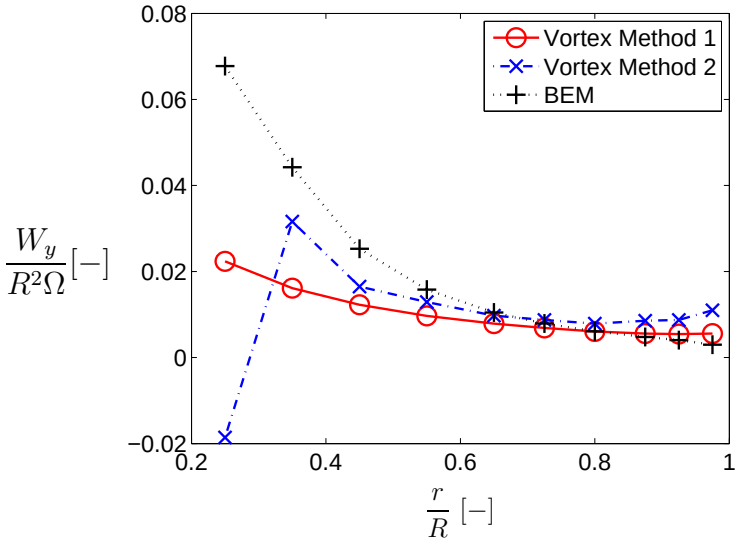

Figure 6.13: Distribution of tangential induction velocity (W_y) along the blade normalized by $R^2\Omega$

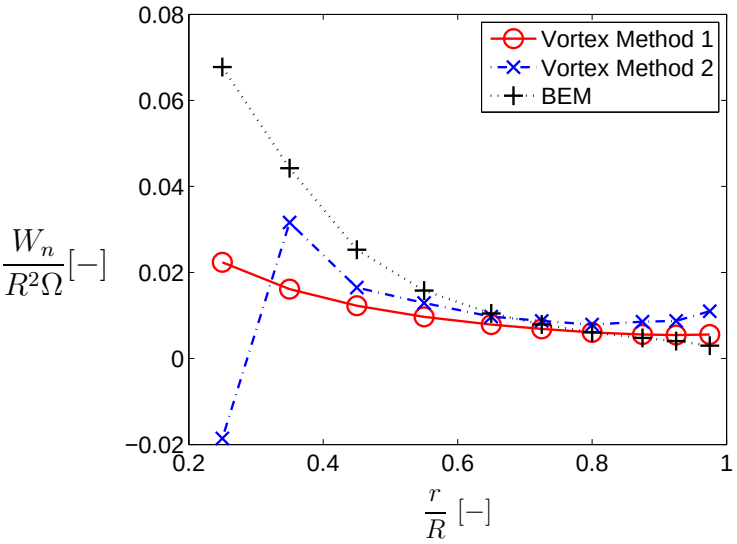

Figure 6.14: Distribution of total induction velocity (W_n) along the blade normalized by $R^2\Omega$

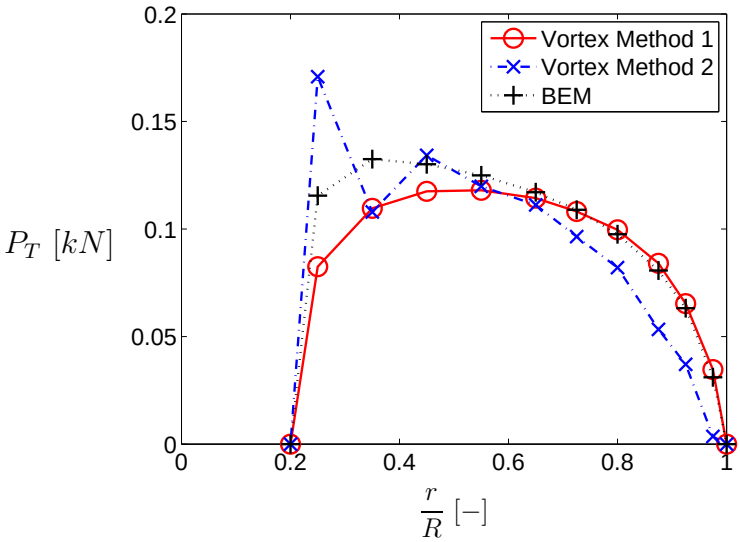

Figure 6.15: Distribution of tangential force (P_T) with respect to the rotor plane

Figures (6.15) and (6.16) show the distribution of normal and tangential forces at the rotor plane. Like the last case, the smooth variation of tangential force and the maximum value of normal force at the tip is obvious. As can be seen in figs.(6.17) and (6.18), the blades of the Case 2 has constant chord length and twist angle.

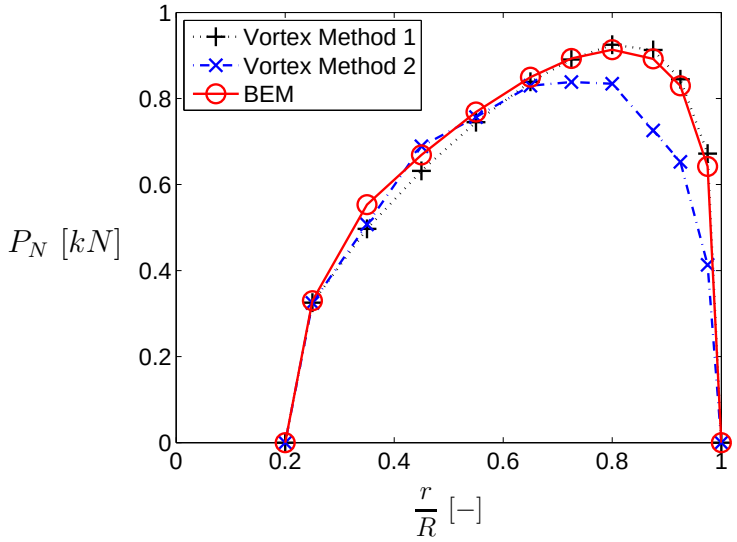

Figure 6.16: Distribution of normal force (P_N) with respect to the rotor plane

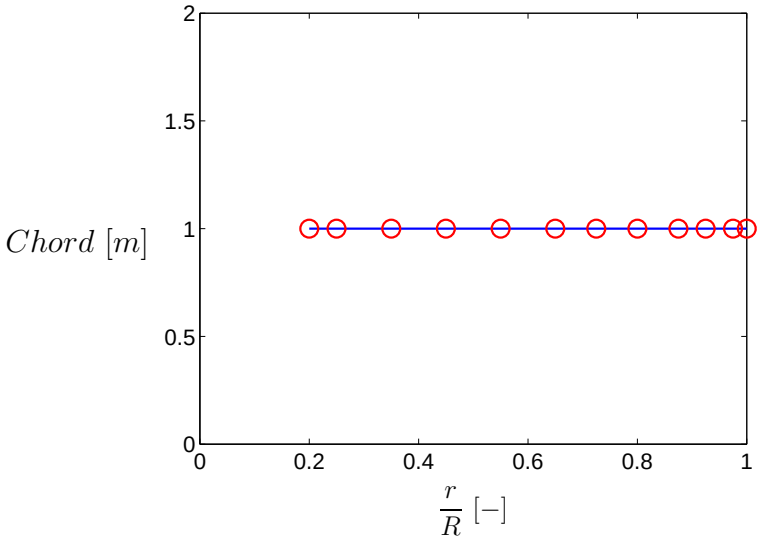

Figure 6.17: Distribution of chord length along the blade

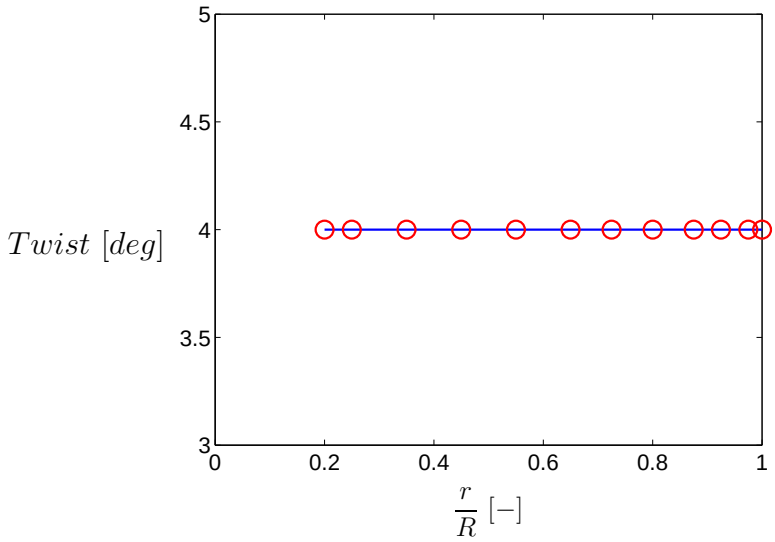

Figure 6.18: Distribution of twist angle along the blade

Node	Radial Position (m)	Twist (deg)	Pitch (deg)	Element Length (m)	Chord (m)	Airfoil Type
1	1.52	14.04	5.00	0.40	0.71	NREL S809
2	1.80	9.67	5.00	0.27	0.68	NREL S809
3	2.07	6.75	5.00	0.27	0.65	NREL S809
4	2.35	4.84	5.00	0.27	0.63	NREL S809
5	2.63	3.48	5.00	0.27	0.60	NREL S809
6	2.90	2.40	5.00	0.27	0.57	NREL S809
7	3.18	1.51	5.00	0.27	0.54	NREL S809
8	3.46	0.76	5.00	0.27	0.51	NREL S809
9	3.73	0.09	5.00	0.27	0.49	NREL S809
10	4.01	-0.55	5.00	0.27	0.46	NREL S809
11	4.29	-1.11	5.00	0.27	0.43	NREL S809
12	4.56	-1.55	5.00	0.27	0.40	NREL S809
13	4.84	-1.84	5.00	0.27	0.37	NREL S809
14	5.12	-2.08	5.00	0.27	0.35	NREL S809
15	5.39	-2.36	5.00	0.27	0.32	NREL S809

Table 6.5: Blade aerodynamics properties of "CER-NREL" HAWT

Item	Description
Rating Power $[kW]$	4.7
No. of Blades	2
Rotor Radius $[m]$	5.53
Hub Radius $[m]$	1.26
Rated Wind Speed $[m/s]$	6.3
Rated Rotor Speed $[rpm]$	72.0
Tip Speed Ratio $(R\Omega/V_0)$	6.5

Table 6.6: Basic machine parameters of "CER-NREL" HAWT

6.3 Case 3

- CER-NREL

The blade aerodynamics properties and basic machine parameters of the "$CER - NREL$" [12] are given in tables (6.5) and (6.6). Figure (6.19)

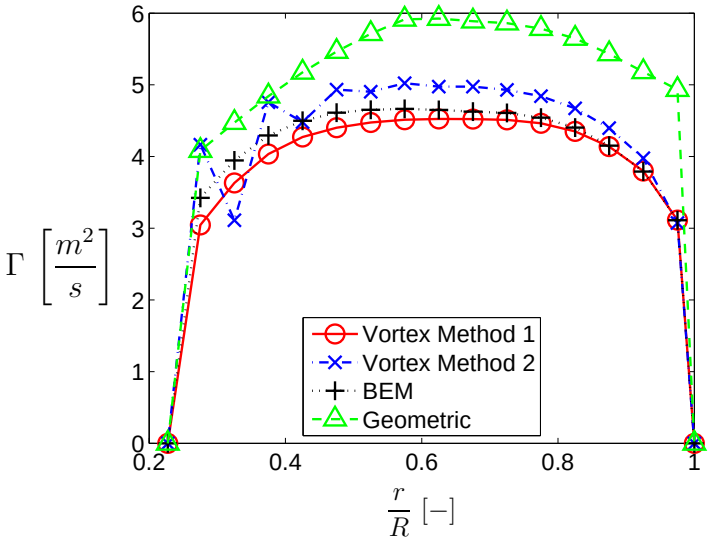

Figure 6.19: Distribution of circulation (Γ) along the blade

shows the distribution of the circulation along the blade for case 3. As can be seen, the reduction of the circulation due to the induced velocity is evident. According to fig.(6.20), the effective angle of attack is in agreement with the downwash concept.

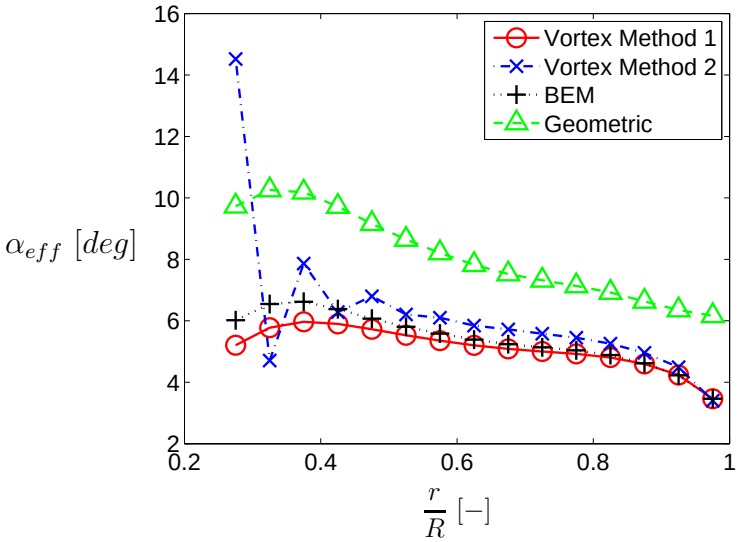

Figure 6.20: Distribution of angle of attack (α_{eff}) along the blade

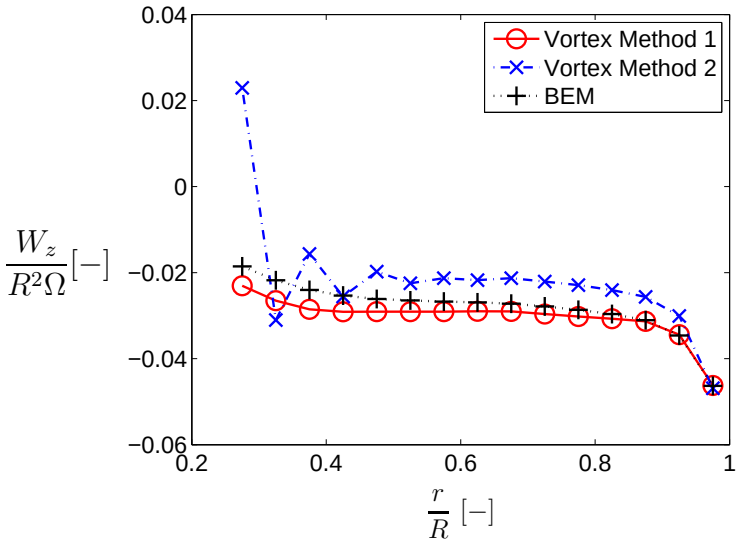

Figure 6.21: Distribution of axial induction velocity (W_z) along the blade normalized by $R^2\Omega$

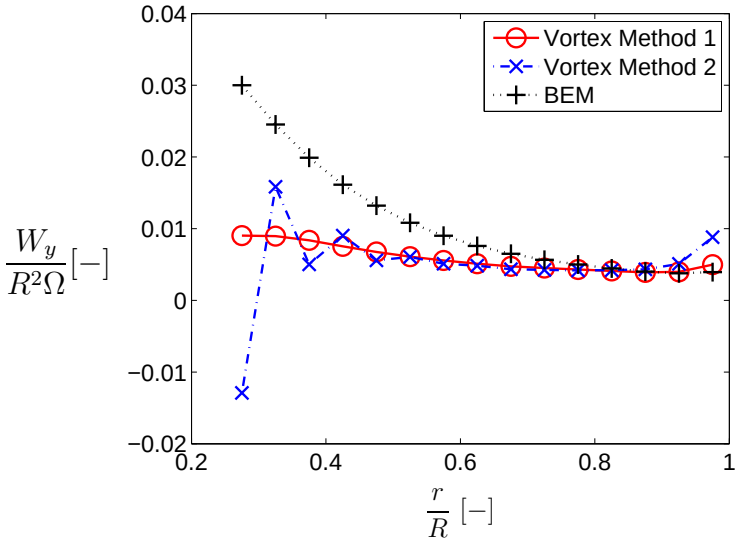

Figure 6.22: Distribution of tangential induction velocity (W_y) along the blade normalized by $R^2\Omega$

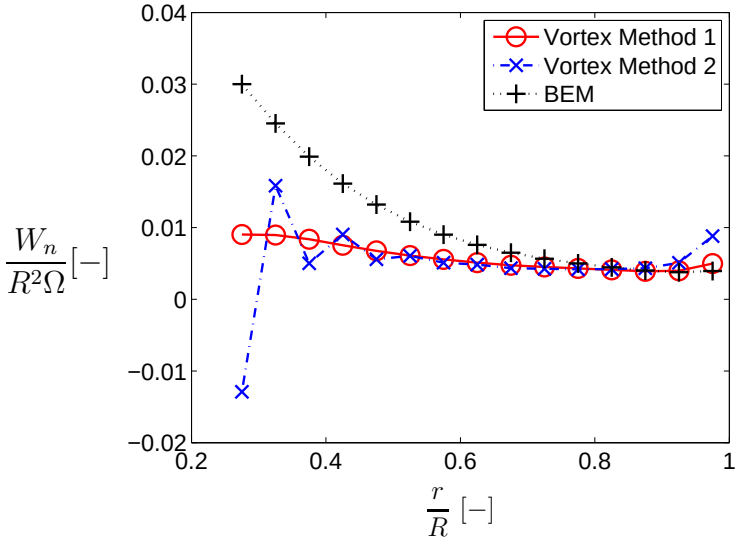

Figure 6.23: Distribution of total induction velocity (W_n) along the blade normalized by $R^2\Omega$

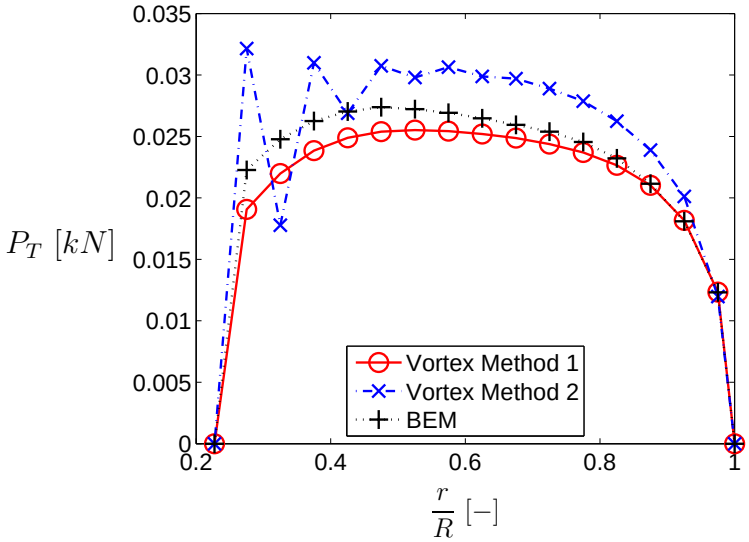

Figure 6.24: Distribution of tangential force (P_T) with respect to the rotor plane

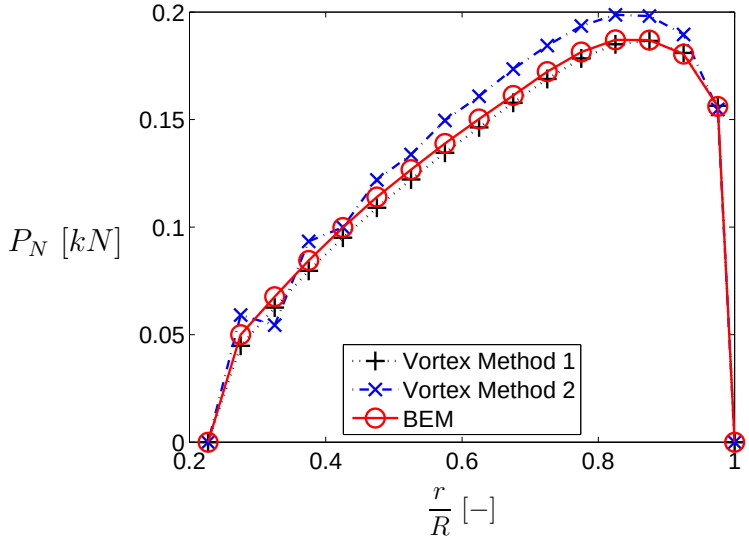

Figure 6.25: Distribution of normal force (P_N) with respect to the rotor plane

The negative values of axial induced velocity, the positive values of tangential velocity and its prevalent role on the total induced velocity is seen in figs.(6.21), (6.22) and (6.23). Similar to the other cases, the smooth variation of the tangential force and the largest values of normal force near the tip can be seen in figs.(6.24) and (6.25). The variation of the chord length

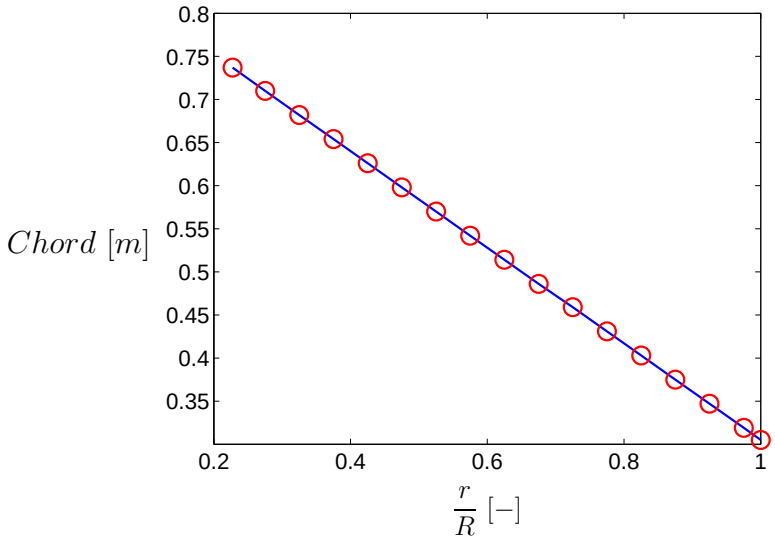

Figure 6.26: Distribution of chord length along the blade

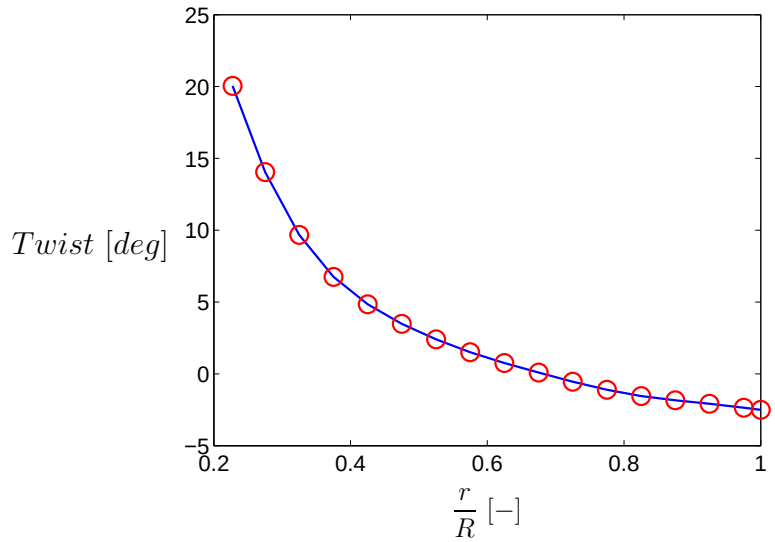

Figure 6.27: Distribution of twist angle along the blade

and twist angle for the case 3 is shown in figs.(6.26) and (6.27).

Node	Radial Position (m)	Twist (deg)	Pitch (deg)	Element Length (m)	Chord (m)	Airfoil Type
1	7	11.50	0	1.5	1.51	FFA-W3-241
2	8	8.30	0	1.00	1.45	FFA-W3-241
3	9	6.60	0	1.00	1.39	FFA-W3-221
4	10	5.20	0	1.00	1.32	FFA-W3-221
5	11	4.50	0	1.00	1.26	FFA-W3-221
6	12	3.55	0	1.00	1.20	FFA-W3-221
7	13	2.77	0	1.00	1.13	LM-2-18
8	14	2.15	0	1.00	1.06	LM-2-18
9	15	1.59	0	1.00	0.99	LM-2-18
10	16	1.12	0	1.00	0.92	LM-2-18
11	17	0.75	0	1.00	0.84	LM-2-18
12	18	0.4	0	1.00	0.74	LM-2-18
13	19	0.15	0	0.75	0.59	LM-2-15
14	19.5	0.06	0	0.50	0.46	LM-2-13
15	20	0.01	0	0.75	0.28	LM-2-13

Table 6.7: Blade aerodynamics properties of "Nordtank-500" HAWT

Item	Description
Rating Power $[kW]$	260
No. of Blades	3
Rotor Radius $[m]$	20.5
Hub Radius $[m]$	6.0
Rated Wind Speed $[m/s]$	8.95
Rated Rotor Speed $[rpm]$	27.1
Tip Speed Ratio ($R\Omega/V_0$)	6.5

Table 6.8: Basic machine parameters of "Nordtank-500" HAWT

6.4 Case 4

- Nordtank-500

The blade aerodynamic properties and basic machine parameters of the "$Nordtank-500$" are given in tables (6.7) and (6.8).

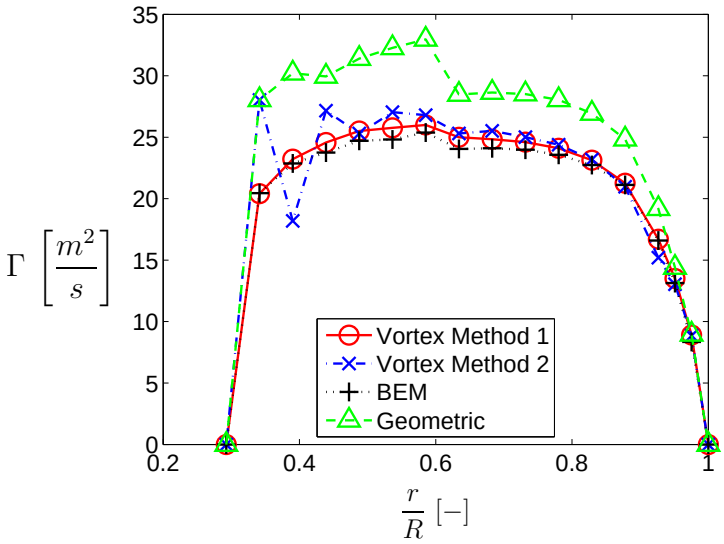

Figure 6.28: Distribution of circulation (Γ) along the blade

In this case, because of lack of exact data for the airfoil type of the blade segments, significant oscillation are found in the all figures. Still, the results show their agreement with the theory and the other cases. Therefore, we can deduce that the resolution to capture the accurate result in vortex method 2 is much more sensitive compared with the BEM method.

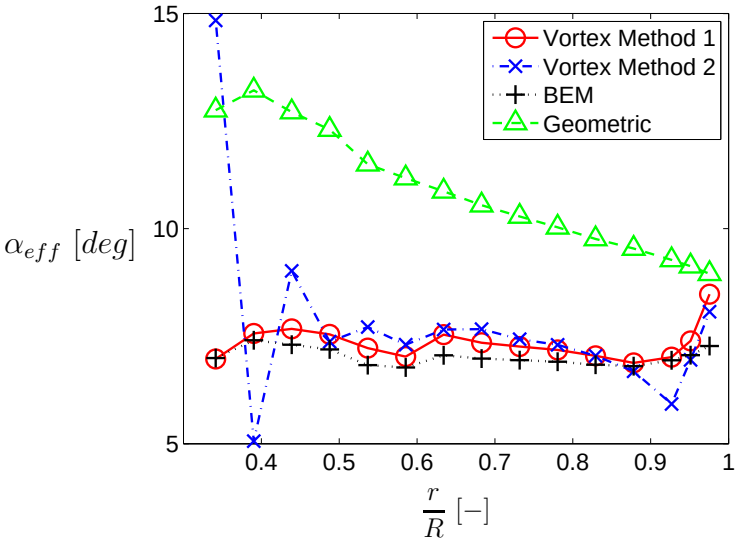

Figure 6.29: Distribution of angle of attack (α_{eff}) along the blade

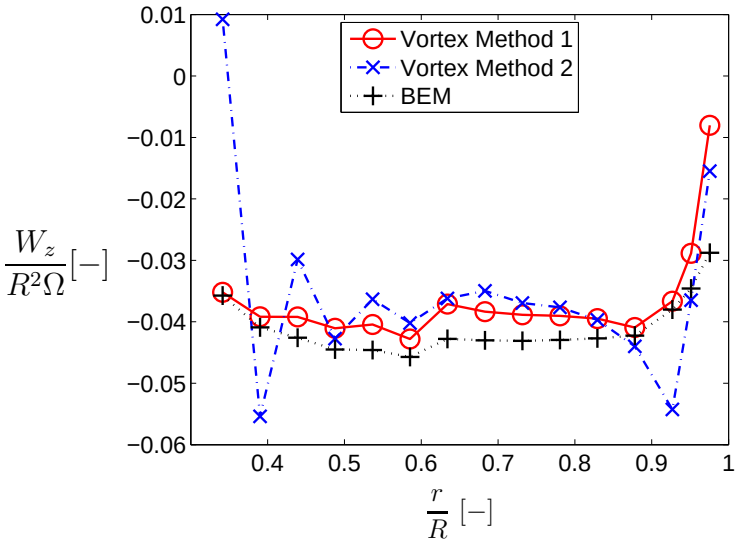

Figure 6.30: Distribution of axial induction velocity (W_z) along the blade normalized by $R^2\Omega$

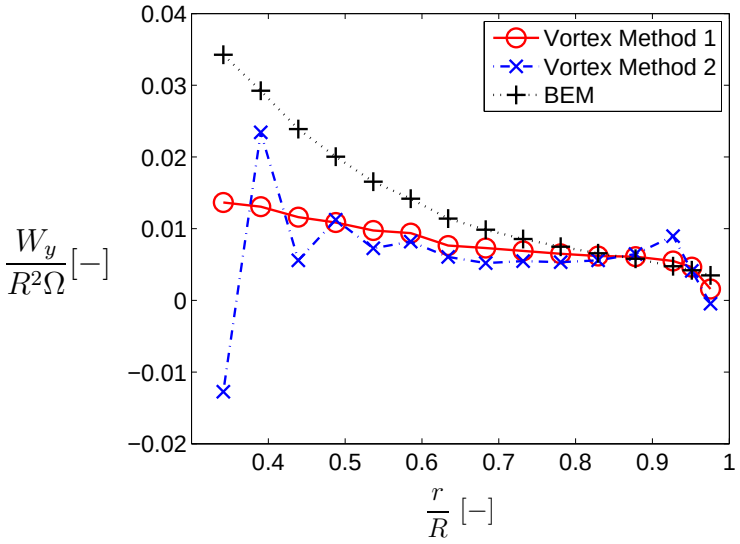

Figure 6.31: Distribution of tangential induction velocity (W_y) along the blade normalized by $R^2\Omega$

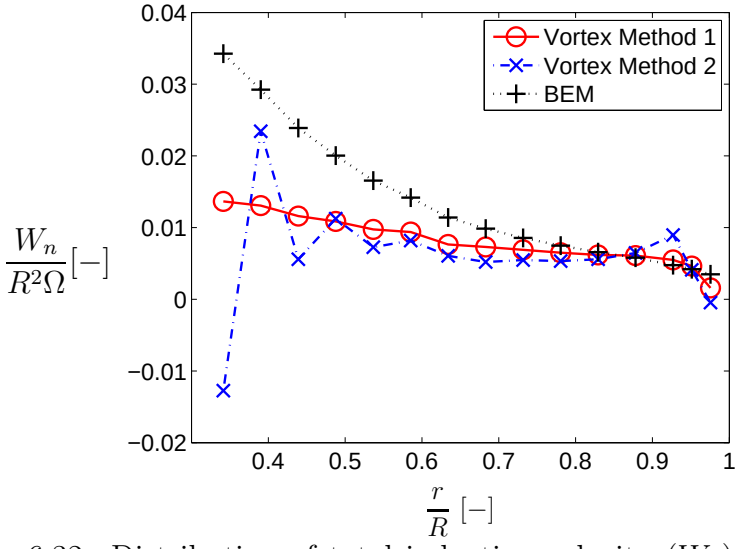

Figure 6.32: Distribution of total induction velocity (W_n) along the blade normalized by $R^2\Omega$

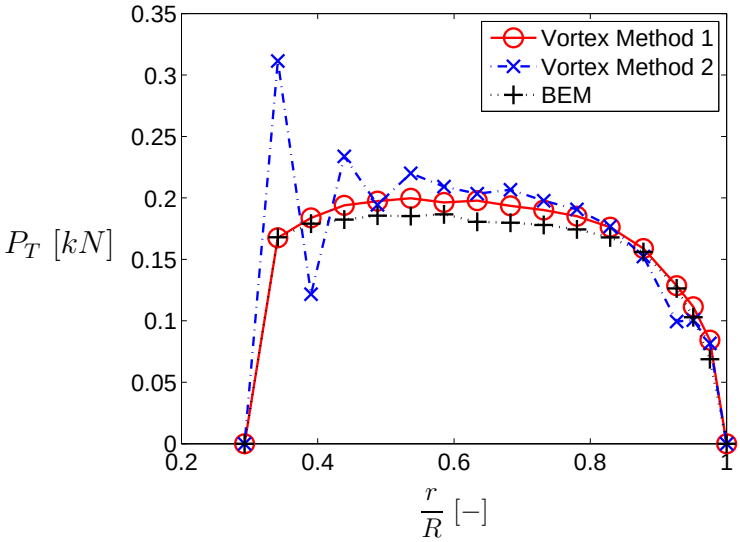

Figure 6.33: Distribution of tangential force (P_T) with respect to the rotor plane

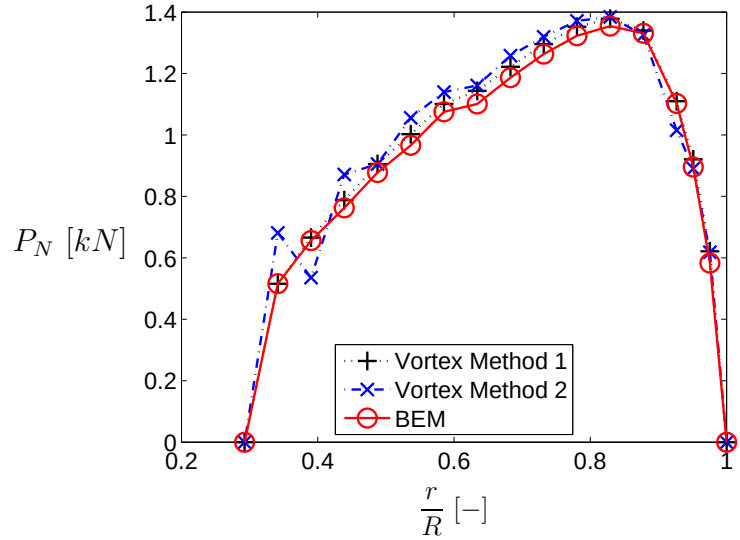

Figure 6.34: Distribution of normal force (P_N) with respect to the rotor plane

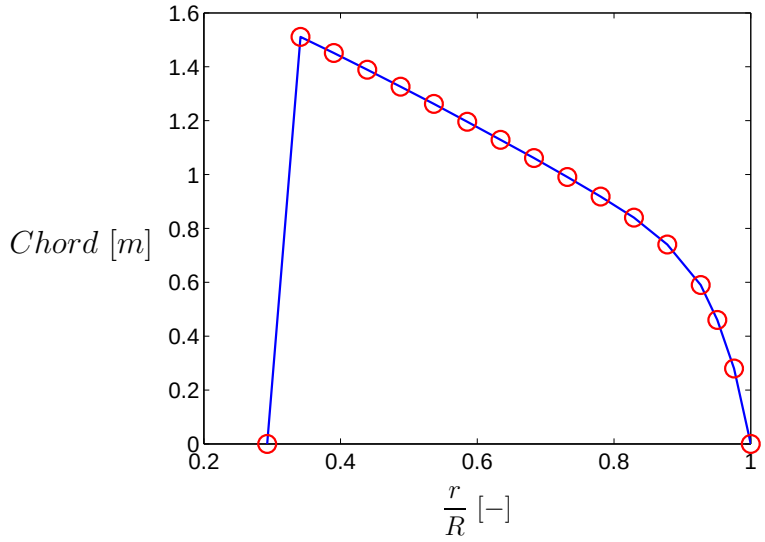

Figure 6.35: Distribution of chord length along the blade

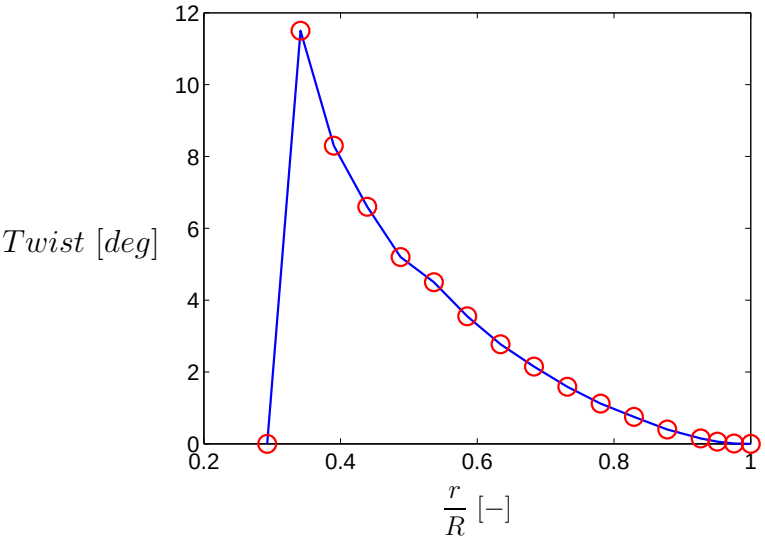

Figure 6.36: Distribution of twist angle along the blade

6.5 Conclusion

The difference between the methods can be categorized as below:

1. The circulation values by BEM and Vortex method 1 are similar. However, BEM method gives somewhat larger values at the root. This means that we need empirical relation for the hub region (like the Prandtl's tip correction factor). Moreover, Vortex method 2 yields larger values for circulation except for the tip.

2. The three methods predict the effective angle of attacks similar to each other.

3. The axial induced velocity for both BEM and Vortex method are approximately the same whereas vortex method 2 shows a greater values except for the tip. The tangential induced velocity decreases from root to tip, but the slope of this reduction for BEM method is greater than the other methods which means that calculated values by BEM is the largest at root.

4. The tangential force seems to be nearly the same for BEM method and Vortex method 1 while the BEM method predicts slightly larger values at the root.

6.6 Future Work

In order to improve the results and to close the models to reality, a lot of efforts should be done. Here, some of them is mentioned.

In order to remove oscillations in the results, the distribution of the control points should be refined by interpolating of airfoil profile data in the regions of tip and root, where the circulation varies rapidly.

Lift and drag coefficients (C_L and C_D) for a certain airfoil profile vary with Reynolds number. This means that they are a function of local Reynolds number. Therefore, the values of C_L and C_D should be looked up (as input data) in tables with an appropriate Reynolds number.

The blade surface roughness should be also included to get more accurate results. In addition, there need some corrections for 3D behaviour of 2D airfoil data, such as rotational stall delay and dynamic-stall hysteresis parameters.

Since the prescribed wake model does not predict highly accurate aerodynamic parameters for HAWT in cases where there are small variations in

the wake geometry specifically when this geometry cannot be prescribed with an acceptable accuracy, then free wake modelling will be a suitable solution where the vortex wake elements are allowed to convect and deform under the action of the local velocity field. In this case, application of the Biot-Savart law should be modified by some physical concepts such as vortex filament core thickness, vortex curvature effect (self induction mechanism) and etc. It may need to add some term(s) to the induced velocity gained by Biot-Savart law. Also, the vortex ring concept may help for construction the model for correctional term(s).

The other unsteadiness parameters including periodic (wind speed, inflow, yaw, ...) and non-periodic (wind turbulence, wake dynamics, ...) flow field factors should be studied.

Appendix A

Derivation of Biot-Savart Equation

The vorticity $\mathbf{\Omega} = \mathbf{\Omega}(\mathbf{r}, t)$ is the curl of the velocity[1]

$$\mathbf{\Omega} = \nabla \times \mathbf{V} \tag{A.1}$$

According to the Green's theorem, which is a special case of Stokes' theorem, the circulation $\Gamma = \oint_C \mathbf{V} \cdot d\mathbf{s}$ around any closed curve C can be related from the vorticity by the equation

$$\Gamma = \oint_C \mathbf{V}.d\mathbf{s} = \iint_S \nabla \times \mathbf{V} \cdot \mathbf{n} dS = \iint_S \mathbf{\Omega} \cdot \mathbf{n} dS \tag{A.2}$$

where S is any surface whose boundary is the curve C.

A.1 Vortex Line, Surface, Tube and Filament

The field lines of the vorticity field are called vortex lines. A vortex line is represented as shown in fig.(A.1). At any point in the flow field, the direction of the vorticity vector is given, by the direction, at that point, of the vortex line passing through that point. Hence,

$$\mathbf{\Omega} \times d\mathbf{s} = 0 \tag{A.3}$$

where **ds** is an element of a vortex line. In Cartesian, if we write

$$\mathbf{\Omega} = (\Omega_x, \Omega_y, \Omega_z) \tag{A.4}$$

[1]Most part of this chapter has been extracted from [13].

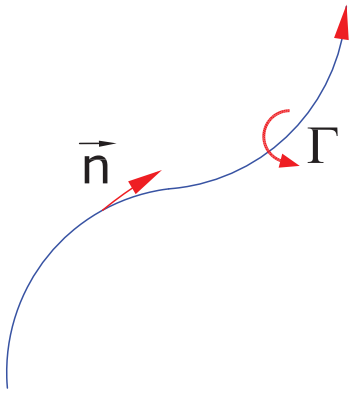

Figure A.1: Vortex line

So, eq.(A.3) becomes

$$\frac{dx}{\Omega_x} = \frac{dy}{\Omega_y} = \frac{dz}{\Omega_z} \tag{A.5}$$

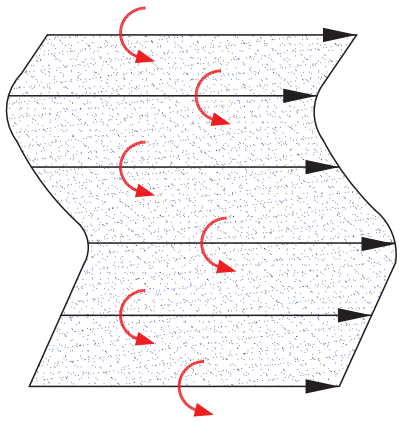

Figure A.2: Vortex surface

If at any instant of time, we draw an arbitrary line in the flow field and draw the vortex lines passing through that line, a surface is formed. Such a surface is called vortex surface and is represented as shown in fig.(A.2).

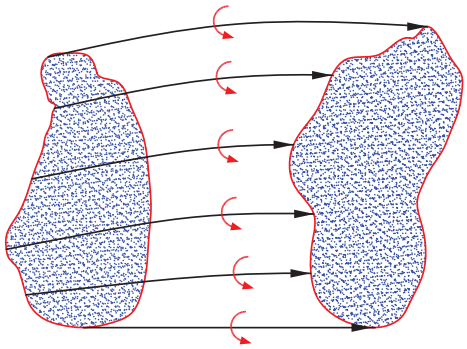

Figure A.3: Vortex tube

If we consider a closed curve and draw all the vortex lines passing through it, a tube is formed. Such a tube is called a vortex tube and is represented as shown in fig.(A.3). A vortex tube of infinitesimal cross-sectional area is known as a vortex filament.

A.2 Vorticity Field as a Divergence Field

Since the vorticity is the curl of another vector field, we have

$$\nabla \cdot (\nabla \times \mathbf{V}) = \nabla \cdot \mathbf{\Omega} = 0 \tag{A.6}$$

Thus, vorticity is a divergenceless field. Consider at any instant, a region of space R enclosed by a closed surface S. We then have

$$\oiint_S \mathbf{\Omega} \cdot \mathbf{n} dS = \iiint_R \nabla \cdot \mathbf{\Omega} dv = 0 \tag{A.7}$$

This equation states that the (net) outflow of vorticity through any closed surface is zero. This is true at every instant of time.

A.3 Spatial Conservation of Vorticity: Strength of a Vortex Tube

Consider at any instant, a vortex tube in the flow field. Denote by R the region space enclosed between the wall of the tube and any two surfaces S_1

and S_2 which cut the tube (see fig.(A.4)). Then, according to eq.(A.7), the outflow of the vorticity through the surface S of the region R vanishes. We therefore write

$$\iint_{S_1} \mathbf{\Omega} \cdot \mathbf{n} dS + \iint_{S_2} \mathbf{\Omega} \cdot \mathbf{n} dS + \iint_{S_w} \mathbf{\Omega} \cdot \mathbf{n} dS = \oiint_{S} \mathbf{\Omega} \cdot \mathbf{n} dS = 0 \tag{A.8}$$

Here S_w denotes the surface of the wall of the tube in the portion under

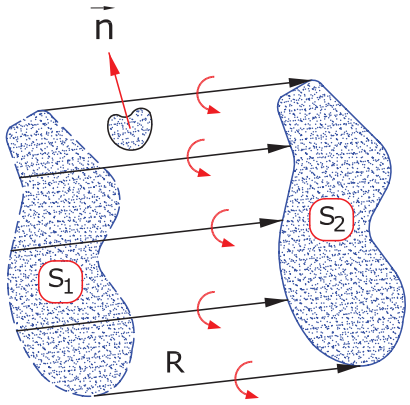

Figure A.4: Illustrating the derivation of the spatial conservation of vorticity

consideration. On the wall of the tube, $\mathbf{\Omega}$ lies in the surface S_w. Hence the integral over S_w vanishes

$$\iint_{S_w} \mathbf{\Omega} \cdot \mathbf{n} dS = 0 \tag{A.9}$$

Consequently, we obtain

$$\iint_{S_1} \mathbf{\Omega} \cdot \mathbf{n} dS + \iint_{S_2} \mathbf{\Omega} \cdot \mathbf{n} dS = 0 \tag{A.10}$$

In this equation $\mathbf{n}$ is an outward normal, outward with reference to the region R. If we draw the normals on the surfaces S_1 and S_2 in the same direction, e.g. (streamwise direction) and denote them by $\mathbf{n}_1$ and $\mathbf{n}_2$ respectively, eq.(A.10) may be rewritten as

$$\iint_{S_1} \mathbf{\Omega} \cdot \mathbf{n}_1 dS = \iint_{S_2} \mathbf{\Omega} \cdot \mathbf{n}_2 dS \tag{A.11}$$

This states that the flow of vorticity through any cross-sectional surface S_1 of a vortex tube is equal to the flow of vorticity through any other cross-sectional surface S_2 of the tube. This is true at every instant of time. If S denotes any cross-sectional surface of the vortex tube, eq.(A.11) may be expressed as

$$\iint_S \mathbf{\Omega} \cdot \mathbf{n} dS = Constant \tag{A.12}$$

This states that the flow of vorticity through any cross-sectional surface of a vortex tube is a constant all along the tube. This is true at every instant of time. In view of the intimate relation between circulation and vorticity, the result in eq.(A.12) may be expressed equivalently in terms of circulation. Let D denote any closed curve that embraces the vortex tube (D encloses the tube and lies on its wall). Then, using eqs.(A.2) and (A.12), we have

$$\Gamma_D = \iint_S \mathbf{\Omega} \cdot \mathbf{n} dS = Constant \tag{A.13}$$

This states that the circulation around any closed curve embracing a vortex tube is constant all along the tube. This is true at every instant of time. Equation (A.13) expresses the spatial conservation of vorticity in the sense implied by that equation. For a vortex filament of variable cross-sectional area dS, this equation takes the form

$$\Gamma_c = \mathbf{\Omega} \cdot \mathbf{n} dS = Constant \tag{A.14}$$

where $\mathbf{n}dS$ is any cross-sectional area of the filament and c is the boundary curve of $\mathbf{n}dS$. If we take $\mathbf{n}$ in the direction of Ω, eq.(A.14) reduces to

$$\Gamma_c = \Omega dS = Constant \tag{A.15}$$

This shows that the vorticity at any section of a vortex filament is inversely proportional to its cross-sectional area. An important consequence of the spatial conservation of vorticity is that a vortex tube, and so also a vortex filament or a vortex line, cannot begin or end abruptly in a fluid. It should either form a closed ring or end at infinity or at a solid or free surface. The circulation around any closed curve embracing a vortex tube, or equivalently the outflow of vorticity through any cross section of the tube, is a characteristic of the tube as a whole and is called the strength of the vortex tube. If we consider a vortex filament of variable cross-sectional area and shrink the area to zero in such a way that the vorticity goes to infinity as the area goes to zero, and the strength. of the filament remains constant, we arrive at the conception of a vortex filament with concentrated vorticity.

A.4 Consequences of the Theorems of Helmholtz and Kelvin

1. A surface which is a vortex sheet at one instant remains a vortex sheet for all times. We further state that fluid particles that are part of a vortex sheet at some instant are part of it for all times. Furthermore, it follows that fluid particles that are part of a vortex tube (or of a vortex filament or of a vortex line) at some instant are part of it for all times.

2. The circulation around a vortex tube, or equivalently the strength of a vortex tube, remains a constant for all times as the tube floats along, regardless of the changes experienced by the vortex tube.

The spatial conservation of vorticity as expressed by eq.(A.13) and the consequences, as described above, of the theorem on the permanence of vorticity or circulation, are usually referred to as Helmholtz's theorems of vortex motion. The spatial conservation of vorticity is purely a kinematic property, for it directly follows from the fact that the divergence of any curl vector is zero, i.e. eq.(A.6).

A.5 Velocity Field Due to Vortex Distribution in an Incompressible Fluid

In applications one is concerned with the problem of expressing the velocity field in terms of the vorticity field. To obtain the velocity $\mathbf{V}(\mathbf{r}, t)$ in terms of the vorticity $\boldsymbol{\Omega}(\mathbf{r}, t)$ we need to invert the equation

$$\boldsymbol{\Omega} = \nabla \times \mathbf{V} \tag{A.16}$$

We do this as follows. Considering an incompressible fluid, we have

$$\nabla \cdot \mathbf{V} = 0 \tag{A.17}$$

On the basis of this relation, we may express $\mathbf{V}$ as the curl of some other vector field, say of $\mathbf{A}(\mathbf{r}, t)$. Hence we set

$$\mathbf{V} = \nabla \times \mathbf{A} \tag{A.18}$$

Since the curl of any gradient vector is zero, the vector $\mathbf{A}$ is indeterminate to the extent of the gradient of a scalar function of position and time. From eq.(A.18), it follows that

$$\nabla \times \mathbf{V} = \nabla \times (\nabla \times \mathbf{A}) = \nabla (\nabla \cdot \mathbf{A}) - \nabla^2 \mathbf{A} \tag{A.19}$$

We now stipulate that

$$\nabla \cdot \mathbf{A} = 0 \tag{A.20}$$

This is permissible since $\mathbf{A}$ is indeterminate to the extent of a gradient vector. From eqs.(A.19), (A.20) and (A.16), we obtain

$$\nabla^2 \mathbf{A} = -\nabla \times \mathbf{V} = -\boldsymbol{\Omega} \tag{A.21}$$

This is Poisson's equation for $\mathbf{A}$. We call $\mathbf{A}$ a vector potential. Once $\mathbf{A}$ is determined as a solution of eq.(A.21), the velocity field may be deduced from eq.(A.18). In Cartesian, if we express

$$\mathbf{A} = (A_x, A_y, A_z) \tag{A.22}$$

$$\boldsymbol{\Omega} = (\Omega_x, \Omega_y, \Omega_z) \tag{A.23}$$

The solution of eq.(A.21) is expressed by Green's formula as

$$\mathbf{A}(\mathbf{r}, t) = \frac{1}{4\pi} \iiint_R \frac{\boldsymbol{\Omega}(\mathbf{s}, t)}{\mid \mathbf{r} - \mathbf{s} \mid} dv(\mathbf{s}) \tag{A.24}$$

where $\boldsymbol{\Omega}(\mathbf{s}, t)\, dv$ is an element of the vortex distribution situated at the point s and R is the region in which the vorticity is distributed (see fig.(A.5)). Note that the integration is with respect to the coordinates of the vortex distribution, i.e. s and not r. The velocity field is then given by

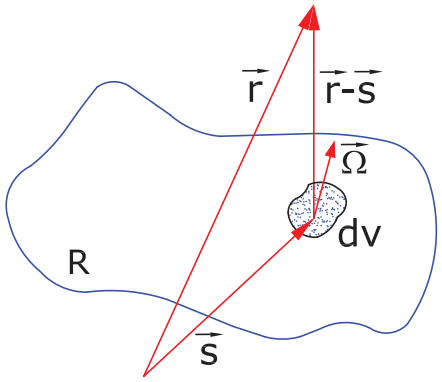

Figure A.5: Nomenclature used in the derivation of the velocity resulting from a vortex distribution

$$\mathbf{V} = \nabla \times \mathbf{A} = \frac{1}{4\pi} \nabla \times \left(\iiint_R \frac{\mathbf{\Omega}(\mathbf{s}, t)}{\mid \mathbf{r} - \mathbf{s} \mid} dv(\mathbf{s}) \right) \tag{A.25}$$

If we denote by $\delta\mathbf{A}$ the contribution to $\mathbf{A}$ at $\mathbf{r}$ due to the-vortex element $\mathbf{\Omega}dv$ situated at S and similarly by $\delta\mathbf{V}$ the contribution to $\mathbf{V}$ at $\mathbf{r}$, we have

$$\delta\mathbf{A}(\mathbf{r}, t) = \frac{1}{4\pi} \frac{\mathbf{\Omega}(\mathbf{s}, t)}{\mid \mathbf{r} - \mathbf{s} \mid} dv(\mathbf{s}) \tag{A.26}$$

$$\delta\mathbf{V}(\mathbf{r}, t) = \frac{1}{4\pi} \nabla_r \times \left(\frac{\Omega(\mathbf{s}, t)}{\mid \mathbf{r} - \mathbf{s} \mid} dv(\mathbf{s}) \right) \tag{A.27}$$

We include the subscript $\mathbf{r}$ on the curl to emphasize that the curl is to be taken with respect to the coordinates of the point $\mathbf{r}$.

A.6 Velocity Field of a Vortex Filament: Biot-Savart Law

Consider a vortex filament of strength Γ. Choose a volume element dv of this filament as the cylinder formed by a cross-sectional surface $\mathbf{n}dS$ and an element of length $\mathbf{dl}$ along the filament (see fig.(A.6)). Then the contribution to the vector potential $\mathbf{A}$ at a field point $\mathbf{r}$, from the vortex element at $\mathbf{s}$ is given by

$$\delta\mathbf{A}(\mathbf{r}) = \frac{1}{4\pi} \frac{\mathbf{\Omega}(\mathbf{s})}{\mid \mathbf{r} - \mathbf{s} \mid} (\mathbf{n}dS \cdot \mathbf{dl}) \tag{A.28}$$

Since we have

$$\mathbf{dl} = \frac{\mathbf{\Omega}}{\Omega} dl \tag{A.29}$$

and

$$\mathbf{\Omega} \cdot \mathbf{n}dS = \Gamma \tag{A.30}$$

Equation (A.28) may be rewritten as

$$\delta\mathbf{A}(\mathbf{r}) = \frac{\Gamma}{4\pi} \frac{\mathbf{dl}}{\mid \mathbf{r} - \mathbf{s} \mid} \tag{A.31}$$

The contribution to the velocity at the point $\mathbf{r}$ from the element of the filament is then given by

$$\delta\mathbf{V}(\mathbf{r}) = \nabla_{\mathbf{r}} \times \left(\frac{\Gamma}{4\pi} \frac{\mathbf{dl}}{\mid \mathbf{r} - \mathbf{s} \mid} \right) \tag{A.32}$$

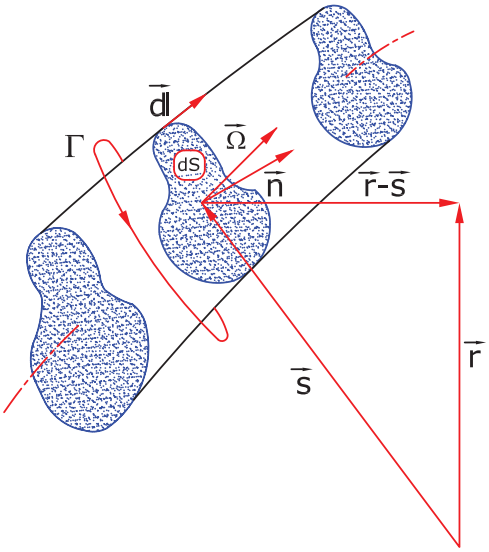

Figure A.6: Nomenclature used in the derivation of the Biot-Savart law

In carrying out the curl operation, we keep **s** fixed. We know that

$$\nabla \times (\phi \mathbf{F}) = (\nabla \phi \times \mathbf{F}) + (\phi \nabla \times \mathbf{F})$$

Here

$$\mathbf{F} = \frac{\Gamma d\mathbf{l}}{4\pi}$$

$$\phi = \frac{1}{\mid \mathbf{r} - \mathbf{s} \mid}$$

Since, $\nabla \times d\mathbf{l} = 0$ then $\phi \nabla \times \mathbf{F} = 0$. Also, $\nabla \phi = -\dfrac{(\mathbf{r} - \mathbf{s})}{\mid \mathbf{r} - \mathbf{s} \mid^3}$. Now, eq.(A.32) reduces to

$$\delta \mathbf{V}(\mathbf{r}) = \frac{\Gamma}{4\pi} \frac{\mathbf{dl} \times (\mathbf{r} - \mathbf{s})}{\mid \mathbf{r} - \mathbf{s} \mid^3} \tag{A.33}$$

This is known as the Biot-Savart law. The velocity at **r** due to the whole vortex filament is obtained by integration of eq.(A.33) over the length of the filament. We thus have

$$\mathbf{V}(\mathbf{r}) = \frac{\Gamma}{4\pi} \int \frac{\mathbf{dl} \times (\mathbf{r} - \mathbf{s})}{\mid \mathbf{r} - \mathbf{s} \mid^3} \tag{A.34}$$

Since Γ is the strength of the filament, it is a constant and hence appears outside the integral.

There is another method for the derivation of the Biot-Savart law. We consider an infinitely thin vortex filament (also closed). Let $\mathbf{n}, \mathbf{b}, \mathbf{t}$ be the unit vectors of normal, bi-normal, and tangent, respectively, and x_n, x_b, x_t are the coordinates along these directions. The vorticity can be written as

$$\boldsymbol{\Omega} = \Gamma \delta\left(x_n\right) \delta\left(x_b\right) \mathbf{t} \tag{A.35}$$

where δ is Dirac's Delta Function. Substituting eq.(A.35) in eq.(1.7)

$$\begin{gathered} \boldsymbol{W} = \frac{\Gamma}{4\pi} \int \delta\left(x_n\right) \delta\left(x_b\right) \frac{\mathbf{t} \times \left(\mathbf{x} - \mathbf{x}'\right)}{\mid \mathbf{x} - \mathbf{x}' \mid^3} dx_n dx_b dx_t \\ \boldsymbol{W} = -\frac{\Gamma}{4\pi} \oint \frac{\boldsymbol{\Delta}\mathbf{r} \times d\mathbf{s}}{\mid \mathbf{x} - \mathbf{x}' \mid^3} \end{gathered} \tag{A.36}$$

where $dV = dx_n dx_b dx_t$ and $\mathbf{t} dx_t = d\mathbf{s}$. Equation (A.36) is derived for the coordinate system bounded to a curve. In an unbounded domain with no interior boundaries and the absolute coordinate system, we can write [14]

$$W\left(\mathbf{x}\right) = -\frac{\Gamma}{4\pi} \int\limits_C \frac{\left(\mathbf{x} - \mathbf{x}'\right)}{\mid \mathbf{x} - \mathbf{x}' \mid^3} \times \frac{\partial \mathbf{x}'}{\partial s'} ds' \tag{A.37}$$

Appendix B

Helix Equation

A helix is a curve in 3-D space. It is characterized by the fact that the tangent line at any point makes a constant angle with a fixed line called the axis.

The parametric equations of a circular helix path s can be written as

$$\mathbf{s} = \begin{cases} x(t) = r\cos(\omega t + \theta_0) \\ y(t) = r\sin(\omega t + \theta_0) \\ z(t) = V_0 t \end{cases} \tag{B.1}$$

where r is circle radius, ω is rotational velocity, θ_0 is initial angle of rotation, t is time and V_0 is translational velocity of helix in z direction (parallel to helix axis), respectively.

According to angular velocity ω definition, one revolution is equal to 2π radians, so

$$\omega = \frac{2\pi}{T} \tag{B.2}$$

where T is period measured in seconds.

Equation of angular motion with constant angular velocity gives

$$\theta = \omega t + \theta_0 \tag{B.3}$$

where for $\theta_0 = 0$ reads

$$\theta = \omega t \tag{B.4}$$

Helix pitch angle ϕ is defined as

$$\phi = \tan^{-1}\left(\frac{V_0}{r\omega}\right) \tag{B.5}$$

Combining eqs.(B.4) and (B.5) yields

$$V_0 t = r\theta\tan\phi \tag{B.6}$$

Now, we can rewrite eq.(B.1) as

$$\mathbf{s} = \begin{cases} x(t) = r\cos(\theta + \theta_0) \\ y(t) = r\sin(\theta + \theta_0) \\ z(t) = r\theta\tan\phi \end{cases} \tag{B.7}$$

or

$$\mathbf{s} = r\cos(\theta + \theta_0)\,\mathbf{i} + r\sin(\theta + \theta_0)\,\mathbf{j} + r\theta\tan\phi\mathbf{k} \tag{B.8}$$

Also, the derivative of $\mathbf{s}$ with respect to θ reads as

$$d\mathbf{s} = d\theta[-r\sin(\theta + \theta_0)\,\mathbf{i} + r\cos(\theta + \theta_0)\,\mathbf{j} + r\tan\phi\mathbf{k}] \tag{B.9}$$

Bibliography

[1] S. Gupta and J. G. Leishman. Comparison of momentum and vortex methods for an aerodynamics analysis of wind turbines. In *43rd AIAA Aerospace Sciences Meeting and Exhibit*, Reno, Nevada, 2005.

[2] R. H. Miller. The aerodynamics and dynamic analysis of horizontal axis wind turbines. *Wind Engineering and Industrial Aerodynamics*, 15:329–340, 1983.

[3] B. Montgomerie. Vortex models for wind turbine loads and performance evaluation. Scientific report-FOI-R–1301–SE, FOI-Swedish Defence Research Agency-Aeronautics, Stockholm, Sweden, 2004.

[4] M. O. L. Hansen, J. N. Sørensen, S. Voutsinas, N. Sørensen, and H. Aa. Madsen. State of the art in wind turbine aerodynamics and aeroelasticity. *Progress in Aerospace Sciences*, 42:285–330, 2006.

[5] M. O. L. Hansen. *Aerodynamics of wind turbines*. Earthscan, New York, 2nd edition, 2008.

[6] J. Whale. An experimental and numerical study of the vortex structure in the wake of a wind turbine. *Wind Engineering and Industrial Aerodynamics*, pages 357–372, 2000.

[7] J. D. Anderson. *Fundamentals of Aerodynamics*. McGraw-Hill, New York, 3rd edition, 2001.

[8] R. Von Mises. *Theory of flight*. Dover Publications, New York, 1st edition, 1945.

[9] H. Dumitrescu and V. Cardos. Wind turbine aerodynamic performance by lifting line method. *Rotating Machinery*, 4:141–149, 1998.

[10] B. R. Jeng, Jr. T. G. Keith, and A. Aliakbarkhanafjeh. Aerodynamic analysis of a horizontal axis wind turbine by use of helical vortex theory.

Technical report-NASA/CR-168054, Department of Mechanical Engineering University of Toledo, Toledo, Ohio, 1982.

[11] J. Jonkman, S. Butterfield, W. Musial, and G. Scott. Definition of a 5-MW reference wind turbine for offshore system development. Technical report, NREL/TP-500-38060, National Renewable Energy Laboratory, Colorado, USA, 2009.

[12] P. Gigure and M. S. Selig. Design of a tapered and twisted blade for the nrel combined experiment rotor. Technical report, NREL/TP-500-38060, National Renewable Energy Laboratory, Colorado, USA, 1998.

[13] K. Karamcheti. *Principles of Ideal-Fluid Aerodynamics*. Krieger, Florida USA, 2nd edition, 1980.

[14] Leonard A. Computing three-dimensional incompressible flows with vortex elements. *Annual Review of Fluid Mechanics*, 17:523–559, 1985.